Mathematical Modeling and Simulation of Aquatic and Aerial Animal Locomotion

Thesis by

Valentin G. Stredie

In Partial Fulfillment of the Requirements

for the Degree of

Doctor of Philosophy

California Institute of Technology

Pasadena, California

2004

(Submitted August 26, 2004)

Acknowledgements

It is a pleasure to thank the many people who made this thesis possible.

First I would like to thank my advisor, Professor Thomas Y. Hou, for the support and guidance I received from him. He is a great mathematician and his incredible experience helped me many times. He's got this extraordinary mathematical and physical perspective; he could understand some of my methods before I could even explain them to him. He could think about models, simulations and applications that could really make a difference. Equally important, I think, was his generosity and kindness. More than an advisor, he was also a good friend giving me advice through difficult times. I would love to recommend him as an advisor for the new applied math grad students.

I am extremely grateful to Professor Theodore Y. Wu who was the genius behind the idea of this thesis. I truly wish some day I will end up knowing at least half the fluid mechanics he knows. He is a wonderful person and during these years I really liked his energy and his enthusiasm. I think he is a great pedagogue, his idea of self-study being incredibly useful. Many times he let me figure out some things even though he knew them. He was giving me some ingenious hints and then after some hard work I was reaching the right conclusion. He was very happy when this was happening and I had only to gain. The things I learned from him will stay with me for a long, long time.

I would also like to thank the man because of whom I started loving mathematics. Professor Constantin Bozdog had this special gift about the way he was teaching math and for me it became like a game, the game of science. We are now very good friends and his moral support meant a lot for me during the grad school years.

The colleagues from the department were very useful sources of mathematical knowledge. Therefore I would like to thank Theo Strinopoulos and Razvan Fetecau for the long

discussions we had about everything, sometimes math... I thank all my friends for their support and encouragement.

Finally, and most importantly, I would like to express special gratitude to my family, my mother and my grandparents. You were there when I needed you and I owe you a lot for that.

My wonderful wife Crina has been, always, my pillar, my joy and my guiding light, and I thank her. For your love and kindness, I dedicate this thesis to you, Crina!

Abstract

In this thesis we investigate the locomotion of fish and birds by applying both new and well known mathematical techniques.

The two-dimensional model is first studied using Krasny's vortex blob method, and then a new numerical method based on Wu's theory[1] is developed. To begin with, we will implement Krasny's ideas for a couple of examples and then switch to the numerical implementation of the nonlinear analytical mathematical model presented by Wu. We will demonstrate the superiority of this latter method both by applying it to some specific cases and by comparing with the experiments. The nonlinear effects are very well observed and this will be shown by analyzing Wagner's result for a wing abruptly undergoing an increase in incidence angle, and also by analyzing the vorticity generated by a wing in heaving, pitching and bending motion. The ultimate goal of the thesis is to accurately represent the vortex structure behind a flying wing and its influence on the bound vortex sheet.

In the second part of this work we will introduce a three-dimensional method for a flat plate advancing perpendicular to the flow. The accuracy of the method will be shown both by comparing its results with the two-dimensional ones and by validating them versus the experimental results obtained by Ringuette in the towing tank of the Aeronautics Department at Caltech.

[1] In this thesis we will use 'Krasny's method' to refer to the method based on the vortex blob technique and 'Wu's method' to refer to the one implemented by Wu. Since we are not aware of an actual method developed by Krasny for an airfoil moving forward at a given angle of attack, we should rather use 'classical vortex method' and 'semi-analytical method' respectively to describe these two implementations. However, we will talk about 'Krasny's method' and 'Wu's method' for easier understanding.

Contents

Chapter 1

Introduction

Flight has fascinated the human mind since its early days of development. The gracefulness and the perfection of a bird in the air inspired us to try to emulate some particular aspects of its superb ability. The first flying devices were paper kites in China about 2000 years ago. After that, men created all kinds of contraptions, which included the ornithopter, which was no more than human-sized bird wings. They had not figured out the effect of taking something of a small scale and making it larger to accommodate a larger client, as flapping wings will work on birds, but will not do the deed for humans, who are generally larger than flying birds.

Years after several other followers failed to create anything successful, it was the Wright Brothers' turn, who are credited with the first sustained flight on December 17, 1903. However, the perfection and elegance of the bird-flapping flight has never been achieved. For these reasons, one can imagine how rich and complex the literature is when we direct our attention to animal flight. In the present chapter, we will try to put our work into context and see what has been done in the past in this vast field.

History and Literature: Theory and Computations. Starting with the work of Sir James Gray who was the head of Cambridge University's Zoology Department from 1937 to 1961, the theory of animal locomotion stimulated G. I. Taylor in making two pioneering investigations. One involved the swimming of snakes and eels, and the other one initiated hydrodynamic studies of flagellar propulsion. However, the main contributions to this domain came later on from Sir James Lighthill and Professor Theodore Wu. Lighthill laid

a theoretical foundation for the swimming of slender fish, while Wu made an extension of classical oscillating airfoil aerodynamics to a linear theory of flexible lifting-surface locomotion, to examine the performance of bending wings of birds in flapping flight and the lunate tails of fast-swimming percomorph and acombroid fishes and rays in swimming.

Re-emphasizing the importance of Wu's (scaling of aquatic locomotion - Wu [1977]), Lighthill's (scaling of aerial locomotion) and Weis-Fogh's (hovering flight) work in fish and bird locomotion, we should also remember the advances made in the field of wing theory and free-surface numerical methods.

One of the pioneers in the study of a wing in flight was T. Theodorsen with his theory of instability and the mechanism of flutter (see Theodorsen [1935]). In 1931, Kaden introduced similarity variables for describing the roll-up of a semi-infinite plane vortex-sheet (see Saffman [1992], p. 147). During the 1950s, several authors presented approximate asymptotic solutions in which the spiral vortex generated behind a sharp edge was replaced by a single point vortex, an example of which is given by Rott [1956]. Moore in 1976 (see Moore [1976]) studied and verified the stability of a class of vortex sheets rolling-up, but could not verify the stability of the problem as noted by Pullin in 1978 (see Pullin [1978]). In the same work, Pullin, for the first time, obtained regular and well-defined start-up vortex spirals from an accurate numerical solution of the Birkhoff-Rott equation (inviscid flow) written in similarity variables. These results were used by Krasny to validate his method. In 1991 (see Krasny [1991]), he provided an extensive discussion of Chorin's vortex blob method (see Chorin [1973]) and applied it for the evolution of a free vortex sheet undergoing a certain perturbation and for the wake forming at the edges of a flat plate advancing perpendicular to the flow. Strong numerical evidence indicated that the vortex blob method converged past the vortex sheet singularity formation time, as the smoothing parameter tended to zero.

Nitsche and Krasny, in 1994, (see Krasny [1994]) developed a numerical method for the vortex ring formation at the edge of a circular tube. Comparison between simulation and experiment indicated that the model captured the basic features of the ring formation process. Then, in 2001, a very interesting model was presented by Chamara and Coller

(Chamara [2001]) for a pair of airfoils with two degrees of freedom: pitching and heaving. They were interested in finding the optimum configuration of the two airfoil system for which the two oscillatory instabilities due to the flutter occurred simultaneously.

Closer to animal locomotion, Dickinson *et al.* measured the unsteady forces on a robotic fruit fly wing and demonstrated the role of wing rotation in force generation (Dickinson [1999]). Also, J. Wang in 2000 (see Wang [2000]) tried to quantify the vortex dynamics of a flying insect, that is essential for hovering, and identify a minimal two-dimensional model that produced sufficient lift. Later, in 2004, Wang, Birch and Dickinson compared computational, experimental and quasi-steady forces in a generic hovering wing undergoing sinusoidal motion along a horizontal stroke plane. In particular, they investigated unsteady effects and compared two-dimensional computations and three-dimensional experiments in several qualitatively different kinematic patterns (see Wang [2004]).

If we look at free-surface flow problems we should mention the work of Baker, Meiron and Orszag in studying the evolution equations. They proposed in 1982 an alternative to the matrix inversion techniques used before. The resulting Fredholm integral equations of the second kind were solved efficiently by iteration in both two and three dimensions. Applications to breaking water waves over finite-bottom topography and inter-facial waves were provided (see Baker [1982]). Finally, Baker and Beale (see Baker [2004]) applied the vortex-blob method to develop a boundary integral method for computing the motion of an interface separating two incompressible, inviscid fluids.

In three dimensions we should point to the work of Brady, Leonard and Pullin who, in 1998 provided a three-dimensional computational method to track the evolution of regularized three-dimensional vortex sheets through an irrotational, inviscid, constant-density fluid. Also, in 2001, Lindsay and Krasny (Lindsay [2001]) developed a fast adaptive Lagrangian particle method for computing free vortex sheet motion in three dimensional flow. To be able to do all the computations efficiently, they also included an adaptive treecode algorithm.

History and Literature: Experiments. In the fluid dynamics literature we were very lucky to find some significant experiments that helped us in verifying our computational

results. Thus, Didden in 1979 (see Didden [1979]) performed an experiment in which a moving piston forces fluid from a circular tube, leading to the formation of a vortex ring. Krasny used this experiment to validate his numerical method.

The fluid mechanics literature is richer in experiments involving a heaving wing. Some were done by Bratt in 1953 (see Bratt [1953]) and more recently by Jones, Dohring & Platzer in 1998 (see Jones [1998]) and by Lai, Yue & Platzer in 2002 (see Lai [2002]). For pitching, the experiment by Koochesfahani (see Koochesfahani [1989]) at Caltech for the visualization of the wake behind a flat plate in pitching motion with various frequencies and pitching axes provided very useful information.

Closer to the natural bird movement, Pennycuick (Pennycuick [1996]), after long observations on a thrush nightingale and a teal, came up with a formula for the wing-beat frequencies of different birds in level cruising flight. In 2000, Earls went even further. It is well known how the most difficult moment of the flight is the take-off. Earls, in 2000, (Earls [2000]), after a study on starlings and quails, showed the movements of the bird wings during this essential moment, talking about kinematics and mechanics. We will use these natural movement descriptions when we analyze a bird's flight in Chapter 3.

For this thesis, in three dimensions, we use some very nice experiments involving a three-dimensional flat plate advancing perpendicular to the flow, performed for his Ph.D. thesis by M. Ringuette in the towing tank at Caltech in 2004 (see Ringuette [2004]).

Wu's Method. In the history of pioneering development of linear unsteady airfoil theory, Herbert Wagner (1925) was the first to have generated an integral equation for calculating the wake vorticity shed by a wing. This approach was further developed by Theodore von Karaman and William Sears (1938), who made a lasting contribution by providing an improved derivation based on the decomposition of the bound vorticity Γ_b into two parts, one for the "quasi-stationary wake-less" flow Γ_0 past the wing, and the other, Γ_1, due to the wing reaction to the vortex sheet. Γ_0 and Γ_1 were both carefully analyzed using linear approximations.

Some work towards the generalization to fully nonlinear theory was done by McCune and co-workers (1990, 1993) but the full generalization to two dimensional flexible lifting surface

performing arbitrary movements was done by Theodore Y. Wu in 2001 (see Wu [2001]). The discussions in this thesis will be based on this newer and improved theory. The analysis of both Γ_0 and Γ_1 captures very well the nonlinear effects while the wake vorticity γ_w is being computed using the Kutta condition in the form of generalized Wagner's integral equation for the conservation of total circulation.

Issues Addressed in This Thesis. The main goal of this thesis is to develop a better method for capturing the nonlinear effects present in highly nonlinear movements of a bird's wing or a fish's fin. These nonlinear effects are very important when we have to study very sensitive movements as highly curved ones (very quick U-turns) or those implying wing-wake interaction. The main difficulty arises when analyzing the fluid properties near the trailing edge of a wing as well as the behavior of the flow inside the vortex ring. These difficulties will be overcome by using Wu's method which provides a very strong nonlinear analytical approach in computing the flow and wing characteristics.

The method will be applied to some significant cases and we will show how it matches the experiment data. Compared to the previous methods, Wu's method will better capture the position and radius of a vortex forming behind a wing advancing at a certain angle of attack. In Section 3.3, we will see how the relative error in the span-wise location of the core of the vortex ring compared to experiment is 9% for Wu's method and 72% for Krasny's. Also the radii of the vortex rings are different, in Wu's method being 25% bigger than in Krasny's. However, Wu's result agrees very well with the experiment in the sense that it verifies the square-root behavior of the radius as predicted by Davenport. The CPU time on an AMD Athlon(tm) XP 1700+ with 512 MHZ for the same initial data (12,000 time-steps) is almost the same: about 90 hours for Wu's method and 85 for Krasny's. Here the complexity of the method proposed by Wu is balanced by the need of a matrix inversion in Krasny's method.

Wu's method will also show more roll-ups inside the vortex ring compared to Krasny's method. To get the same number of roll-ups for Krasny's we will have to decrease the blob and therefore to decrease the time step accordingly. This will increase considerably the total CPU time.

For nonlinear motions, Wu's method shows very good results when compared with the experiments for heaving and pitching. Some more interesting examples will be studied involving highly curved Heaviside, Fourier and bending motions. The lift and the thrust will be analyzed, emphasizing the effect of the free vortex sheet over the flying wing.

One of the big improvements we could note using Wu's method is what we obtain computationally for Wagner's theoretical result. The theory says that in the case of a forward flying wing with an angle of attack, the initial lift is half the final lift. Our result is significantly better than the ones found in the literature (see Katz [2001]). We get a ratio of initial lift over final lift of about 0.64 while using Krasny's method this was around 0.74. The one obtained by Katz and Plotkin is about 0.85.

We will try to demonstrate that all these improvements are due to the fact that Wu's method captures the leading order effect of the first released vortex element. The error that Krasny's method introduces in this first element will propagate in the wake at every time step and will be the source of discrepancies between the results obtained with the two approaches.

The thesis begins with an introduction to Krasny's vortex-blob method. The understanding of his work was a very important step for us and it was crucial in the implementation and development of a numerical method for Wu's theory. Krasny's ideas are taken from his paper from 1994 (see Krasny [1994]) in which he studied the vortex formation at the edge of a circular tube. Krasny's method provides important insight for a number of fluid mechanics and numerical issues. We generalize Krasny's method to a flat plate moving perpendicular to the flow. We refer to Krasny [1991] for more discussions of the method.

We will continue with the extensive presentation of Wu's theory for a flexible plate advancing at an angle of attack. This is inspired form Wu's 2001 paper "On Theoretical Modeling of Aquatic and Aerial Animal Locomotion" (see Wu [2001]). The very complex mathematical formulation provides a nonlinear approach inspired from a theory initially adopted by Wagner, von Karman and Sears. It is based on the decomposition of the bound vorticity into two parts, one representing the "quasi-steady wake-less" flow over the wing, and the other representing the additional bound vorticity in reaction to the trailing wake

vortices, required to reinstate the original time-varying normal velocity on the bound sheet.

We will provide an extensive description for the implementation of these methods and will include some very interesting comparisons both between the two methods and between Wu's method and experiment. First we will present our results for the vortex formation at the edge of a circular tube. They verify well against Krasny's results and against the experimental ones obtained by Didden in 1979 (see Didden [1979]). We continue with the problem of a flat plate advancing perpendicular to the flow and then with the implementation of Krasny's method for a wing advancing at a given angle of attack. To the best of our knowledge, the numerical implementation of the latter case is not available in the literature and therefore, the method we are presenting here is partly inspired from the cases discussed in this thesis involving Krasny's method, partly from the simple numerics found in Katz [2001]. The corresponding section and the following ones involving Wu's method will present an analysis that documents the structure and development of a tip vortex shed from a conventional wing. Such flows are of engineering importance because they dominate the wakes of lifting vehicles. In real experiments they are also of scientific interest as examples of turbulent flows dominated by rotation.

In order to demonstrate that Wu's method behaves better than the ones developed before, we will compare it against the experiment done by Davenport (see Davenport [1995]), and then we will apply it to some highly nonlinear motions such as heaving, pitching, mixed heaving-pitching, and bending. We will compute some relevant quantities such as thrust and lift and interpret the results obtained. A very nice way of validating Wu's method is to see its output for Wagner's famous result: if a wing undergoes an abrupt change in incidence angle, the initial lift at $t = 0^+$ will be half of the final lift. We try to see what happens to this result in the case of an abrupt Heaviside or Fourier flexible motion.

In the last part of the thesis, we will propose a three-dimensional mathematical model for a flat plate advancing perpendicular to the flow. The three-dimensional approach for the computation of the bound circulation is inspired from the panel method presented in "Low speed aerodynamics" by J. Katz and A. Plotkin (Katz [2001]). This is ingeniously combined with Krasny's two-dimensional method to solve for the free sheet vortex elements.

The results match the experiments done by Ringuette in 2004 at Caltech (see Ringuette [2004]) in terms of the total circulation along chord-wise sections of the wake. Also, the results agree very well with the two-dimensional ones for a chord-wise center section of a very high aspect ratio wing. However, the numerical method fails to observe the separation found in the experiment after the so called "formation number". This is due to the viscosity of the fluid and it can only be artificially implemented in our potential flow.

The three-dimensional results are very important for developing a more complex three dimensional theory. As in the two-dimensional case, this could be the first step towards a more in depth analysis. The first results obtained in this thesis are very promising for a future work which could be of great importance for the study of swimming and flying. The main difficulty though, would be the three-dimensional generalization of Wu's theoretical model.

Organization of the Thesis. Chapter 2 will present the theoretical approach and the numerical algorithms for Krasny's and Wu's methods. For Krasny's method we will use two of his papers - see Krasny [1991] and Krasny [1994]. Wu's approach will be inspired from his paper, "On theoretical modeling of aquatic and aerial animal locomotion" (see Wu [2001]).

Chapter 3 will show our implementation for these methods on various examples. Krasny's method will be applied to a piston forcing the fluid out of a tube, to a wing advancing perpendicular to the flow and to a wing advancing at a given angle of attack. Wu's method will be applied for a wing advancing at a given angle of attack, for a wing in heaving, pitching, bending motions as well as for a wing in highly curved Heaviside and Fourier motions. The two methods will be compared against experiments and we will demonstrate the superiority of Wu's method. Also, the lift and thrust will be analyzed in some significant cases and Wagner's result will be numerically implemented using Wu's method.

Chapter 4 will present the implementation of the three-dimensional method along with some very interesting comparisons with the experiments done in 2004 by Davenport.

Chapter 5 is devoted to concluding remarks and future directions.

Chapter 2

Theory for the Mathematical Model of the Vortex in Potential Flow

2.1 Krasny's Vortex Blob Method

2.1.1 Vortex Formation at the Edge of a Circular Tube

Introduction Inspired from an experiment done by Didden in 1979, Krasny and Nitsche (1994) implemented a numerical method for the axisymmetric flow shedding a vortex wake. Didden's experiment investigated the movement of a piston inside a circular tube which was forcing the fluid out and was generating a vortex ring at the edge of the tube. Comparison between the numerical simulation and experiment indicated that the theoretical model captured the basic features of the ring formation process.

The vortex-sheet model has been used extensively to compute separating flow past a sharp edge. The computations employed a time-stepping procedure in which discrete vortex elements of suitable strength were released from the edge at regular intervals. Instead of using point vortices, Krasny used blobs, meaning that he gave a non-zero radius (δ) to the released vortex elements. This was used to regularize the roll-up of the free vortex sheet (see Chorin [1973]). The artificial smoothing parameter $\delta > 0$ was used in the equation governing the motion of the sheet and information about the vortex sheet was gotten by considering the limit of the result as $\delta \to 0$.

Another difficult problem, aside from the roll-up, is the separation at a sharp edge.

Krasny's approach, as it will be discussed later, takes care of this by carefully analyzing the relation between the circulation shedding rate and the slip velocities on both sides of the edge by using the Kutta condition.

Krasny's goal was to prove that the vortex-sheet model provides an asymptotic approximation for slightly viscous flow. As it was said before, he succeeded in doing this by comparing his computational results with some very accurate measurements from a well-controlled laboratory experiment. Work done before Krasny (see Tryggvason, Dahm & Sbeih - 1991) showed that the zero smoothing limit of $\delta \to 0$ agreed with the zero viscosity limit $\nu \to 0$ in the case of the Kelvin-Helmholtz problem for the periodic vortex-sheet roll-up in two-dimensional flow. This study compared the vortex-blob simulations with finite-difference solutions of the Navier-Stokes equations. While the vortex-blob method proved to give very good results when applied to Kelvin-Helmholtz problem, Krasny tried to offer a validation of this method for flows past a sharp edge.

The following theoretical and numerical results follow closely the theory presented in Krasny [1994] and Krasny [1991].

Free Vortex Sheet The model is implemented using cylindrical coordinates $(x^f(\Gamma,t), r^f(\Gamma,t))$, with $0 \leqslant \Gamma \leqslant \Gamma_T(t)$ and $0 \leqslant t$, where Γ is the Lagrangian circulation along the sheet and $\Gamma_T(t)$ is the total circulation at time t. A regularized filament of unit strength located at $(\tilde{x}, \tilde{r})$ will influence a point at (x, r) by

$$\psi_\delta(x, r; \tilde{x}, \tilde{r}) = \frac{1}{4\pi} \int_0^{2\pi} \frac{r\tilde{r}\cos\theta}{(\rho^2 + \delta^2)^{1/2} d\theta}, \tag{2.1}$$

where ψ_δ is the stream function, $\rho^2 = (x - \tilde{x})^2 + r^2 + \tilde{r}^2 - 2r\tilde{r}\cos\theta$ and δ is the vortex-blob smoothing parameter. This is where the blob appears in the equations governing the sheet. Lamb (1931) shows that the stream function can be expressed in terms of the complete elliptic integrals of the first and second kind, $F(\lambda)$ and $E(\lambda)$, as

$$\psi_\delta(x, r; \tilde{x}, \tilde{r}) = \frac{1}{2\pi}(\rho_1 + \rho_2)(F(\lambda) - E(\lambda)), \tag{2.2}$$

where $\lambda = (\rho_2 - \rho_1)/(\rho_2 + \rho_1),\ \rho_1^2 = (x-\tilde{x})^2 + (r-\tilde{r})^2 + \delta^2,\ \rho_1^2 = (x-\tilde{x})^2 + (r+\tilde{r})^2 + \delta^2$, and

$$F(\lambda) = \int_0^{2\pi} \frac{d\theta}{\sqrt{1-\lambda^2 \sin^2\theta}},\ E(\lambda) = \int_0^{2\pi} \sqrt{1-\lambda^2 \sin^2\theta}\, d\theta, \tag{2.3}$$

To learn more about numerical calculations of elliptic integrals and elliptic functions, see (Bulirsch [1965]).

The velocity induced by a circular filament has axial and radial components given by the definition of the stream function

$$u_\delta(x,r;\tilde{x},\tilde{r}) = \frac{1}{r}\frac{\partial \psi_\delta}{\partial r}(x,r;\tilde{x},\tilde{r}),\ v_\delta(x,r;\tilde{x},\tilde{r}) = -\frac{1}{r}\frac{\partial \psi_\delta}{\partial x}(x,r;\tilde{x},\tilde{r}). \tag{2.4}$$

The partial derivatives of ψ_δ are given by the chain rule

$$\frac{\partial \psi_\delta}{\partial x} = \frac{x-\tilde{x}}{\rho_1}\frac{\partial \psi_\delta}{\partial \rho_1} + \frac{x-\tilde{x}}{\rho_2}\frac{\partial \psi_\delta}{\partial \rho_2},\ \frac{\partial \psi_\delta}{\partial r} = \frac{r-\tilde{r}}{\rho_1}\frac{\partial \psi_\delta}{\partial \rho_1} + \frac{r+\tilde{r}}{\rho_2}\frac{\partial \psi_\delta}{\partial \rho_2}, \tag{2.5}$$

which, after finding $F'(\lambda)$ and $E'(\lambda)$ in terms of $F(\lambda)$ and $E(\lambda)$, gives

$$\frac{\partial \psi_\delta}{\partial \rho_1} = \frac{1}{2\pi}\left(F(\lambda) - \frac{1}{2}\left(1+\frac{\rho_2}{\rho_1}\right)E(\lambda)\right),\ \frac{\partial \psi_\delta}{\partial \rho_2} = \frac{1}{2\pi}\left(F(\lambda) - \frac{1}{2}\left(1+\frac{\rho_1}{\rho_2}\right)E(\lambda)\right). \tag{2.6}$$

When $r \neq 0$, the induced velocity is computed directly using (2.4), while, for $r = 0$ the velocity is computed by evaluating the limit $r \to 0$ in (2.4)

$$u_\delta(x,0;\tilde{x},\tilde{r}) = \frac{1}{2}\frac{\tilde{r}^2}{((x-\tilde{x})^2 + \tilde{r}^2 + \delta^2)^{3/2}},\ v_\delta(x,0;\tilde{x},\tilde{r}) = 0. \tag{2.7}$$

In summary, the induced velocity is computed by integrating over the sheet

$$\begin{pmatrix} u^f \\ v^f \end{pmatrix}(x,r) = \int_0^{\Gamma_T} \begin{pmatrix} u_\delta \\ v_\delta \end{pmatrix}(x,r;x^f(\Gamma,t),r^f(\Gamma,t))d\Gamma. \tag{2.8}$$

Bound Vortex Sheet The piston and the tube are given again in cylindrical coordinates, parametrized by arc length s

$$(x^b(s), r^b(s)) = \begin{cases} (0, s), & 0 \leqslant s \leqslant R \\ (s - R, R), & R \leqslant s \leqslant R + L \end{cases}, \tag{2.9}$$

where L and R are the length and the radius of the cylinder respectively.

The velocity induced by the bound vortex sheet is given by

$$\begin{pmatrix} u^b \\ v^b \end{pmatrix}(x, r) = \int_0^{R+L} \begin{pmatrix} u_0 \\ v_0 \end{pmatrix}(x, r; x^b(s,t), r^b(s,t))\gamma(s,t)ds, \tag{2.10}$$

where $\gamma(s,t)$ is the bound-sheet strength. It can be seen that δ is set to zero on the bound-sheet but it is positive on the free-sheet. Krasny explains this by the necessity of resolving the roll-up in the free-sheet, while there is not such requirement on the bound sheet since its shape is fixed. Even more than that, we set $\delta = 0$ on the bound-sheet to prevent ill-conditioning in the equation for the bound-sheet strength, as it will be seen later on. For now, let's just note that the velocity induced by both the free and the bound sheet is given by

$$\begin{pmatrix} u \\ v \end{pmatrix}(x, r) = \begin{pmatrix} u^f \\ v^f \end{pmatrix}(x, r) + \begin{pmatrix} u^b \\ v^b \end{pmatrix}(x, r). \tag{2.11}$$

There is a difficulty occurring at the edge $(x, r) = (L, R)$, where the singular kernel on the bound sheet cannot be balanced by the regularized kernel on the free sheet. However, Krasny shows in his paper (see Krasny [1994]) that this can be overcome by application of the normal boundary condition on the tube wall. He also verifies the effect of the jump in δ upon the induced velocity in the article's appendix.

Discretization In the numerical implementation we have two different sets of filaments: free filaments - their number increases in time because at every time step another one is released in the free sheet, and bound filaments. The free filaments are denoted by

$(x_j^f(t), r_j^f(t))$, and they depend on the circulation parameters $\Gamma_j,\ j = 0, ..., N_f$. The bound vortices are denoted by $(x^b(s_j), r^b(s_j))$, and they are placed on the piston and tube walls according to

$$s_j = \begin{cases} \frac{jR}{N_1^b}, & j = 0, ..., N_1^b \\ R + L\sin\left(\frac{\pi}{2}\frac{j-N_1^b}{N^b-N_1^b}\right), & j = N_1^b, ..., N^b. \end{cases} \tag{2.12}$$

In other words, the bound filaments are uniformly spaced on the piston, but they cluster at the edges of the tube which provides better resolution at those edges. This is a frequently used technique in fluid dynamics.

To find the new position of the free filaments, Krasny applies the trapezoidal rule to integrals (2.8) and (2.10) and computes the total induced velocity (2.11). From that he finds

$$\frac{dx_j^f}{dt} = u(x_j^f, r_j^f), \quad \frac{dr_j^f}{dt} = r(x_j^f, r_j^f). \tag{2.13}$$

Of course the first goal would be to find the bound-sheet strength. This will be done by inverting a linear system that comes from writing down the boundary conditions

$$\begin{cases} v(x_j^m, r_j^m) = 0, & j = N_1^b, ..., N^b \\ u(x_j^m, r_j^m) - u(x_{j-1}^m, r_{j-1}^m) = 0, & j = 2, ..., N_1^b \\ u(\frac{1}{2}L, 0) = U_p(t). \end{cases} \tag{2.14}$$

The first condition is given by the fact that the tube walls are impenetrable, so radial velocity is zero, the third one matches the velocity of the piston in the center of the tube and the second one sets uniform tangential velocity along the piston. Given this, we obtain a linear system in N^b equations and N^b unknowns solved by Krasny using Gaussian elimination. Krasny shows how the need of taking $\delta = 0$ on the bound sheet appears from the fact that the solution of the linear system (2.14) oscillates and fails to converge under mesh refinement when $\delta > 0$.

Vortex shedding Now we will talk about the edge of the tube. The circulation shedding rate there is given in terms of the slip velocities at the edge, inside and outside the tube

u_-, u_+

$$\frac{d\Gamma_T}{dt} = \frac{1}{2}(u_-^2 - u_+^2). \tag{2.15}$$

These slip velocities satisfy

$$u_- - u_+ = \gamma_e, \qquad \frac{1}{2}(u_+ + u_-) = \bar{u}, \tag{2.16}$$

where γ_e is the sheet strength at the edge of the tube (computed when solving the linear system (2.14)) and $\bar{u}$ is the average slip velocity.

This is how the circulation shedding rate at the edge and the average slip velocity are obtained

i) set $\bar{u} = u(L, R)$ which is computed by applying the trapezoidal rule to the axial component of (2.11);

ii) obtain the sheet strength γ_e by solving the linear system (2.14);

iii) having $\gamma_e, \bar{u}$ compute u_+, u_- from (2.16). Since no attached flow is allowed, whenever u_+ or u_- is negative we set it to zero;

iv) having u_+, u_- compute $d\Gamma_t/dt$ and $\bar{u}$ from (2.15) and (2.16).

Time-stepping, numerical parameters and results Finally we are able to describe the algorithm for the numerical method. At each time step there are four stages to be treated:

i) solve the linear system (2.14) to get the bound-sheet strength values γ_e;

ii) evaluate the velocity of the free filaments $u(x_j^f, r_j^f), v(x_j^f, r_j^f)$ from (2.11);

iii) evaluate $d\Gamma_t/dt$ and $\bar{u}$ as described above using (2.15) and (2.16);

iv) update $(x_j^f, r_j^f), \Gamma_t, U_p(t)$ and prepare for the next time step.

A new filament is shed only in the first stage of a time-step. Krasny is also using a point insertion technique which means he inserts additional filaments in the free sheet whenever the distance between consecutive filaments is bigger than some ϵ or when the angular separation (with respect to the spiral center) is larger than $2\pi/N_{rev}$.

The simulation performed by Krasny is set up to match Didden's experiment (Figure 2.1). The tube radius is R=2.5, the tube length is L=10, and the speed is $U_0 = 1.6$. The

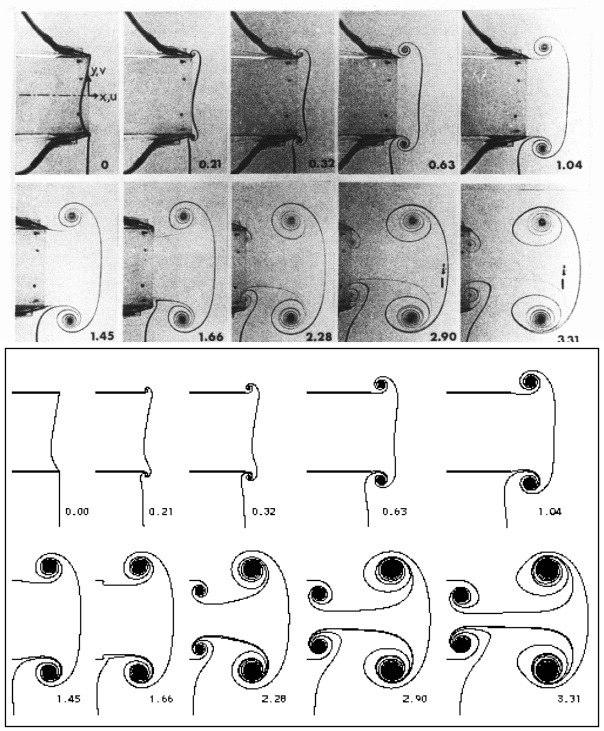

Figure 2.1: Tube with piston immersed in fluid - flow visualization of vortex ring formation - experiment by Didden (1979); simulation by Krasny using $\delta = 0.2$

piston stops moving at $t_{off} = 1.6$ when a counter-rotating vortex appears at the edge of the tube. It can be seen that, with a blob of $\delta = 0.2$, Krasny's experiments (Figure 2.1) reproduce very accurately Didden's plots. Simulations are also performed varying the blob radius and it turns out that as δ is reduced the spiral core is more tightly rolled up.

In Krasny and Nitsche's paper more plots can be found showing how accurate the simulation is compared with the experiment (see Figure 2.2).

2.1.2 Vortex Formation at the Edges of a Free Falling Two-Dimensional Plate

Another example through which Krasny wants to show how vortex blob computations approximate real fluid motion is the movement of flat plate normal to the flow. This generates a vortex sheet roll-up at the edges of the plate.

A vortex sheet is defined by a curve $z(\Gamma, t)$ in the complex plane depending on two

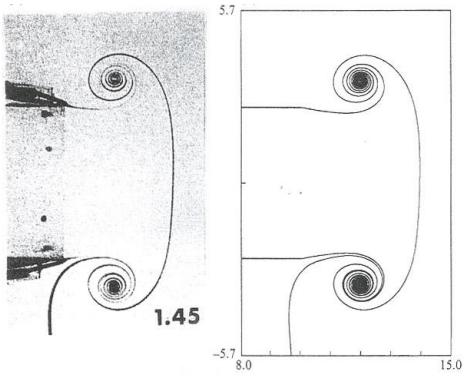

Figure 2.2: Comparison at t=1.45; experiment versus simulation with $\delta = 0.2$

parameters: circulation and time. The evolution equation is

$$\overline{\frac{\partial z}{\partial t}}(\Gamma, t) = \int K(z(\Gamma, t) - z(\tilde{\Gamma}, t))d\tilde{\Gamma}, \qquad K(z) = \frac{1}{2\pi\imath z}, \tag{2.17}$$

where the Cauchy principal value of the integral is taken. This is a special case of the Biot-Savart law, which expresses the velocity as an integral over the vorticity in incompressible flow. Again, Chorin's vortex blob method is applied, and the singular kernel in (2.17) is replaced by the smooth approximation K_δ which approaches our original kernel as δ approaches zero. For example, in free space this becomes

$$K_\delta(z) = K(z)\frac{|z|^2}{|z|^2 + \delta^2}. \tag{2.18}$$

Using this kernel in the evolution equation will give us a smoothed approximation to the vortex sheet. The curve is discretized into vortex blobs $z_j(t)$ as discussed in the previous section and the integral with the smoothed kernel can be approximated by a quadrature rule

$$\overline{\frac{\partial z_j}{\partial t}} = \sum_k K_\delta(z_j - z_k)\Gamma_k. \tag{2.19}$$

By integrating in time these equations we could get the motion of the vortex blobs.

Numerical method In Krasny's method the plate coincides with the interval $-1 \leqslant x \leqslant 1$ and it moves vertically with speed 1/2. Again, as before, the flow contains a bound vortex sheet composed by point vortices and a free vortex sheet composed by blob vortices. At every time step a new filament is released from both edges of the plate. The velocity induced at a vortex element (x_j, y_j) (either a vortex point or vortex blob) having circulation Γ_j is given by (according to equation 2.19)

$$(\frac{dx_j}{dt}, \frac{dy_j}{dt}) = \sum_{k \neq j} \frac{(-(y_j - y_k), (x_j - x_k))\Gamma_k}{2\pi((x_j - x_k)^2 + (y_j - y_k)^2 + \delta^2)}. \tag{2.20}$$

In this equation one should be careful on considering $\delta = 0$ whenever the index k refers to one of the bound point vortices. Along the bound sheet, since the plate is horizontal, i.e., y is constant, the bound vortex sheet strength $\gamma(x, t)$ satisfies a Cauchy singular integral equation of the first kind,

$$\frac{1}{2\pi} \int_{-1}^{1} \frac{\gamma(x, t) d\tilde{x}}{(x - \tilde{x})} = -v(x, t). \tag{2.21}$$

Krasny argues that the necessity of using vortex points on the bound sheet is due to the impossibility of solving the above equation for a general right side if the kernel is smoothed. To provide better resolution at the edges, the bound point vortices are not placed uniformly on the plate but they cluster towards the edges according to $x_j = \cos\theta_j, \theta_j = j\pi/n$ and equation (2.21) is satisfied at the midpoint of each interval. Another equation comes from the fact that the total circulation is conserved in accordance with Kelvin's theorem. Hence, equations (2.21) transform into a linear system which, solved by Gaussian elimination, will give us the strengths $\gamma(x_j, t)$.

Krasny uses the Kutta condition to determine the circulation of the free vortices

$$\frac{d\Gamma}{dt} = \frac{1}{2}(U_-^2 - U_+^2) = \overline{U} \cdot \gamma, \tag{2.22}$$

where $\gamma \sim \Delta\Gamma/\Delta x$ is calculated by a finite difference formula. Here, as we have seen before, U_- and U_+ are the one-sided velocities at the edge, $\overline{U}$ is the average velocity, and γ is the vortex sheet strength at the edge. The separating flow condition is used to prevent an attached slip flow from contributing to the shedding process (if either $U_+ < 0$ or $U_- < 0$

that value is set to zero). Krasny's method uses an adaptive point insertion technique and an adaptive time step.

Validation Krasny validates his results by comparing them with the ones obtained by Pullin in 1978. Pullin used point vortices to represent the vortex sheet, a single point vortex to represent the inner spiral turns, and conformal mappings to determine the strength of the bound vortex sheet. The pair of counter-rotating vortices forming in the recirculating region behind the plate agree very well between the two methods. Taking as an example $\delta = 0.025$ and $t = 1$ Krasny's results could be checked by superimposing the shape of the vortices over the one obtained by Pullin; they agree quite well.

2.1.3 Vortex Formation behind a Two-Dimensional Wing at Angle α

Krasny has not explained in his papers how exactly he would apply his vortex-blob theory to forward flying wings. Some plots appeared in his articles regarding the vortex sheet roll-up past a semi-infinite flat plate. To get one step closer to numerically implement Wu's method, we try to implement Krasny's method first for comparison with Wu's. The implementation is based on the theory from the two previous sections and some very useful ideas from Katz & Plotkin's "Low Speed Aerodynamics". Our implementation could be found in the next chapter along with results and some very interesting comparisons between the two models.

2.2 Wu's Analytical Method

Classical slender-body theory of fish locomotion As noted in the introduction, the slender-body theory was developed by Lighthill (1960, 1970), Wu (1971c,d), Wu and Newman (1972), Newman (1973), Newman and Wu (1973) and others, for understanding the fish locomotion. This theory is applicable to a very general class of body geometry and movement, from the propulsive motions in carangiform and thunniform to those in amiiform and gymnotiform. In all cases the body may be regarded as slender, characterized by a small slenderness parameter, δ, defined as the ratio of maximum body depth to body length,

$\delta = 2b/l$. The theory is based on the assumption that the amplitude of the undulatory wave motion passed along the body is small compared to body length, so that its higher nonlinear effects can be neglected. The Reynolds number, for the cases of practical interest is usually high, ranging over $10^4 - 10^7$. Wu and Newman showed in 1972 that the effect of body thickness in the direction of bodily displacement (in the z-direction) from the stretched-straight position (in the xy-plane) is secondary in effect and can be neglected. Later on, Newman (1973) and Newman and Wu (1973) showed this effect could be amended if desired by employing conformal mapping to map cross-sectional body contour into a slit so as to make use of the solution to zero-thickness case. With the effect of body thickness neglected, the transverse bodily motion can be prescribed (see Figure 2.3) to vary with time t as

$$z = h(x, y, t) \quad with \quad x, y \in S_b;\ 0 < x < l;\ |y| < b(x), \tag{2.23}$$

where the (x,y,z) coordinate system is fixed in the body frame, and the stream is considered having velocity U in the x direction which basically matches the fish steady swimming velocity in still water. S_b denotes the stretched-straight body plan-form lying in the xy-plane and 2b is the body depth. With the assumption that the fluid is incompressible ($\frac{d\rho}{dt} = \frac{\partial \rho}{\partial t} + u \cdot \nabla \rho = 0$) and the flow irrotational (vorticity=curl(u)=0), there exists a scalar potential $\phi_0(x, y, z, t)$ such that

$$\phi_0 = Ux + \phi(x, y, z, t), \tag{2.24}$$

where the velocity potential ϕ gives the perturbation velocity

$$\mathbf{u} = (u, v, w) = \nabla_0 \phi \quad (\nabla_0 = (\partial_x, \partial_y, \partial_z), \tag{2.25}$$

and satisfies Laplace's equation $\phi_{xx} + \phi_{yy} + \phi_{zz} = 0$.

Since we are studying the slender-body theory, the slenderness parameter δ and the body displacement function h are very small compared to the body length l. Therefore we can consider only the leading terms in the Laplace equation and reduce this to a two-dimensional

Laplace equation in y and z

$$\phi_{yy} + \phi_{zz} = 0. \tag{2.26}$$

Accordingly, the Bernoulli equation can be linearized too, to give

$$D\phi = \Phi \qquad (D \equiv \partial/\partial t + U\partial/\partial x), \tag{2.27}$$

$$\Phi = (p_\infty - p)/\rho, \tag{2.28}$$

where Φ is Prandtl's acceleration potential depending on pressure and density. From (2.26) and (2.27) it can be seen that Φ also satisfies the two-dimensional Laplace equation. Therefore we can work with the complex variables (see Wu 1971, 1983)

$$\zeta = y + \imath z, \quad f = \phi + \imath\psi, \quad F = \Phi + \imath\Psi, \quad \nu = v - \imath w = df/d\zeta. \tag{2.29}$$

The complex coordinate ζ, complex velocity potential f, complex acceleration potential F and complex velocity ν are analytic functions of one another and are related by

$$Df = F \qquad (D \equiv \partial/\partial t + U\partial/\partial x), \tag{2.30}$$

$$D\nu = dF/d\zeta. \tag{2.31}$$

The boundary conditions for this problem can be given both in terms of ϕ and Φ as follows:

I. Boundary conditions in terms of ϕ: II. Boundary conditions in terms of Φ

(i) $(\phi_z)_\pm = Dh \equiv W(y;x,t)$, (i) $(\Phi_z)_\pm = DW(y;x,t)$ $((x,y) \in S_b)$,

(ii) $D\phi_\pm = 0$, (ii) $\Phi_\pm = 0$, $((x,y) \in S_w)$,

(iii) $\phi_\pm = 0$, (iii) $\Phi_\pm = 0$, $((x,y) \in S_c)$,

(iv) $D\phi_\pm = 0$, (iv) $\Phi_\pm = 0$, $((x,y)$ *on T.E.*$)$,

$$f = O(\zeta^{-1}),\ F = O(\zeta^{-1}),\ \nu = O(\zeta^{-2}),\ (|\zeta| \to \infty).$$

Here, in conditions (i) we discuss the body plan-form $(S_b : |y| < b(x), 0 < x < l)$, in (ii) S_w describes the wake plan-form (see Figure 2.3) resulting from projecting the vortex

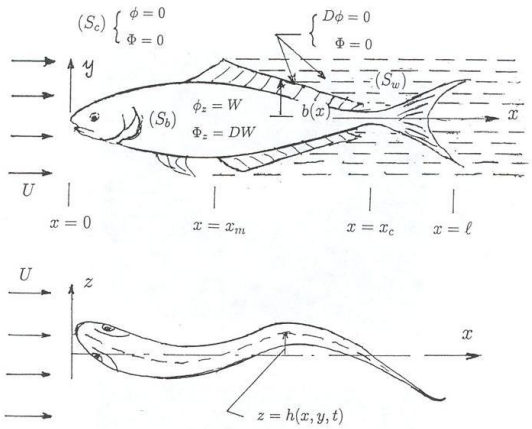

Figure 2.3: The various sections of flow regions for analyzing fish propulsion:(A) anterior leading edge section ($0 < x < x_m$);(B) trailing side-edge section ($x_m < x < x_c$); and (C) caudal fin section ($x_c < x < l$).

sheet shed from trailing edges of side fins onto the $z = 0$ plane ($S_w : b(x) < |y| < b_m = b(x_m), b'(x) < 0$) and in (iii) S_c denotes the region in the $z = 0$ plane complementary to $S_b + S_w$. In (iv) we describe the Kutta condition, namely that we have continuous pressure at the trailing edge (T.E.) of side fins and caudal fin. Finally, conditions (v) are required by the Kelvin's circulation theorem.

The nonlinear theory of two-dimensional flexible lifting-surface locomotion The theory of two-dimensional lifting-surface locomotion is very important, both because it provides a very good limiting case for asymptotic evaluation of lifting surfaces of large aspect-ratio found in many cases of aquatic and aerial animal locomotion, and because it provides a very good starting point for the development of a three-dimensional generalized theory.

Thus, we consider the irrotational flow of an incompressible and inviscid fluid generated by a thin (no thickness) two-dimensional surface S_b, having an arbitrary motion through the fluid, its flexibility being inspired by the movement of animals in nature. We are going to parametrize this motion by using a Lagrangian coordinate ξ to express a point

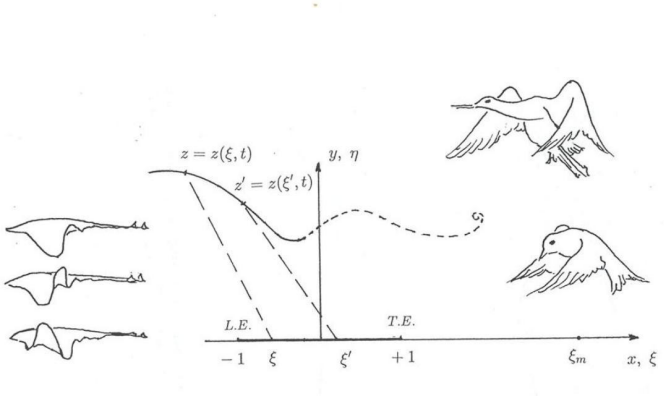

Figure 2.4: The Lagrangian coordinate system, (ξ, η), used to describe arbitrary motion of a two-dimensional flexible lifting surface moving along arbitrary trajectory through water in a reference frame (x, y) fixed with the fluid at infinity.

$X(\xi, t), Y(\xi, t)$ on S_b varying in time as

$$S_b(t): \ \mathbf{x} = \mathbf{X}(\xi, t) = (X(\xi, t), Y(\xi, t)) \quad (-1 < \xi < 1, t \geqslant 0). \tag{2.32}$$

The simplest choice of ξ is the initial material position of $S_b(t = 0)$ which is taken to be in its stretched-straight shape so that $X(\xi, 0) = \xi, Y(\xi, 0) = 0$ $(-1 < \xi < 1)$, lying in an unbounded fluid initially at rest in an inertial frame of reference (see Figure 2.4). The body surface $S_b(t)$ might be flexible but it is considered inextensible, so that

$$X_\xi^2 + Y_\xi^2 = 1. \tag{2.33}$$

Of course, the tangential $\mathbf{s}$ and normal $\mathbf{n}$ vectors are given by

$$s(\xi, t) = \partial\mathbf{X}/\partial\xi = (X_\xi, Y_\xi), \quad \mathbf{n}(\xi, t) = (-Y_\xi, X_\xi). \tag{2.34}$$

The velocity of a point ξ on $S_b(t)$ is given by

$$\mathbf{U}(\xi, t) = \partial\mathbf{x}/\partial t = (X_t, Y_t) \quad (-1 < \xi < 1, t \geqslant 0), \tag{2.35}$$

and its tangential and normal components are found by projecting the velocity onto the corresponding vectors

$$U_s(\xi,t) = \mathbf{U}\cdot\mathbf{s} = (X_\xi X_t + Y_\xi Y_t), \quad U_n(\xi,t) = \mathbf{U}\cdot\mathbf{n} = (X_\xi Y_t - Y_\xi X_t). \tag{2.36}$$

As we have seen before, the flow field is expressed in Eulerian coordinates, so the velocity of the incompressible and irrotational flow has a velocity potential $\psi(x,y,t)$ and a stream function $\phi(x,y,t)$. As seen from (2.30) and (2.31) the complex coordinate z, complex potential f and complex velocity w are given by

$$z = x + \imath y, \quad f = \psi + \imath\phi, \quad w = u - \imath v = df/dz \tag{2.37}$$

and they are analytic functions of one another.

Now we'll try to express all the boundary conditions in terms of these variables and to do that we will adopt a set of coordinates (ξ,η), with the η-axis pointing in the direction of the normal vector $\mathbf{n}$, where $\eta = 0$ coincides with $S_b(t)$ for $(-1 < \xi < 1, t \geqslant 0)$. After the motion starts, a free vortex sheet is shed from the trailing edge (T.E. at $\xi = 1$) to form a wake surface $S_w(t)$ described by the extended material coordinate ξ for $\xi > 1$

$$S_w(t):\ \mathbf{x} = \mathbf{X}(\xi,t) = (X(\xi,t), Y(\xi,t)) \quad (1 < \xi < \xi_m, t \geqslant 0), \tag{2.38}$$

where ξ_m identifies the trajectory $(X(\xi_m,t), Y(\xi_m,t))$ of the very first vortex filament released into the wake (i.e. the furthest wake point with respect to the trailing edge). Hence, at every time step a new stretch is being created in the wake just beyond the trailing edge $\delta\mathbf{X}(1,t) = \mathbf{U}(1,t)\delta t$, tangentially to the trajectory of the trailing edge.

Using analytic continuation, we can think of (ξ,η) as forming a complex reference plane $\zeta = \xi + \imath\eta$ so that the two planes, ζ and $z = x + \imath y$ are related by a conformal transformation which will be denoted by $z = z(\zeta,t)$. There is no need to determine the actual conformal mapping $z = z(\zeta,t)$ since we only have to use its analytic relationship in a small neighborhood of $S_b(t) + S_w(t)$.

Now it is time to introduce a transformation between the Eulerian coordinates (x,y,t)

and the Lagrangian material ones (ξ, η, t')

$$x = \tilde{x}(\xi, \eta, t'), \quad y = \tilde{y}(\xi, \eta, t'), \quad t = t', \quad F(x(\xi, \eta, t'), y(\xi, \eta, t'), t) = \tilde{F}(\xi, \eta, t'), \tag{2.39}$$

where F denotes any differentiable function. By the chain rule, for this kind of general function we get

$$\frac{\partial \tilde{F}}{\partial t'} = \left.\frac{\partial \tilde{F}}{\partial t'}\right|_{\xi,\eta} = \frac{\partial F}{\partial t} + u\frac{\partial F}{\partial x} + v\frac{\partial F}{\partial y} \equiv \frac{dF}{dt}, \tag{2.40}$$

which is material time differentiation in a frame of reference that follows the fluid particle (ξ, η) at a time instant $t' = t$. Using these relations we will derive some useful properties for the quantities of interest. To start with a general flow variable, we will denote its value on the $\pm$ side of S_b or S_w by

$$\tilde{F}(\xi, \eta = \pm 0, t') = \tilde{F}_{\pm}(\xi, t') \quad (-1 < \xi < \xi_m, t \geqslant 0). \tag{2.41}$$

The variables with subindices $\pm$ are called surface variables and they are computed for the upper and lower boundaries of the surface. Their derivatives are given by (2.40),

$$\frac{\partial \tilde{F}_{\pm}}{\partial t'} = \left(\frac{dF}{dt}\right)_{\pm} = \left(\frac{\partial F}{\partial t}\right)_{\pm} + \mathbf{u}_{\pm} \cdot (\nabla F)_{\pm}, \quad (\mathbf{u}_{\pm} = (u_{\pm}, v_{\pm}),\ \nabla = (\partial_x, \partial_y)), \tag{2.42}$$

and

$$\frac{\partial \tilde{F}_{\pm}}{\partial \xi} = \mathbf{s} \cdot (\nabla F)_{\pm}, \quad \left(\frac{\partial \tilde{F}}{\partial \eta}\right)_{\pm} = \mathbf{n} \cdot (\nabla F)_{\pm}, \tag{2.43}$$

where the operator $\partial_{t'}$ means the material rate of change, the operator ∂_ξ gives the surface gradient and ∂_ξ the normal gradient.

To compute the velocities of the particles along both sides of $S_b \cup S_w$ at $\mathbf{X}(\xi, t)$ we have

$$\mathbf{u}_{\pm}(\xi, t') = \partial \mathbf{x}_{\pm}(\xi, t')/\partial t', \quad (-1 < \xi < \xi_m, t' > 0), \tag{2.44}$$

which in complex form becomes

$$\frac{\partial z_{\pm}}{\partial t'}(\xi, t') = \overline{w}_{\pm}(\xi, t'), \tag{2.45}$$

where the over-line means complex conjugate. Decomposing the velocity into tangential and normal components, we get

$$u_s^{\pm} - \imath u_n^{\pm} = (u_{\pm} - \imath v_{\pm})(\mathbf{X}_\xi + \imath \mathbf{Y}_\xi) = w_{\pm}(\xi, t') \frac{\partial \mathbf{Z}(\xi, t')}{\partial \xi}, \tag{2.46}$$

where $\mathbf{Z} = \mathbf{X} + \imath \mathbf{Y}$.

The kinematic condition, which will also be our boundary condition in the numerical implementation, requires that any fluid particle that is at some point in time on the boundary surface will remain moving along it at all times. This can be written as

$$on\ S_b(t) \cup S_w(t): \quad u_n^+(\xi, t') = u_n^-(\xi, t') = U_n(\xi, t') \quad (-1 < \xi < \xi_m, t > 0). \tag{2.47}$$

This means of course that there is no flow through the surface. Tangential to the surface the condition should be different since the tangential velocity at the boundary surface develops a jump in magnitude across the surface. Hence, $S_b(t)$ becomes a bound vortex sheet while $S_w(t)$ is a free vortex sheet which is convected away with the fluid. The above relations say that $U_n(\xi, t')$ is prescribed on $S_b(t)$ but is unknown on $S_w(t)$, this having to be calculated by imposing a dynamic condition on $S_w(t)$, namely that the pressure has to be continuous on $S_w(t)$

$$p_+(\xi, t') = p_-(\xi, t') \qquad (1 \leqslant \xi < \xi_m, t > 0), \tag{2.48}$$

which means there is no pressure jump across the free sheet, including the trailing edge at $\xi = 1$ which is the Kutta condition. The pressure is given by the Bernoulli equation

$$\frac{p}{\rho} + \frac{\partial \phi}{\partial t} + \frac{1}{2}(u_s^2 + u_n^2) = \frac{p}{\rho} + \frac{\partial \phi}{\partial t'} - \frac{1}{2}(u_s^2 + u_n^2) = 0, \tag{2.49}$$

where the latter one follows from using (2.40). Furthermore, using condition (2.47) we get

$$\frac{1}{\rho}(p_- - p_+) = \left(\frac{\partial \phi}{\partial t}\right)_+ - \left(\frac{\partial \phi}{\partial t}\right)_- + \frac{1}{2}(u_s^+ + u_s^-)(u_s^+ - u_s^-) \quad (z \in S_b \cup S_w) \tag{2.50}$$

$$= \frac{\partial}{\partial t'}(\phi_+ - \phi_-) - \frac{1}{2}(u_s^+ + u_s^-)(u_s^+ - u_s^-) \quad (z \in S_b \cup S_w). \tag{2.51}$$

To find a unique solution to our problem, we follow the approach from (2.17) and write the integral representation of a surface distribution of a mass dipole of strength μ over the boundary surface, which gives the complex potential $f = \phi + \imath\psi$ in the form

$$f(z,t) = \frac{1}{2\pi\imath}\int_{S_b\cup S_w}\frac{\mu(\xi',t)}{z'-z}dz' \qquad (z' = z(\xi',t'), z \notin S_b \cup S_w). \tag{2.52}$$

Applying Plemelj's formula (see Muskhelishvili [1946], §17, eq. (17.2)) for a point z approaching a point on the sheet $Z(\xi,t)$ from the $\eta = \pm 0$ side, we get

$$f_\pm(z,t) = \pm\frac{1}{2}\mu(\xi,t) + \frac{1}{2\pi\imath}\int_{S_b\cup S_w}\frac{\mu(\xi',t)}{z'-z}dz' \qquad (z = Z(\xi,t) \in S_b \cup S_w), \tag{2.53}$$

computed taken the Cauchy's principal value of the integral. Having the dipole strength μ related to the jump discontinuity in ϕ

$$\mu(\xi,t) = \phi_+(\xi,t) - \phi_-(\xi,t) \tag{2.54}$$

and the relation between vorticity γ along the ξ-axis and the jump in tangential velocity across the boundary of the vortex sheet

$$\gamma(\xi,t) = \frac{\partial\mu}{\partial\xi}(\xi,t) = \frac{\partial}{\partial\xi}(\phi_+ - \phi_-) = u_s^+ - u_s^-, \tag{2.55}$$

we are able to compute the complex velocity $w(z,t) = df/dz$

$$\begin{aligned} w(z) &= \frac{1}{2\pi\imath}\int_{S_b\cup S_w}\mu(\xi',t)\left[-\frac{d}{dz'}\frac{1}{z'-z}\right]dz' = \frac{1}{2\pi\imath}\int_{S_b\cup S_w}\mu(\xi',t)\left[-\frac{\partial}{\partial\xi'}\frac{1}{z'-z}\right]d\xi' \\ &= \frac{1}{2\pi\imath}\int_{S_b\cup S_w}\frac{\gamma(\xi',t)}{z'-z}d\xi' \quad (\gamma = \partial\mu/\partial\xi,\ z \notin S_b \cup S_w). \end{aligned}$$

Here, to get the second integral we changed the variable and then to get the third one we integrated by parts and used (2.47). Further more, by applying Plemelj's formula again we get

$$w_\pm(z,t) = \pm\frac{1}{2}\gamma(\xi,t)/\frac{dz}{d\xi} + \frac{1}{2\pi\imath}\int_{S_b\cup S_w}\frac{\gamma(\xi',t)}{z'-z}d\xi' \quad (z = Z(\xi,t) \in S_b \cup S_w). \tag{2.56}$$

Now combining this last relation (2.56) and (2.46), it follows

$$u_{s\pm} - \imath u_n = \pm\frac{1}{2}\gamma(\xi,t) + \frac{1}{2\pi\imath}\frac{dz}{d\xi}\int_{S_b\cup S_w}\frac{\gamma(\xi',t)}{z'-z}d\xi'. \tag{2.57}$$

Of course, this result validates (2.47) and gives

$$u_n^+(\xi,t) = u_n^-(\xi,t) = \frac{1}{2\pi}\Re\left\{\frac{dz}{d\xi}\int_{S_b+S_w}\frac{\gamma(\xi',t)}{z'-z}d\xi'\right\}, \tag{2.58}$$

$$u_{sm} \equiv \frac{1}{2}(u_s^+ + u_s^-) = \frac{1}{2\pi}\Im\left\{\frac{dz}{d\xi}\int_{S_b+S_w}\frac{\gamma(\xi',t)}{z'-z}d\xi'\right\}. \tag{2.59}$$

These equations will play a very important role in the implementation of the numerical method. The first one shows the continuity of the normal velocity across the vortex sheet, while the second one gives an average of the tangential component of the velocity across the boundary $S_b \cup S_w$. These relations again give an interpretation of the boundary conditions

on S_b: $u_n(\xi,t)$ is prescribed and $\gamma(\xi,t)$ is unknown;

on S_w: $\gamma(\xi,t)$ is material invariant and $u_n(\xi,t)$ and $u_{sm}(\xi,t)$ are unknown.

Here, we should discuss this material invariance of the vorticity in more detail. It refers to Helmholtz's theorem, which states that in an irrotational flow of an incompressible inviscid fluid, free vorticity cannot be generated in any interior bulk of the fluid but only at a boundary surface. Once it gets generated it will be conserved in time. Hence, imposing this vorticity conservation with the local fluid, we get

$$\frac{\partial\gamma_w}{\partial t} + u_{sm}\frac{\partial\gamma_w}{\partial\xi} = 0, \tag{2.60}$$

which can be used as the Kutta condition like (2.48). This will help compute the trajectory of the free vortex sheet by a time-marching procedure.

There is one more thing we have to take care of since there will be another equation needed in the numerical method. This comes from the total net vorticity, where, using Kelvin's theorem, we know that the total circulation is conserved in time. The circulation

$\Gamma(t)$ is given by

$$\Gamma(\xi,t)=\oint \mathbf{u}\cdot d\mathbf{x}=\oint_{P_-}^{P_+} d\phi=\phi_+(\xi,t)-\phi_-(\xi,t)=\mu(\xi,t)\quad(-1<\xi<\xi_m,\ t>0),\ (2.61)$$

where points P_- and P_+ are chosen directly across the vortex sheet at location ξ, so that the line connecting them, along which we integrate, does not intersect the vortex sheet boundary. Circulation can also be given in terms of the vorticity distribution

$$\Gamma(\xi,t)=\oint \mathbf{u}\cdot d\mathbf{x}=\int_0^{\xi}\gamma(\xi,t)d\xi\quad(-1<\xi<\xi_m,\ t>0).\tag{2.62}$$

Kelvin's theorem states that the total circulation is conserved, hence, around any closed contour Σ that completely encircles the entire vortex sheet, the circulation remains the same in time

$$\Gamma_\Sigma(t)=\int_0^{\xi_m}\gamma(\xi,t)d\xi=\Gamma(0).\tag{2.63}$$

If the flow starts from rest, the initial value of the total circulation is zero. One more thing of particular interest would be to split the integral in (2.63) in two parts to find a relation between the circulation of the bound vortex sheet and the one for the free vortex sheet

$$\Gamma_b(t)=\oint \mathbf{u}\cdot d\mathbf{x}=\int_0^{1}\gamma(\xi,t)d\xi=-\int_1^{\xi_m}\gamma(\xi,t)d\xi=-\Gamma_w(t).\tag{2.64}$$

We did this because, eventually, we are interested in the circulation of the newly released vortex filament. To be able to compute this circulation we consider the variation $\delta\Gamma_b=\Gamma_b(t+\delta t)-\Gamma_b(t)$ on the bound sheet for a very small time interval δt. According to Kelvin's theorem the variation of circulation on the bound sheet for this small period of time is equal with opposite sign to the circulation of the newly released vortex filament during this span of time. In other words

$$\delta\Gamma_b(t)=-\delta\Gamma_w(t)=-\gamma(1,t)\delta\xi=-\gamma(1,t)[U_s(1,t)+u_{sm}(1,t)]\delta t,\tag{2.65}$$

where $U_s(1,t)$ is the (given) tangential velocity of the trailing edge. The circulation of the

previously shed free sheet does not appear in this relation, since it remains conserved in time.

The theory presented above is sufficient to produce a time-marching numerical procedure described by Wu, (Wu [2001]). However, Wu takes the theory even further and after some more theoretical results, he proposes a new numerical method based on the time-marching procedure and on the extended theory. Here we will first present the theoretical results from this paper and then describe the complete numerical recipe.

Generalized Wagner-von Karman-Sears method As it was said in the introduction, quite a few brilliant mathematicians worked on the development of linear unsteady airfoil theory. The ones who made the biggest contribution are Theodore von Karman and William R. Sears. Their theory is based on a result found by Herbert Wagner (1925) who came up with an integral equation to calculate the wake vorticity shed from a wing. Von Karman and Sears improved Wagner's theory and developed a very ingenious decomposition of the bound vorticity distribution γ_b into two parts, one for the "quasi-stationary, wake-less" flow, γ_0, and the other, γ_1 due to the effect of the trailing vortex sheet on the wing. The uniqueness and importance of this method reside in the fact that it does afford a direct generalization to the fully nonlinear theory. Theodore Wu (2001) improved this idea even further, generalizing it to two-dimensional flexible lifting surface performing arbitrary motion for modeling aquatic and aerial animal locomotion.

Following the ideas of von Karman and Sears, we split the bound vorticity in two parts as follows

$$\text{on } S_b(t): \qquad \gamma(\xi,t) = \gamma_0(\xi,t) + \gamma_1(\xi,t) \qquad (-1 < \xi < 1),$$

$$\text{on } S_w(t): \qquad \gamma(\xi,t) = \gamma_w(\xi,t) \qquad (1 < \xi < \xi_m),$$

where $\gamma_0(\xi,t)$ is the "quasi-stationary, wake-less" vorticity mentioned above, and $\gamma_1(\xi,t)$ is the additional bound vorticity due the effect of the trailing wake vortices $\gamma_w(\xi,t)$. To determine these vortex distributions we will follow the next three steps:

1. determine $\gamma_0(\xi,t)$ using the prescribed $U_n(\xi,t)$ with t fixed and no unsteady wake;

2. determine $\gamma_1(\xi,t)$ due to the effect of the wake so that we reinstate the unsteady

$U_n(\xi, t)$;

3. determine $\gamma_w = \gamma_w(\xi, t)$ by using the Kutta condition.

We should emphasize that this approach will take into account the nonlinear effects given by the actual displacement of the vortex sheet, which makes this theory significantly different than the linear one.

Following the three steps given above, we start interpreting the mathematical equations from this point of view. In the first step, we will omit the wake effect and regard time as a fixed parameter. This will transform equation (2.58) into

$$U_n(\xi, t) = \frac{1}{2\pi} \Re \left\{ \frac{dz}{d\xi} \int_{-1}^{1} \frac{\gamma_0(\xi', t)}{z' - z} d\xi' \right\} for(-1 < \xi < 1), \tag{2.66}$$

which basically is an integral equation that will give us $\gamma_0(\xi, t)$ under the Kutta condition. To be able to get that, we rewrite (2.66) to single out the Cauchy kernel

$$\begin{aligned} U_n(\xi, t) &= \frac{1}{2\pi} \int_{-1}^{1} \left[\frac{1}{\xi' - \xi} + g(\xi', \xi) \right] \gamma_0(\xi', t) d\xi' \equiv (G_0 + G_1)\gamma_0, \\ g(\xi', \xi) &= \Re \left\{ \frac{dz}{d\xi} \frac{1}{z' - z} \right\} - \frac{1}{\xi' - \xi}, \end{aligned} \tag{2.67}$$

where $(\xi' - \xi)^{-1}$ is the Cauchy kernel while $g(\xi', \xi)$ is a smooth kernel. For slightly curved body movement, $|g(\xi', \xi)|$ is small which give us the idea to solve (2.67) by iteration or by perturbation analysis, writing $\gamma_0(\xi, t)$ as a series expansion in terms of the small bound of $|g(\xi', \xi)|$. Note that in the case of a flat-plate airfoil both z and z' will be on the wing, making $dz/d\xi$ a constant, and therefore making $g(\xi', \xi)$ zero, which is the linear case as expected.

With this said, let's write the expansion for $\gamma_0(\xi, t)$

$$\gamma_0 = \gamma_{00} + \gamma_{01} + \gamma_{02} + ... \tag{2.68}$$

Substituting (2.68) in (2.67) we get after we match terms of the same magnitude

$$G_0\gamma_{00} = \frac{1}{2\pi}\int_{-1}^{1}\frac{1}{\xi'-\xi}\gamma_{00}(\xi',t)d\xi' = U_n(\xi,t), \tag{2.69}$$

$$G_0\gamma_{0k} = -\frac{1}{2\pi}\int_{-1}^{1} g(\xi',\xi)\gamma_{0,k-1}(\xi',t)d\xi' \equiv -G_1\gamma_{0,k-1}. \tag{2.70}$$

The leading order equation can be solved in a closed form under the Kutta condition, giving

$$\gamma_{00}(\xi,t) = -\frac{2}{\pi}\sqrt{\frac{1-\xi}{1+\xi}}\int_{-1}^{1}\sqrt{\frac{1+\xi'}{1-\xi'}}\frac{U_n(\xi',t)}{\xi'-\xi}d\xi' \equiv G_0^{-1}U_n \quad (-1<\xi<1). \tag{2.71}$$

This can be easily verified by substituting (2.71) in (2.69) and using the Poincaré-Bertrand formula (see Muskhelishvili [1946], §23, eq. (23.7))

$$\int_L \frac{d\xi'}{\xi'-\xi}\int_L \frac{h(\xi',\xi'')}{\xi''-\xi'}d\xi'' = -\pi^2 h(\xi,\xi) + \int_L d\xi''\int_L \frac{h(\xi',\xi'')}{(\xi'-\xi)(\xi''-\xi')}d\xi'. \tag{2.72}$$

Putting everything together, we find all terms in the decomposition of $\gamma_0(\xi,t)$

$$\gamma_0(\xi,t) = G_0^{-1}(U_n+N_0), \qquad N_0 = \sum_{m=1}^{N}(-1)^m(G_1G_0^{-1})^m U_n \equiv G_N U_n. \tag{2.73}$$

This way, given U_n (the body motion) by (2.36) we have found the vorticity γ_0 which will also give us the corresponding circulation

$$\Gamma_0(t) = \int_{-1}^{1}\gamma_0(\xi,t)d\xi = -2\int_{-1}^{1}\sqrt{\frac{1+\xi}{1-\xi}}[U_n(\xi,t)+N_0(\xi,t)]d\xi. \tag{2.74}$$

This ends step 1. We are going to move on to analyze step 2. Before doing that some more explanations need to be given. In step 2 we are supposed to find γ_1 due to the effect of the wake. We will find it in terms of the wake vorticity though, γ_w and then at the end, having γ_1 determined and both γ_1 and γ_w written in terms of γ_w, we will write Kelvin's circulation theorem and determine γ_w from there. Having γ_w determined, we will be able to find γ_1 as well from the relation we determine in step 2.

First, from (2.58) we have the expression for the normal velocity $U_{n1}(\xi,t)$ induced at

$z(\xi,t)$ on S_b by the free vortex sheet γ_w given by

$$U_{n1}(\xi,t)=\frac{1}{2\pi}\Re\left\{\frac{dz}{d\xi}\int_1^{\xi_m}\frac{\gamma_w(\xi',t)}{z'-z}d\xi'\right\}\equiv(K_0+K_1)\gamma_w\equiv K\gamma_w,\quad(-1<\xi<1)\tag{2.75}$$

$$K_0\gamma_w=\frac{1}{2\pi}\int_1^{\xi_m}\frac{\gamma_w(\xi',t)}{\xi'-\xi}d\xi',\qquad K_1\gamma_w=\frac{1}{2\pi}\int_1^{\xi_m}g(\xi',\xi)\gamma_w(\xi',t)d\xi',\tag{2.76}$$

where $g(\xi',\xi)$ is the same as the one defined in step 1 except that in this case the ranges for ξ' and ξ are: $1<\xi'<\xi_m$ and $-1<\xi<1$. If we denote by U_{n1} the normal velocity induced by the wake vortex γ_w on the wing S_b, then γ_1, the corresponding induced vorticity will satisfy (2.66) but with U_n replaced by $-U_{n1}$. Then exactly as in (2.73) we get for γ_1

$$\gamma_1(\xi,t)=-G_0^{-1}[U_{n1}+N_1],\qquad N_1=\sum_{m=1}^{N}(-1)^m(G_1G_0^{-1})^mU_{n1}=G_NU_{n1}\quad(N\leqslant\infty).\tag{2.77}$$

If we substitute (2.75) in (2.77) and do some algebra we get

$$\gamma_1(\xi,t)=\gamma_{10}(\xi,t)+\gamma_{1N}(\xi,t),\qquad\gamma_{10}=-G_0^{-1}K_0\gamma_w,\qquad\gamma_{1N}=-G_0^{-1}G_NU_{n1},\tag{2.78}$$

$$\gamma_{10}=\frac{1}{\pi}\sqrt{\frac{1-\xi}{1+\xi}}\int_1^{\xi_m}\sqrt{\frac{\xi'+1}{\xi'-1}}\frac{\gamma_w(\xi',t)}{\xi'-\xi}d\xi'\quad(-1<\xi<1),\tag{2.79}$$

$$\gamma_{1N}=\frac{1}{\pi^2}\sqrt{\frac{1-\xi}{1+\xi}}\int_1^{\xi_m}\gamma_w(\xi',t)d\xi'\int_{-1}^{1}\sqrt{\frac{1+\xi''}{1-\xi''}}\frac{g(\xi',\xi'')+G_NK(\xi',\xi'')}{\xi''-\xi}d\xi'',\tag{2.80}$$

where γ_{10} was gotten by integration with the order of integrations interchanged.

This vorticity γ_1 will be responsible for the generation of more circulation Γ_1 around the wing

$$\Gamma_1(t)=\int_{-1}^{1}\gamma_1(\xi,t)d\xi=\Gamma_{10}(t)+\Gamma_{1N}(t),\tag{2.81}$$

$$\Gamma_{10}=\int_{-1}^{1}\gamma_{10}(\xi,t)d\xi=\int_1^{\xi_m}\left(\sqrt{\frac{\xi+1}{\xi-1}}-1\right)\gamma_w(\xi,t)d\xi,\tag{2.82}$$

$$\Gamma_{1N}=\frac{1}{\pi}\int_1^{\xi_m}\gamma_w(\xi,t)d\xi\int_{-1}^{1}\sqrt{\frac{1+\xi'}{1-\xi'}}[g(\xi,\xi')+G_NK(\xi,\xi')]d\xi'.\tag{2.83}$$

Now, the total circulation around the wing S_b is of course $\Gamma_b = \Gamma_0 + \Gamma_1$ while the total circulation around the free vortex sheet Γ_w is given by

$$\Gamma_w(t) = \int_1^{\xi_m} \gamma_w(\xi, t) d\xi. \tag{2.84}$$

As we said before, now it is time to apply Kelvin's theorem which states that the total circulation around both the bound and the free vortex sheet is conserved

$$\Gamma_b + \Gamma_w = \Gamma_0 + \Gamma_1 + \Gamma_w = 0, \tag{2.85}$$

which gives

$$\Gamma_0 + \int_1^{\xi_m} \sqrt{\frac{\xi+1}{\xi-1}} \gamma_w(\xi, t) d\xi + \Gamma_{1N} = 0, \tag{2.86}$$

or the generalized nonlinear Wagner's integral equation for the trailing vortex distribution γ_w. In this last equation, Γ_{1N} and N_0 from (2.74) refer to nonlinear effects. If we disregard these two terms the original Wagner's linear equation is obtained.

The numerical algorithm To discretize all the equations above to be used in our numerical method, we choose a time sequence $t_0 = 0, t_1, t_2, ...,\ (t_{k+1} - t_k = \Delta t_k, k = 0, 1, 2, ...)$, with sufficiently small Δt_k. At time t_0 the body is found in the stretched-straight position in the unbounded flow which is at rest. After Δt_1, i.e. at time t_1, the bound sheet moves at a new position according to (2.32). In the mean time a free filament is released in the wake S_w or in other words, a first onset grid is opened behind the trailing edge at a distance $\delta\xi$ (see 2.65) to receive the shed vortex element. The unknown vorticity $\gamma(\xi, t)$ on the wing is determined from the two components $\gamma_0(\xi, t)$ and $\gamma_1(\xi, t)$. $\gamma_0(\xi, t)$ will be determined from (2.73). For determining $\gamma_1(\xi, t)$ we first have to solve for $\gamma_w(\xi, t)$ from (2.86) and then use (2.78), (2.79) and (2.80). This way the total vorticity on the wing is determined $(\gamma_0(\xi, t) + \gamma_1(\xi, t))$ and also the vorticity of the newly released wake element $\gamma_w(\xi, t_1)$. Hence, we know the vorticity along the whole sheet $(1 < \xi < 1 + \Delta\xi_1)$ and we could determine $u_s^{\pm}$ from (2.57) and u_n on $\Delta\xi_1$ of $S_w(t_1)$ from (2.58). This way we can revise the data on $S_w(t_1)$ by iteration for any improvement on the length and direction of

$\Delta\xi_1$.

At t_2, we move the wing again according to (2.32) to the new position $\mathbf{X}(\xi, t_2)$. The vortex released at the previous time step will be convected with the flow velocity and its circulation will be preserved in time, thus it will be known. The movement of the wing will open again a new onset grid in the wake, allowing a new free vortex element in the wake at a distance $\Delta\xi_2$. We can again go through all the calculations performed at the previous time step, i.e., compute the vorticity of the whole vortex sheet, compute the normal and tangential velocities and eventually updating the data on S_w. This way we have just constructed an algorithm that will take us from any known time step t_k to the next one t_{k+1}. As one could see, an incredibly important role is played by the determination of the vorticity of the currently shed free vortex element. The in-depth numerical procedure for discretizing the equations given above will be presented in the next chapter.

Chapter 3

Numerical Implementation of the Mathematical Model

3.1 Numerical Implementation of Krasny's Methods

3.1.1 Vortex Forming at the Edge of a Circular Tube with Results; Comparison With Krasny's Results and With Didden's 1979 Experiment

To implement this method we follow Krasny's results (Krasny [1994]) which were described in Section (2.1.1). Our numerical implementation uses $N_1^b = 8$ bound filaments on the radius of the piston (i.e. half the piston since we have axial symmetry). On each tube wall we have $N^b - N_1^b = 50$ filaments. The piston has diameter 5 (so radius $R = 2.5$) and the tube length is $L = 10$. The bound vortices are equally spaced on the piston but they use some sine-distribution on the tube wall so that we have more filaments at the edge of the tube (see (2.12)).

To closely follow Krasny's implementation we choose a variable time step: until $t = 0.5$ the time step linearly increases from an initial $\Delta t_0 = 0.004$ to a final reading of $\Delta t_1 = 0.02$. The piston keeps moving until time $t_{off} = 1.6$ when it stops abruptly and a counter rotating vortex begins forming. The time step is constant except for an interval of length 0.2 around the stopping time. Here, the time step decreases linearly down to $\Delta t_0/10 = 0.0004$ and then symmetrically increases back to $\Delta t_1 = 0.02$. We need this mesh refinement to better capture the ending of the initial vortex formation and the beginning of the counter-rotating one. Also to mimic the real experiment, the piston accelerates from zero velocity to a

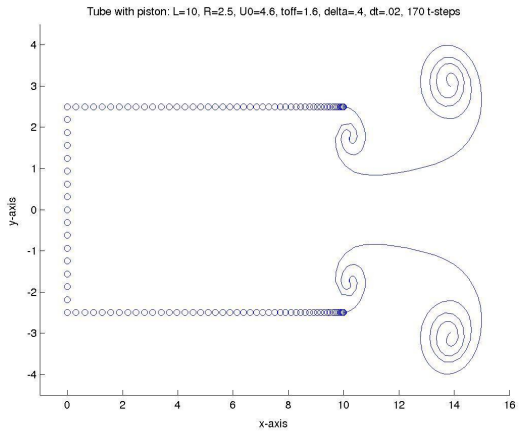

Figure 3.1: Krasny's method for piston pushing the fluid out from a tube, with adaptive speed $U_0 \approx 4.6$, blob $\delta = 0.4$, variable time-step $dt \approx 0.02$, tube length $L = 10$, tube radius $R = 2.5$, time when piston stops $t_{off} = 1.6$. Plot after 170 time steps.

constant velocity $U_0 = 4.6$ in time $t_u = 0.3$. To get the plot in Figure (3.1), we use a blob $\delta = 0.4$ and 170 time-steps. We use here only the point insertion technique with respect to distance (see Section (2.1.1)), and for that we choose $\epsilon = 0.4$.

First, we compose our linear system having the sheet-strength values $\gamma(s_j, t)$ as the N_b-unknowns. The strengths are computed at the bound points while the boundary conditions (2.14) are satisfied at midpoints. The first condition, giving zero radial velocity on the tube wall, will provide $N_b - N_b^1$ equations from a discretization of (2.10) and (2.8). To compute the velocities, we use (2.4), and to compute the complete elliptic integrals of the first and second kind from (2.3), we use an idea from (Bulirsch [1965]) which gives us a very accurate result with ten digits of accuracy.

The second condition, which states that the tangential velocity is the same inside the tube, will give us $N_b^1 - 1$ equations, again by computing the corresponding induced velocities as explained above. The third condition, which matches the piston velocity in the center of the tube ($r = 0, x = L/2$) will provide the last missing equation and will be computed based on formula (2.7). On all these computations we set $\delta = 0$ on the bound sheet and $\delta > 0$ on the free sheet for the reasons explained in Section (2.1.1). Hence, we have a linear system with N_b equations and N_b unknowns which is easily solved in Matlab by using the *inv* function which gives the inverse of a matrix.

Remark 1. *The right hand side of the linear system consists of velocities induced by the free sheet given by (2.8). In here, the circulation of the free vortices is known from the previous time step since it is conserved in time.*

Since now we have the sheet-strength values, we can determine the convection velocities of the free filaments by using (2.11). The velocity $\bar{u}$ of the currently released filament is computed using (2.15) and (2.16). This way we prevent having attached slip flow at the edge of the tube. The free filaments along with the newly released filament can be convected now with the computed velocities and the computation for the next time step can start.

The comparison of our results (Figure 3.1), Krasny's, and the ones gotten by Didden in 1979 (Didden [1979]) are very promising in our quest to better understand the various aspects of vortex theory. The next step, before analyzing Wu's method, is to implement Krasny's ideas for a wing advancing perpendicular to the flow. This will be described in the next section.

3.1.2 Vortex Forming at the Edges of a Vertically Moving Flat Plate; Comparison With Krasny's Results

The discussion in this section is based on the theory presented in (Krasny [1991]) and summarized in Section (2.1.3). Here we go one step further and analyze the wake behind a two-dimensional plate advancing perpendicular to the flow.

The whole idea is, as in the piston-tube problem presented in the previous section, to form the linear system, to invert it and then to determine the velocity of the currently released free filament. This time the system will be formed based on the evolution equation (2.17) with a smoothed kernel given by (2.18) and (2.19). The discretization of this equation is given in (2.20). The linear system will have as unknowns the circulation of the bound filaments. Since the problem is symmetric we will have a stationary point in the center of the plate, having circulation zero.

In our implementation we take $N + 1 = 81$ points on a plate with radius $R = 1$ which moves upwards with a velocity $U_0 = 1/2$. The plate reaches this velocity after an acceleration that takes $t = 0.01$. During this acceleration the time-steps are smaller but

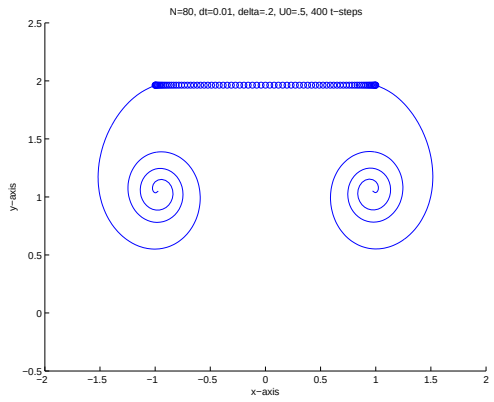

Figure 3.2: Krasny's method for a wing advancing upwards, normal to the flow, with adaptive speed $U_0 \approx 0.5$, blob $\delta = 0.2$, variable time-step $dt \approx 0.01$. Plot after 400 time steps having $N = 80$ bound vortex points.

they increase linearly as described in the previous section, and when the velocity becomes constant the time step becomes constant as well, with $dt = 0.01$. The blob is chosen to be $\delta = 0.2$ and the the bound vortex points on the wing have a cosine distribution so that we have more points and therefore a better resolution at the edges of the plate. The boundary condition requires that there is no normal flow through the plate which means matching the normal velocity from (2.20) with the advancing velocity of the plate. This will be done at the midpoints giving therefore N equations. However we want to compute the circulation at every bound point, i.e. $N + 1$ unknowns, issue that will be solved remembering that we have a stationary point in the center of the plate with circulation zero. Hence, we have a linear system with N equations and N unknowns which will be solved by inverting the matrix in Matlab with the *inv* function and will provide the circulation on the plate.

The sheet strength value at the edge of the plate γ_e, will be computed by a finite difference formula applied to the bound circulation $\gamma \sim \Delta\Gamma/\Delta x$. The edge strength will allow us to compute the circulation and the velocity of the newly shed vortex exactly as in the case of the piston-tube problem. For that we will use (2.15) and (2.16) or just (2.22). First, we compute the slip velocities $\overline{U}$ at both edges of the plate. This will be done using relation (2.20). Then we compute the slip velocities above and below the edge U_+ and U_- using (2.16) and whenever one of them is negative we set it to zero to prevent

attached slip flow. With the updated U_+ and U_- we recompute $\overline{U}$, which will be now the tangential velocity of the currently released vortex filament, and also the circulation of this free filament from (2.22).

Remark 2. *(i) In (2.22), $d\Gamma/dt$ represents the time variation of the total circulation of the free sheet and (ii) the newly shed vortex filament is released tangentially to the plate, i.e. in the x-direction, with the computed tangential velocity $\overline{U}$.*

The numerical computation for Figure (3.2) is performed with the data given at the beginning of this section and a blob $\delta = 0.2$. The plot is obtained after 400 time-steps. We can see a very nice roll-up which agrees very well with the results gotten by Krasny (see Krasny [1991]) and Pullin (see Pullin [1978]). The success of the implementation of these two methods makes us go even further and try to develop an algorithm in the spirit of Krasny's ideas for a wing advancing at a given angle of attack. We could not find any description of the method for this case, however, designing it is very important for understanding wing mechanics. Please see the next section (3.1.3) for a discussion of this algorithm.

3.1.3 Vortex Forming behind a Wing Advancing at a Given Angle of Attack

Our implementation of Krasny's idea for a wing advancing at a given angle of attack is based on the evolution equation (2.17). The idea presented in the previous two sections will work here too, since by discretizing this evolution equation we get a linear system that will give us the circulation on the wing. The discretization of the equation shows that if a vortex element of circulation Γ is located at (x_0, y_0), then the velocity induced by this element at an arbitrary point $P(x, y)$ will be

$$\begin{aligned} u &= \frac{\Gamma}{2\pi} \frac{(y - y_0)}{(x - x_0)^2 + (y - y_0)^2} \\ v &= \frac{-\Gamma}{2\pi} \frac{(x - x_0)}{(x - x_0)^2 + (y - y_0)^2}. \end{aligned} \tag{3.1}$$

Let's consider the wing to be formed of bound points distributed so that we have better resolution at the trailing and leading edges given by the presence of more vortices (cosine-

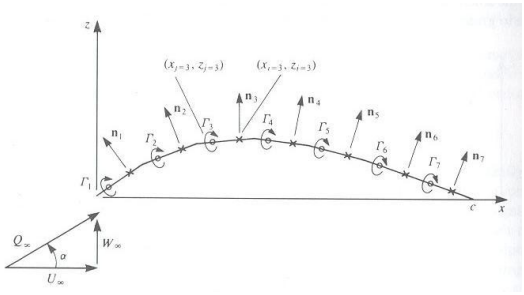

Figure 3.3: Discrete vortex representation of the thin, lifting airfoil model.

distribution). Following an idea from Katz, (Katz [2001]), we will be using two sets of additional points on the wing. The vortices will be placed at the segment quarter chord, while the normal vectors n will be placed at collocation points situated at the three-quarter chord of the segments, and this way the Kutta condition will be satisfied automatically (see Figure (3.3)). Therefore, the boundary condition (no flow through the wing) will be imposed at the collocation points and the circulation will be determined at the location of the vortices. This way equations (3.1) will not have singularities when both points are on the wing. However, when the points will be in the wake, a blob will be used, meaning that we will add a small δ^2 to the denominators of (3.1).

Suppose we take N points on the wing (in our calculations $N = 40$). Then we will have $N-1$ vortex points and $N-1$ collocation points. If at a certain time step we have N_w vortex filaments in the wake, then the velocity of each bound vortex point of the wing is a sum of the velocities induced by the $N-1$ bound vortices and N_w free vortices. These induced velocities are computed using (3.1). The strength of all the wake vortices except the one shed at the current time step is known from the previous time step since it conserves in time. Therefore the unknowns here are the values of the circulation of bound vortices ($N-1$ unknowns) and also the strength of the latest wake vortex. Hence we have N unknowns and only $N-1$ equations, i.e. imposing the boundary condition at every collocation point. The N^{th} linear equation will be given by the Kelvin condition which states that the total circulation is conserved. This means that the sum of the total bound and free circulation

is zero if we start from a rest state. So our system will be of the form

$$\begin{aligned} a_{i1}\Gamma_1 + a_{i2}\Gamma_2 + a_{i3}\Gamma_3 + \ ... \ + a_{i,N-1}\Gamma_{N-1} + a_{iw}\Gamma_{1w} &= b_i \quad i = 1, .., (n-1) \\ \Gamma_1 + \Gamma_2 + \Gamma_3 + \ ... \ + \Gamma_{N-1} + \Gamma_{1w} &= b_0 = -\sum_{k>1} \Gamma_{kw}, \end{aligned}$$

where the right-hand-side terms are the ones known, corresponding to the known wake strengths.

Remark 3. *The location of the currently released filament is also known, this being placed in the center of the path covered by the trailing edge at the current time step.*

Having said this, we are able to solve for the strengths of the bound vortices and the latest released wake filament by solving the linear system. Going back to equations (3.1) we can now compute the velocities of all the free vortices and move them accordingly. This ends one time step in our computation. To start the next one, we will move the wing with the prescribed velocity and compute all the above quantities again.

The result will be compared latter in this chapter with the one obtained using Wu's method but for now we could be satisfied with it since it displays all the features we're looking for. For instance, we get more and more roll-ups as we decrease the blob and the interior of the vortex has a very good resolution. For our computations we choose variable time steps, apply insertion techniques both with respect to the distance between the free vortices and to the angular separation and all work fine. The plot in Figure (3.4) is obtained with a speed $U_0 = 10$, inclination angle $\alpha = 18^\circ$ and blob $\delta = 0.2$. The time step is chosen relatively small $dt = 0.0002$ since we leave our method to run for 10,000 time-steps. This corresponds to the wing covering a distance equal to 10 chord lengths (the chord length is $c = 2$). We can see that even after such a long computation, the method is very robust giving a very nice roll-up.

At this point, knowing all these tricks about vortex theory, we are ready to attack Wu's method. Even more than that, now we have some very important results to use for comparison with this method.

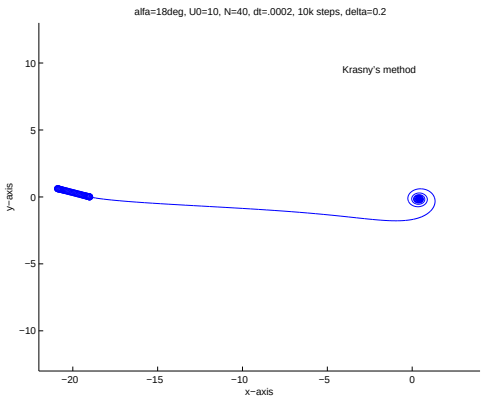

Figure 3.4: Krasny's method for a wing advancing with an angle of attack $\alpha = 18°$, with speed $U_0 = 10$, blob $\delta = 0.2$, time-step $dt = 0.0002$. Plot after 10,000 time steps having $N = 40$ bound vortex points.

3.2 Numerical Implementation of Wu's Method

3.2.1 Vortex Forming behind a Wing Advancing at a Given Angle of Attack Modeled With Wu's Method

We will describe here the numerical method implemented for applying Wu's theory. The code is written in Matlab. To discretize the bound vortex sheet we choose 40 points $(x_b(i), y_b(i))$ on the wing having a chord of 2. Also, the bound filaments are chosen to form a cosine-mesh, $\xi_j = \cos\theta_j,\ \theta_j = j\pi/n$, to provide better resolution at the edges. The wing is inclined at α degrees. We prescribe the flow velocity U_0, the time step dt and a constant f being the distance from the trailing edge where we put the current released free filament, also referred in our theory as $\delta\xi$. The current free vortex is released tangentially to the plate from the trailing edge so that the segment connecting it to the trailing edge will make an angle α with the x-axis.

We will also need some extra points on the wing, namely the centers of the segments connecting two bound vortex points $(x_h(i), y_h(i))$. These midpoints will help us compute the Cauchy's principal value for some integrals later on, which is a very common idea in fluid mechanics.

First, we compute γ_0 knowing the normal imposed velocity on the wing $U_n \sin(\alpha)$. From

(2.67) we can compute γ_0 either by iteration or by a series expansion

Iteration	Series expansion
we have $U_n = (G_0 + G_1)\gamma_0$ $\Rightarrow\ \gamma_0 = G - 0^{-1}U_n - G_0^{-1}G - 1\gamma_0$ Let $\gamma_0^{(n+1)} = G_0^{-1}U_n - G_0^{-1}G_1\gamma_0^{(n)}$	$\gamma_0 = \gamma_{00} + \gamma_{01} + \gamma_{01} + ...$ $G_0\gamma_{00} = U_n\ \Rightarrow\ \gamma_{00} = G_0^{-1}U_n$
guess γ_0 (best guess would be $G_0^{-1}U_n$)	$\gamma_{00} = G_0^{-1}U_n$
$\gamma_0^{(1)} = G_0^{-1}U_n - G_0^{-1}G_1\gamma_0^{(0)}$	$\gamma_{01} = -G_0^{-1}G_1\gamma_{00}$ so $\gamma_0 = \gamma_{00} + \gamma_{01} = G_0^{-1}U_n - G_0^{-1}G_1\gamma_{00}$
$\gamma_0^{(2)} = G_0^{-1}U_n - G_0^{-1}G_1\gamma_0^{(1)}$	$\gamma_{02} = -G_0^{-1}G_1\gamma_{01}$ $\Rightarrow\ \gamma_0 = \gamma_{00} + \gamma_{01} + \gamma_{02}$ $\Rightarrow\ \gamma_0 = G_0^{-1}U_n - G_0^{-1}G_1\gamma_{00} - G_0^{-1}G_1\gamma_{01}$ $= G_0^{-1}U_n - G_0^{-1}G_1(\gamma_{00} + \gamma_{01})$
$\gamma_0^{(3)} = G_0^{-1}U_n - G_0^{-1}G_1\gamma_0^{(2)}$	$\gamma_0 = G_0^{-1}U_n - G_0^{-1}G_1(\gamma_{00} + \gamma_{01} + \gamma_{02})$
.....	
$\Rightarrow\ \gamma_{0n} = \gamma_{00} + \gamma_{01} + \gamma_{02} + ... + \gamma_{0,n-1}$	

The numerical computation of γ_0 is extremely tedious and we'll devote our attention to that for the next paragraphs.

We observe that, from (2.71) we get

$$\gamma_{00}(\xi, t) = -\frac{2}{\pi}\sqrt{\frac{1-\xi}{1+\xi}}\int_{-1}^{1}\sqrt{\frac{1+\xi'}{1-\xi'}}\frac{U_n(\xi', t)}{\xi' - \xi}d\xi'. \tag{3.2}$$

One would expect to be able to get a contribution of $\sqrt{1+\xi}$ outside the integral to cancel the singularity due to the factor in front of this integral, so that γ_{00} is bounded for ξ close to one, i.e., at the leading edge. However, this will not happen. To see that, let's consider a smooth $U_n(\xi, t)$ which corresponds to smooth moves of the wing. Let's take an even easier example, considering a constant velocity, and without losing generality, consider $U_n \equiv 1$. For this, we are able to compute the integral analytically, as one can see from the following lemma.

Lemma 1. *Under the Kutta condition and the integrability condition, the solution of the Cauchy integral equation of the first kind,*

$$\frac{1}{\pi\imath}\fint_{-1}^{1}\frac{\phi(y)}{y-x}dy = 1 \quad is \quad \phi(y) = \imath\sqrt{\frac{1+y}{1-y}}, \quad for\ any\ y \in (-1,1).$$

For a proof of the lemma please refer to Appendix (A). According to this lemma, we have

$$\int_{-1}^{1}\sqrt{\frac{1+\xi'}{1-\xi'}}\frac{d\xi'}{\xi'-\xi} = \pi, \qquad \forall\ \xi' \in (-1,1), \tag{3.3}$$

which clearly states that we will not be able to get rid of the square root discontinuity in front of the integral just by manipulating the integral itself. Interpreting the physics, this means that the vorticity γ_0 has a square root discontinuity at the leading edge. However, this is not a problem, since we are looking for the circulation on the wing which is the integral of the vorticity (see 2.74). By integrating the square root discontinuity, this will vanish and we will have a nice, smooth bound circulation.

Finally, the vorticity γ_0 will be computed using (2.68) through (2.71) following these steps:

1. From (2.71) compute

$$\overline{\gamma_{00}}(\xi) = \int_{-1}^{1}\sqrt{\frac{1+\xi'}{1-\xi'}}\frac{U_n(\xi',t)}{\xi'-\xi}d\xi', \tag{3.4}$$

which is not a genuine vorticity since it misses the

$$-\frac{2}{\pi}\sqrt{\frac{1-\xi}{1+\xi}}$$

factor in front. As we said before, we omit this factor so that we do not deal with discontinuities in our numerical procedure;

2. From (2.70) compute

$$\begin{aligned} G_0\gamma_{01} &= -\frac{1}{2\pi}\int_{-1}^{1} g(\xi',\xi)\left[-\frac{2}{\pi}\sqrt{\frac{1-\xi'}{1+\xi'}}\overline{\gamma_{00}}\right]d\xi' \\ &= \frac{1}{\pi^2}\int_{-1}^{1} g(\xi',\xi)\sqrt{\frac{1-\xi'}{1+\xi'}}\overline{\gamma_{00}}(\xi')d\xi' \equiv U_n^1, \end{aligned} \tag{3.5}$$

here we put back the factor we omitted before, so that everything agrees with (2.70). Also we introduce a term U_n^1 (which will be some sort of an analog to U_n from (2.71)) just for the sake of recognizing some pattern in our recursive algorithm.

3. Having said this, using (2.70), (2.71) becomes

$$\gamma_{01}(\xi,t) = -\frac{2}{\pi}\sqrt{\frac{1-\xi}{1+\xi}}\int_{-1}^{1}\sqrt{\frac{1+\xi'}{1-\xi'}}\frac{U_n^1(\xi',t)}{\xi'-\xi}d\xi' \equiv G_0^{-1}U_n^1 \quad (-1<\xi<1),$$

and as in step 1 we will compute

$$\overline{\gamma_{01}}(\xi) = \int_{-1}^{1}\sqrt{\frac{1+\xi'}{1-\xi'}}\frac{U_n^1(\xi',t)}{\xi'-\xi}d\xi'; \tag{3.6}$$

4. now as in step 2 we compute U_n^2 from (2.70)

$$G_0\gamma_{02} = \frac{1}{\pi^2}\int_{-1}^{1} g(\xi',\xi)\sqrt{\frac{1-\xi'}{1+\xi'}}\overline{\gamma_{01}}(\xi')d\xi' \equiv U_n^2; \tag{3.7}$$

5. Again as in steps 1 and 3 we invert now the operator G_0 and get

$$\overline{\gamma_{02}}(\xi) = \int_{-1}^{1}\sqrt{\frac{1+\xi'}{1-\xi'}}\frac{U_n^2(\xi',t)}{\xi'-\xi}d\xi'. \tag{3.8}$$

The above procedure can be continued indefinitely giving us not vorticities $\gamma_{00},\gamma_{01},\gamma_{02},...$ but $\overline{\gamma_{00}},\overline{\gamma_{01}},\overline{\gamma_{02}},....$ However, when we compute $\Gamma_{00},\Gamma_{01},\Gamma_{02},...$ we integrate

$$\Gamma_{0k} = \int_{-1}^{1} -\frac{2}{\pi}\sqrt{\frac{1-\xi}{1+\xi}}\overline{\gamma_{0k}}(\xi)d\xi,$$

and we get rid of the discontinuity.

The algorithm above can be coded by writing three Matlab procedures or functions. First one will give us the smooth kernel $g(\xi', \xi)$, the second one will compute $\overline{\gamma_{0k}}$ and the third one U_n^k. Let's see how they are computed.

For the kernel $g(\xi', \xi)$ from (2.67) we used midpoints to represent ξ and the bound points for ξ'. We used finite differences to compute $dz/d\xi$ after we explicitly wrote the real part of the complex quantity.

Computing $\overline{\gamma_{0k}}$ on midpoints gets a bit trickier since by simply applying the trapezoidal rule in computing the integral we get a very poor result. We say poor here because we can always compare our result, for some constant velocity U_n^k, with the result given by Lemma 1 to serve as a standard reference. Therefore we choose another way, commonly used in lifting flow problems, changing the variable $\xi' = \cos y'$ to get

$$\begin{aligned} \overline{\gamma_{0k}}(\xi) &= \int_{-1}^{1} \sqrt{\frac{1+\xi'}{1-\xi'}} \frac{U_n^k}{\xi' - \xi} d\xi' \\ \overline{\gamma_{0k}}(\cos y) &= \int_0^{\pi} (1 + \cos y') \frac{U_n^k}{\cos y' - \cos y} dy'. \end{aligned} \tag{3.9}$$

This now will be solved using trapezoidal rule for points y' and y chosen this time between 0 and π so that they correspond to the bound points on the wing and to the midpoints, respectively. This method gives a very accurate computational result for the above integral since we do not have to deal with the square root singularity anymore.

To compute U_n^k we'll make the same change of variable, getting

$$\begin{aligned} U_n^{k+1}(\xi, t) &= \frac{1}{\pi^2} \int_{-1}^{1} \sqrt{\frac{1-\xi'}{1+\xi'}} g(\xi', \xi) \overline{\gamma_{0k}}(\xi') d\xi' \\ U_n^{k+1}(\cos y, t) &= \frac{1}{\pi^2} \int_0^{\pi} (1 - \cos y') g(\cos y', \cos y) \overline{\gamma_{0k}}(\cos y') dy', \end{aligned} \tag{3.10}$$

where U_n^k is computed on the bound points of the wing using again the trapezoidal rule.

We stop the computation whenever the norm of $\overline{\gamma_{0k}}$ gets smaller than some given epsilon, in this case we chose $\epsilon = 10^{-11}$. Adding up all $\overline{\gamma_{0k}}$ we get $\overline{\gamma_0}$ which gives the circulation Γ_0 over the body by

$$\Gamma_0 = \int_{-1}^{1} -\frac{2}{\pi} \sqrt{\frac{1-\xi}{1+\xi}} \gamma_0(\xi) d\xi, \tag{3.11}$$

which is computed again using a change of variable as in (3.10) and then applying the trapezoidal rule. This ends our computation of the quasi-stationary body circulation Γ_0.

Method for computing γ_1 From (2.75) we get

$$\begin{aligned} U_{n1}(\xi,t) &= \frac{1}{2\pi}\Re\left\{\frac{dz}{d\xi}\int_1^{\xi_m}\frac{\gamma_w(\xi',t)}{z'-z}d\xi'\right\} && (3.12)\\ &= \frac{1}{2\pi}\gamma_w(1,t)\Re\left\{\frac{dz}{d\xi}\int_1^{1+\delta\xi_m}\frac{d\xi'}{z'-z}\right\}+\frac{1}{2\pi}\Re\left\{\frac{dz}{d\xi}\int_{1+\delta\xi_m}^{\xi_m}\frac{\gamma_w(\xi',t)}{z'-z}d\xi'\right\} && (3.13)\\ &= A\gamma_w(1,t)+B, && (3.14)\end{aligned}$$

where

$$\begin{aligned} A &= \frac{1}{2\pi}\Re\left\{\frac{dz}{d\xi}\int_1^{1+\delta\xi_m}\frac{d\xi'}{z'-z}\right\}\\ B &= \frac{1}{2\pi}\Re\left\{\frac{dz}{d\xi}\int_{1+\delta\xi_m}^{\xi_m}\frac{\gamma_w(\xi',t)}{z'-z}d\xi'\right\}, \end{aligned}$$

and $\gamma_w(1,t)$ is the vorticity of the latest shed free vortex (the one between $\xi=1$ and $\xi=1+\delta\xi_m$), which is considered constant on the little gap being just opened in the wake over $\delta\xi_m$.

Now using (2.76) and the linearity of the operators G_0^{-1} and G_1 (and implicitly of G_N) we get

$$\begin{aligned} \gamma_1(\xi,t) &= -G_0^{-1}(U_{n1}+N_1) = -G_0^{-1}[A\gamma_w(1,t)+B+G_N(A\gamma_w(1,t)+B)] && (3.15)\\ &= -G_0^{-1}(A+G_NA)\gamma_w(1,t)+-G_0^{-1}(B+G_NB) && (3.16)\\ &= -G_0^{-1}(A+N_{1A})\gamma_w(1,t)+-G_0^{-1}(B+N_{1B}) = \gamma_{1A}\gamma_w(1,t)+\gamma_{1B}, && (3.17)\end{aligned}$$

where N_{1A} and N_{1B} have the obvious meaning in accordance with (2.76). Of course, in (3.17), γ_{1A} does not represent genuine vorticity, being just a multiplicative factor, but we still denote it by γ for the simplicity of understanding. It becomes clear now how γ_1 is computed: just recall the procedures used in computing γ_0 but this time with $(-A)$ and $(-B)$ instead of U_n to determine γ_{1A} and γ_{1B} and then use the last relation from (3.17). A and B are computed using the trapezoidal rule. Still, $\gamma_w(1,t)$ is unknown and therefore we

(a) **(b)**

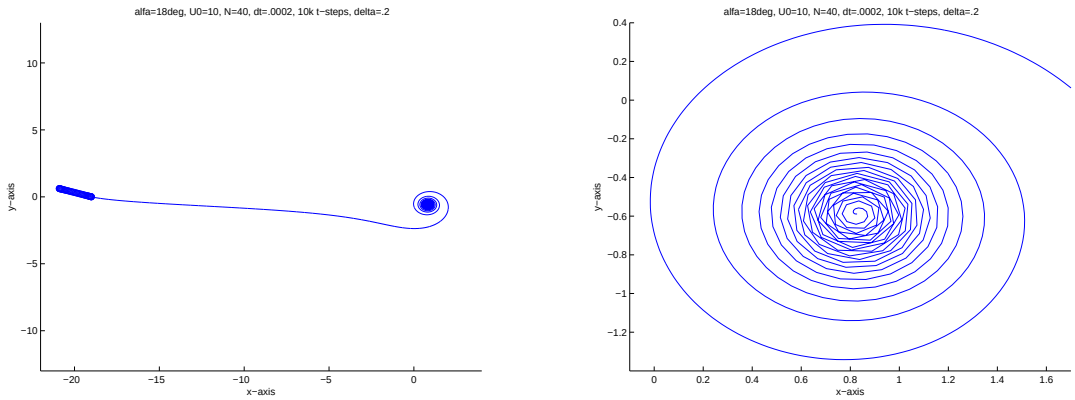

Figure 3.5: Wu's method for vortex forming behind a wing flying at $\alpha = 18°$, $U_0 = 10$, time step $dt = 0.0002$ and blob $\delta = 0.2$. In figure **(b)** one can see how accurate the method is when we zoom inside the vortex. Plot after 10,000 time-steps.

have to take our analysis even further.

Using Kelvin's relation for the conservation of circulation (see (2.85)) we get

$$\begin{aligned} 0 &= \Gamma_0 + \Gamma_1 + \Gamma_w && (3.18)\\ &= \Gamma_0 + \left[\gamma_w(1,t)\int_{-1}^{1}\gamma_{1A}d\xi + \int_{-1}^{1}\gamma_{1B}d\xi\right] + \left[\gamma_w(1,t)\delta\xi_m + \int_{1+\delta\xi_m}^{\xi_m}\gamma(\xi,t)d\xi\right] && (3.19)\end{aligned}$$

where the bound circulation Γ_1 is split in two parts corresponding to A and B, and the wake circulation is also split in two parts, one corresponding to the latest released vortex filament and the second to the rest of the free sheet.

In conclusion, we have

$$\gamma_w(1,t) = -\frac{\Gamma_0 + \int_{-1}^{1}\gamma_{1B}d\xi + \int_{1+\delta\xi_m}^{\xi_m}\gamma(\xi,t)d\xi}{\delta\xi_m + \int_{-1}^{1}\gamma_{1A}d\xi}. \qquad (3.20)$$

Here all the terms are known from our previous discussion. Of course, $\int_{1+\delta\xi_m}^{\xi_m}\gamma(\xi,t)d\xi$ is known from the conservation of the free circulation from one time step to the next. Hence we know $\gamma_w(1,t)$ and therefore both γ_w and γ_1.

Having the circulation and vorticity on both the bound and the free sheet, we can now

compute the convection velocities for the free vortex filaments. These velocities will be computed using relations (2.58) and (2.59) in which

$$\Re\left\{\frac{dz}{d\xi}\int_{S_b+S_w}\frac{\gamma(\xi',t)}{z'-z}d\xi'\right\} = \frac{dx}{d\xi}\int_{S_b+S_w}\frac{(x'-x)\gamma(\xi',t)}{(x'-x)^2+(y'-y)^2}d\xi' + \frac{dy}{d\xi}\int_{S_b+S_w}\frac{(y'-y)\gamma(\xi',t)}{(x'-x)^2+(y'-y)^2}d\xi', \tag{3.21}$$

$$\Im\left\{\frac{dz}{d\xi}\int_{S_b+S_w}\frac{\gamma(\xi',t)}{z'-z}d\xi'\right\} = -\frac{dx}{d\xi}\int_{S_b+S_w}\frac{(y'-y)\gamma(\xi',t)}{(x'-x)^2+(y'-y)^2}d\xi' + \frac{dy}{d\xi}\int_{S_b+S_w}\frac{(x'-x)\gamma(\xi',t)}{(x'-x)^2+(y'-y)^2}d\xi'. \tag{3.22}$$

Note that these relations also give the normal and tangential velocities. In convecting the free vortices it would be easier though, to work with the x and y components of the velocities. Also, when we discretize the integrals, the sum will contain a $+\delta^2$ in the denominator (the blob) whenever ξ' is on S_w. However, δ is set to zero when ξ' is on S_b. After all these steps, we are ready to go to the next time step and to compute all the required unknowns again.

This ends the description of our method. An example is provided in Figure (3.5). The example shows how accurate the method is by zooming inside the vortex. We do not use in this case any point insertion technique just to show how good the raw result is. The numerical implementation uses an advancing wing velocity $U_0 = 10$, an angle of inclination $\alpha = 18°$, a blob $\delta = 0.2$ and a fixed time step $dt = 0.0002$. The plot is obtained after 10,000 time-steps, or after the wing traveled 10 chord lengths (the wing's chord length is 2).

3.3 Comparison of the Two Methods for the Rigid Wing

3.3.1 Comparing the Results

Both Krasny's method and Wu's method produce very nice results. Krasny also observes that the smaller the blob δ gets, the more accurate the method becomes in terms of capturing the physical effect of viscosity. By that it should be understood that we would like to capture better what happens in the center of the vortex, and by decreasing the blob we get more and more roll-ups. Comparing the two methods for identical sets of initial data (see Figure 3.6) we can see that Wu's method behaves much better in capturing the roll-ups inside the

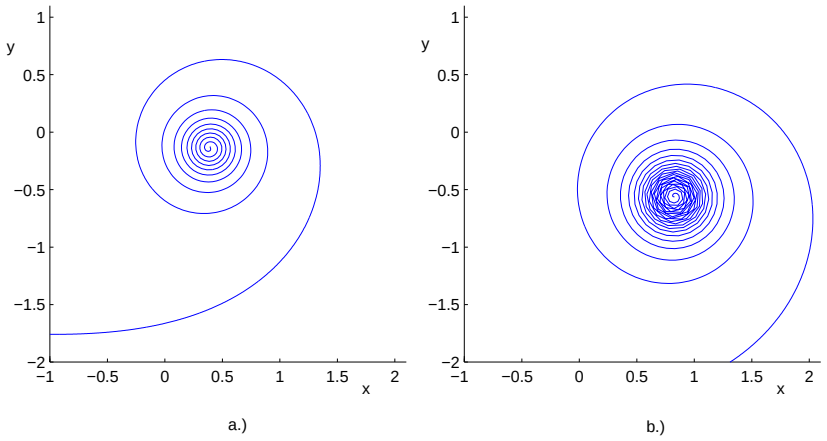

Figure 3.6: a.) Vortex obtained with Krasny's method; b.) Vortex obtained with professor Wu's method.

vortex ring. Krany's method would produce the same results for a smaller blob which will require a smaller time-step for accuracy and therefore a longer computational time. The plots presented in Figure (3.6) are obtained for a flat plate of chord $c = 2$, inclined at an angle $\alpha = 18°$, traveling with a speed $U_0 = 10$, with a time-step $dt = 0.0002$ and after ten thousand time-steps. For both plots, the blob is chosen to be $\delta = 0.2$. No point insertion technique is used in these plots to better see the accuracy of the methods. The plot obtained using Wu's method proves to be very stable for small blobs when the number of roll-ups becomes very big.

The difference between the two plots resides, perhaps more importantly, in the position and radius of the vortex ring. The center of the ring obtained with Krasny's method is located at $(x, y) = (0.395, -0.151)$ while Wu's method gives us a ring with center located at $(x, y) = (0.827, -0.588)$. The radius of the first one is $R = 0.97$ while for the second one the radius is $R = 1.218$. So one can see that by Wu's method we get a slightly bigger vortex ring located a bit lower and more to the right than the one gotten by the other method. To verify the right position of the vortex and also to validate the ring dimensions we will refer in the next subsection to experiments performed using a NACA wing.

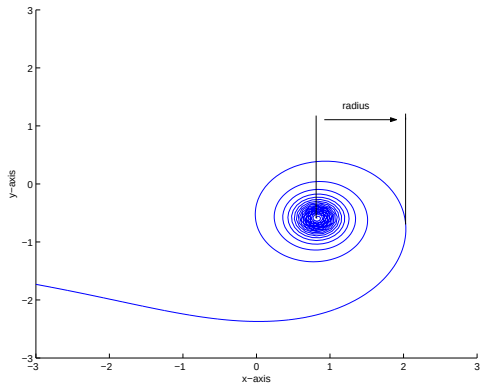

Figure 3.7: The way the radius of the vortex was measured.

3.3.2 Validating the Numerical Computations

Radius of the vortex One of the few experiments we could find in the literature involving the structure and development of a tip vortex shed from a conventional wing is that performed in 1995 by William J. Davenport (Davenport [1995]). His experiments were performed in the Virginia Tech Stability Wind Tunnel and a rectangular-planform NACA 0012 wing with a 0.203 m chord, and a blunt tip was used to generate the vortices. The measurements we are going to refer to were done with a chord Reynolds number $U_\infty c/\nu$ of 530000 (corresponding to a velocity of about 37.3 m/s) with the wing at an angle of attack α of 5°. Davenport's results were taken at cross-sections 5c, 10c, 15c, 20c, 25c and 30c downstream of the wing leading edge (here c represents the chord length). He showed using these six points of data that the scale of the spiral grew approximately as the square root of the distance traveled by the wing (see Figure 9, pp.84, in Davenport [1995]).

Even though the difference between this experiment and our numerical model is obvious (NACA wing has thickness), Davenport's results are as close as possible to our model, and by comparison we can demonstrate that our model and method are indeed valid approximation of real-life physics.

The simulation using professor Wu's method is performed with the following characteristics: a chord length $c = 2$, an advancing speed of 10, an angle α of 5° to match Davenport's experiment, a blob of 0.2 and a time-step of 0.0005. The wing is left to travel for 12,000

time steps which corresponds to 30 chord lengths and the sample of data for the behavior of the radius is taken after every 100 time-steps or every quarter-chord-length traveled. The code is run on a AMD Athlon(tm) XP 1700+ with 512 MHZ, and it runs for about 90 hours. The radius is measured from the center of the vortex (considered to be the location of the first filament released) to the right most point of the wake (see Figure 3.7).

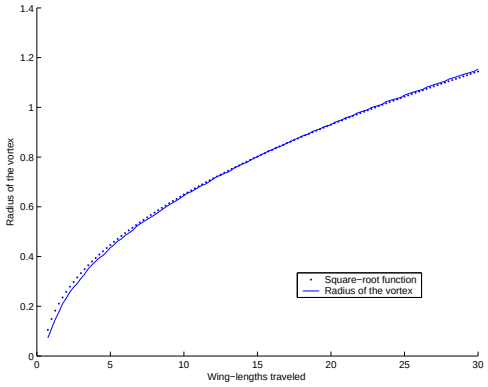

Figure 3.8: Plot of the radius of the vortex versus the square-root function. Here the x axis represents the number of chord-lengths traveled by the wing.

The results are very accurate, and the large number of data points taken offers a very detailed view of the analogy with the experiment. In Figure (3.8) we can see that the behavior of the radius in time mimics very well the behavior of the square-root function represented by a dotted line. The slight discrepancy at the beginning of the motion could be due to the fact that we miss thickness in our model.

Also, to validate the position of the vortex found in Figure (3.6), we note that Davenport's experiment results are very close to the results obtained using Wu's method. Davenport computes the span-wise position of the core η as a function of x/c in the baseline flow. The distance η is defined as the y-coordinate of the vortex core center relative to the wing tip. After the wing travels $x/c = 10$ chord lengths, Davenport reports a position of about $\eta/c = 0.27$, which in our case, for the data used in Figure (3.6), would mean $\eta = 0.54$ since the chord is 2. This is very close to what Wu's method gives us: $\eta = 0.588$ and rather far from the result obtained using Krasny's method: $\eta = 0.151$. Again, the small discrepancy

could be due to the thickness of the NACA wing.

3.4 Results Obtained for Nonlinear Motions

Some very interesting cases to be analyzed in the following sections are those for heaving and pitching motions. While the heaving or fluttering motion is closer to that of a bird's wing in flight, the pitching motion is better related to the movement of a fish's fin. Since both movements have very close correspondents in nature we will try to see how our method compares with the experiments found in the literature. Nevertheless, we will try to argue that they do provide thrust, and, in the case of a mixed heaving and pitching motion, we will try to describe the kind of flight that generates lift and the one that generates thrust.

3.4.1 Wu's Method for Heaving Motion

The fluid mechanics literature is richer in experiments involving a heaving wing. Some experiments were done by Bratt in 1953 (see Bratt [1953]) and more recently by Jones, Dohring & Platzer in 1998 (see Jones [1998]) and by Lai, Yue & Platzer in 2002 (see Lai [2002]). To further validate our unsteady method and to aid in defining its limits of applicability, the unsteady wake structures numerically generated are compared with the wake structures found experimentally.

If we consider a flapping wing and denote by $V_p = hk$ the non-dimensional plunging velocity, where h is the plunge amplitude in terms of the chord c and k is the reduced frequency $\omega c/U_0$, then it is well known from the above experiments, that in viscous fluids, stationary airfoils and airfoils plunging sinusoidally with low V_p generate viscous related drag. As the V_p is increased the drag is reduced and eventually thrust is produced. However, the potential-flow code predicts zero drag for a stationary airfoil and thrust for a plunging airfoil at any finite frequency. Therefore, qualitative and quantitative comparisons of the wake structures are made for a sufficiently big V_p such that the experiment will show a thrust mode as well. The qualitative agreement demonstrated in Figure (3.9) is excellent. In the experiment, the distance between the centers of the vortices in the second pair of vortices is about 0.4 when the plate length is 1 while for the computational result, the same

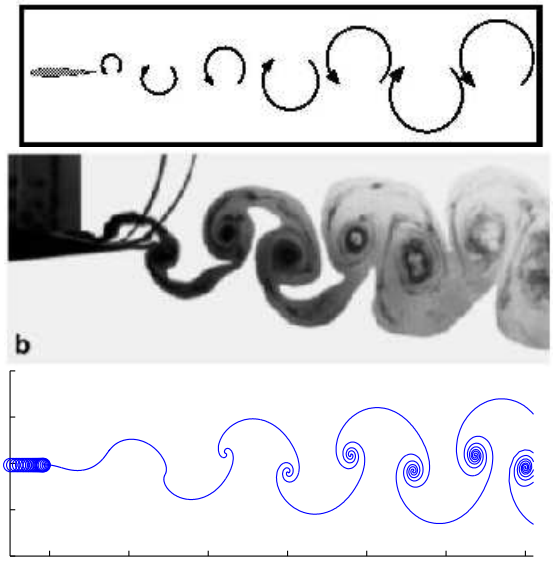

Figure 3.9: Heaving wing; Upper: rotational orientation of eddies; Center: experiment done by Lai in 2002; Lower: Wu's numerical method.

distance is 0.8 for a plate of length 2. The upper image shows a schematic illustration of the rotational orientation of the eddies. This kind of placement will obviously generate thrust. The numerical plot is the lower image and then the experiment from (Lai [2002]) is the center one. For the numerical plot we use a foil advancing to the left in a stationary flow, flapping at 10 Hz with a non-dimensional plunge velocity of $V_p = 0.076$ which perfectly match the experiment data. The amplitude is $h = 0.038$ and the wing velocity is $U_0 = 5$. Here, a small blob is used $\delta = 0.11$, the time step is $\Delta t = 0.001$ and the execution is stopped after 2630 time steps. The experiment was conducted in the water tunnel facility at the Department of Aeronautics and Astronautics, Naval Postgraduate School, Monterey, California.

To demonstrate the production of thrust, we analyze the velocity profile at a point located at $0.41c$ behind the trailing edge. To better capture the thrust production we should have integrated this profile along a $x = ct$. section; however, this punctual analysis should give a good interpretation of the thrust. One could see from Figure (3.10)) that the mean velocity at this point is positive indicating the presence of a jet. This shows how

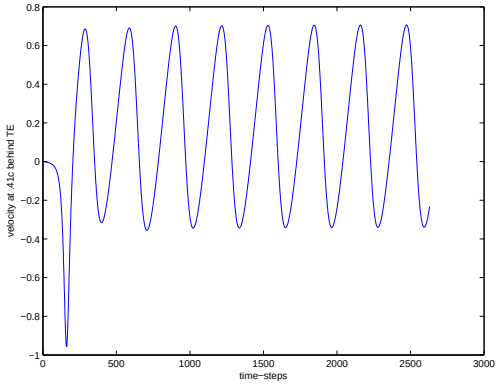

Figure 3.10: Heaving wing; Profile of the velocity at 0.41c downstream behind the trailing edge.

important the study of the wake is, the released vortices being able to create thrust and therefore to move the bird or the fish forward.

The first drop in the velocity which makes it negative is due to the beginning of the motion, however, after the first quarter of the motion period, thrust will be generated. If we are looking at the physical interpretation, this represents the period before the flow particles situated at $0.41c$ downstream from the trailing edge get influenced by the disturbance created by the pitching wing.

3.4.2 Pitching Motion

A very similar wake is produced in the case of a pitching motion (see Figure 3.11). Here, the upper part represents the plot obtained by Wu's method while the lower one represents the experiment done in 1989 by Koochesfahani (see Koochesfahani [1989]) at Caltech. This time the wing is advancing from left to right having a high pitching frequency ($f = 5 \Rightarrow w = 2\pi f \approx 31.14$) around the quarter-chord center which matches the conditions in the experiment. The amplitude is $\pm 2^\circ$ and the advancing speed is 10. The blob is $\delta = 0.2$, the time step $\Delta t = 0.0005$ and the procedure is stopped after 3000 time steps. Again the comparison shows a very accurate behavior compared with the experiment. The position and orientation of the vortices in the wake suggest a jet-like wake behind the pitching foil.

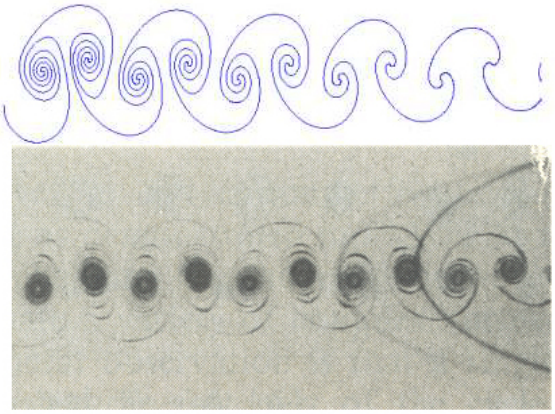

Figure 3.11: Pitching motion; Upper: Wu's numerical method; Lower: experiment done by Koochesfahani in 1989.

Koochesfahani shows though, that at low frequencies in real flow, the drag effect is dominant due to the viscosity. This could be a research door for the biologists to see what kind of frequencies exist in the case of rapid fish movements and how they agree with the numerical and water tank experiments.

3.4.3 Mixed Pitching and Heaving Motion

A bird wing is an airfoil combining the functions of an aircraft wing and propeller blade to give lift and thrust. This is done by a mixed motion of the wing involving both heaving and pitching. This more complex movement is very nonlinear and we'll try to analyze it using Wu's method.

Just to see the shape of the wake behind a wing performing a mixed motion, we use Wu's method for the following case (see plot a. in Figure (3.12)): a heaving movement having amplitude $h = 0.038$ and angular frequency $w_h = 8$ combined with a pitching movement around a point situated at $xc = 0.15$ from the leading edge, having pitching amplitude of $\pm 3^\circ$ and pitching angular frequency of $w_p = 8$. The wing starts from a rest position that coincides with the $[-1, 1]$ segment on the Ox axis and has a phase difference between heaving and pitching of zero degrees. It also moves to the left with a speed $U_0 = 3.12$ and a vortex element is shed in the wake after every time step $\Delta t = 0.002$. The plot is made

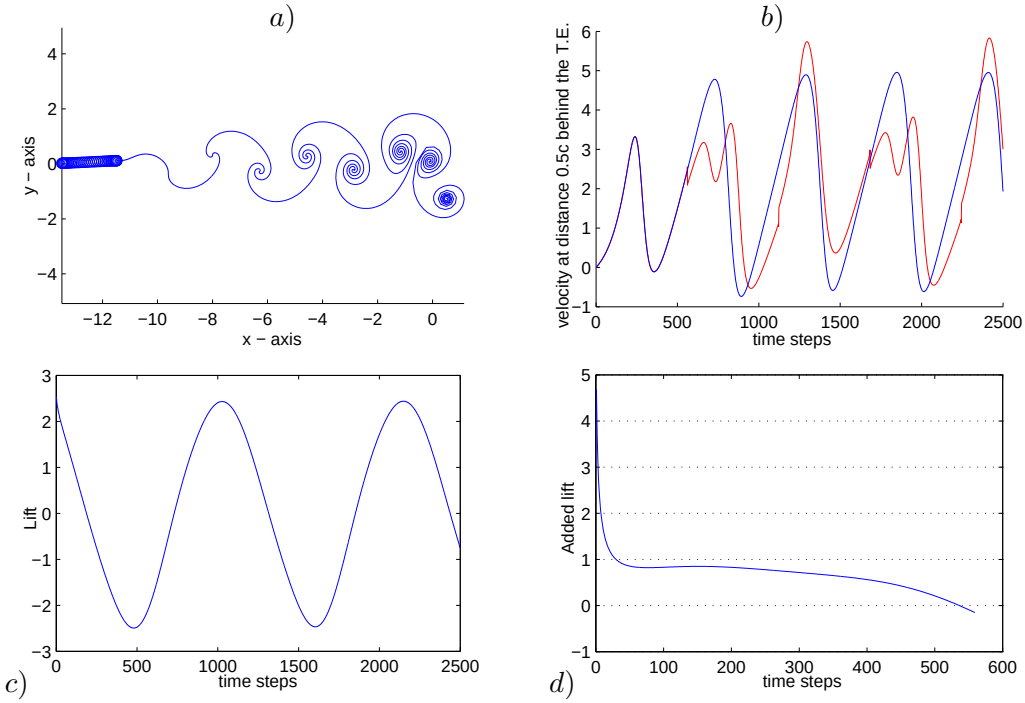

Figure 3.12: Wu's method for a mixed heaving-pitching motion. a) An example of mixed heaving-pitching motion; b) Comparison of flow velocities at a distance 0.5c behind T.E. for cruising flight (blue) and ascending flight (red); c) Lift for cruising flight; d) Added lift for two half-periods for ascending flight

after 2000 time steps.

However, we want to describe more realistically the actual movement of a bird's wing. For that, we have to take into consideration some more aspects from the natural movement. We know that in order to generate lift and thrust, the down-stroke and the upstroke of a bird's wing are not similar. The down-stroke is more powerful by keeping the wing section almost horizontal, while in the upstroke the wing is inclined, having the trailing edge lower than the leading edge. We will show that this movement generates lift and therefore we will call this ascending flight. However, a wing which does not incline for the upstroke, i.e. having a pure heaving motion, will not create any lift because of the symmetry of this motion. Without considering the bird's weight, we could argue that this kind of motion will keep the bird at a constant altitude and we will show that it generates more thrust than the first motion. Therefore we will call this cruising motion.

To better see the difference between these two movements, we analyze them using Wu's

method. The ascending motion is composed of a heaving with amplitude $h = 0.425$ and angular frequency $w_h = 8$. While for the down-stroke we have only this heaving motion, for the upstroke we combine it with a pitching motion. Thus, when the wing starts the upstroke, we start to incline it with an amplitude $\theta_0 = 4°$ and an angular frequency $w_p = 8$ equal to that of the heaving so that when the wing ends the upstroke it will find itself again in a horizontal position.

The cruising flight is modeled using a pure heaving motion with the same characteristics as above. For both motions we pick a flight velocity of $U_0 = 8$ and a time step for the numerical method $\Delta t = 0.0007$. The blob is $\delta = 0.2$ and the pitching motion is realized around the trailing edge. The lift is computed as in Section 3.4.7.

Plot b. in figure (3.12) shows the velocity of a particle located at a distance $0.5c = 1$ behind the trailing edge. Since the fluid is stationary and only the wing is moving, we can see that, having a positive average velocity behind the trailing edge, thrust will be generated in both cases. However, one will notice that in the case of cruising flight (the blue plot) more thrust is generated than in the case of ascending flight. For instance, during the half-period corresponding to the upstroke, the thrust for the cruising motion is 20% larger than the other one which makes this motion more suitable when the bird wants to advance.

However, if we take a look at the lift, we will see that, due to the symmetry of the motion, the overall lift in the case of a cruising flight is practically zero (see plot c. Figure (3.12)). Not the same thing can be said about the ascending case. In this case, if we add up the lift produced during the upstroke and the one produced during the down-stroke we will see that the resulting lift is quite relevant (see plot d. Figure (3.12)).

In conclusion, we have demonstrated that these two types of mixed motions provide quite different results: the cruising movement produces thrust but no lift while the ascending one produces less thrust but considerable lift. It is worth mentioning though, that in a real flight things change a bit. To be able to support its own weight, the bird will use some pitching even during cruising so that the generated lift will cancel this new force. Also during the ascending flight, the amplitude of pitching will have to increase because of the same reason.

Another fact observed in nature is that on the upstroke of the wing beat, the feathers at

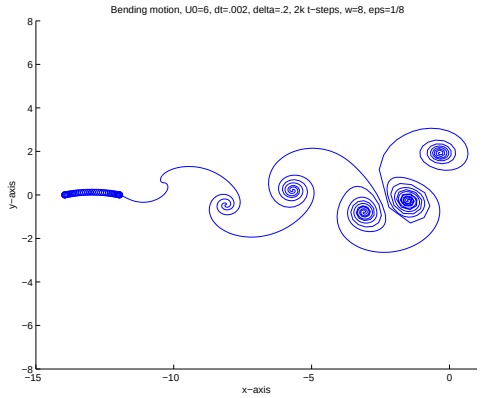

Figure 3.13: Wu's method for a bending motion.

the end of many bird wings twist sideways to let the air slip through with little resistance. This will increase even more the lift compared to the pure heaving motion.

3.4.4 Bending Motion

In this subsection, we would like to demonstrate the ability of Wu's method in dealing with nonlinearity. We use an example of a plate with zero thickness but having a variable camber. The incidence angle of the chord is zero but there is an actual incidence angle given by the camber. The deformation of the wing used in Figure (3.13) is given by $y = \epsilon(1-x^2)$, with the amplitude $\epsilon = 1/8\sin(\omega t)$. The angular frequency is $\omega = 8$, the advancing speed is $U_0 = 6$, the time step $\Delta t = 0.002$ and the blob $\delta = 0.2$. The plot is obtained after 1100 time steps and very accurately catches the formation and structure of the wake vortices.

This example has very nice applications when combined with a flapping motion. In that case, it would describe the motion of a wing composed by a flexible membrane like the one found in bats (*Chiroptera*) or in some insects.

3.4.5 Analysis of the First Released Vortex Element

To better understand the differences we noticed between Wu's and Krasny's methods, we analyze the first released vortex element for a rigid wing (of length 2) advancing at a given angle of attack. We are able to compute the circulation of this first vortex analytically and

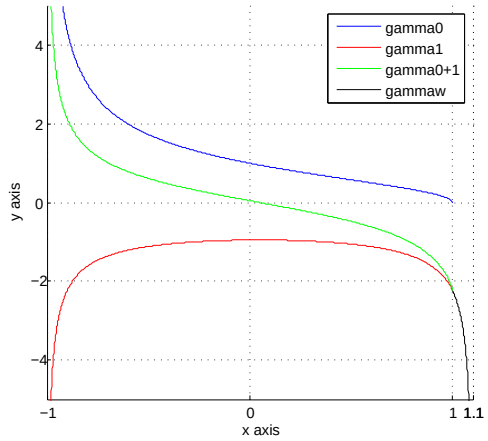

Figure 3.14: Plot of the vorticity functions for one released vortex filament.

therefore to compare this exact circulation with the ones given by the two computational methods.

The analytical formula for the vorticity on the body without any wake effect (γ_0) is given by equation (2.73) after a simple change of variables. The vorticity on the wake (γ_w) is computed using equation (2.86) along with Lemma 1. Finally the vorticity induced on the body by the wake (γ_1) is computed from formula (2.79). (For more details please consult Sears [1938]). When the wing goes abruptly from horizontal position to an inclination alpha so that the wake-free circulation on the body is $\Gamma_0 = 1$, we have the following formulas for the discussed vorticities

$$\gamma_0 = \frac{1}{\pi}\sqrt{\frac{1-x}{1+x}} \tag{3.23}$$

$$\gamma_w = -\frac{1}{\pi}\sqrt{\frac{1}{1+Ut-x}} \tag{3.24}$$

$$\gamma_1 = -\frac{1}{\pi}\frac{1}{\sqrt{(1+x)(1+Ut-x)}}. \tag{3.25}$$

In figure (3.14) we plot these functions without the $1/\pi$ factors and for an initial vortex placed at a distance $\sigma = 0.1$ behind the trailing edge. A couple of things can be observed from this plot. Firstly, we can see that both γ_0 and γ_1 are unbounded at the leading

edge of the wing which is in accordance with the known wing theory results. The more important aspect, however, is the fact that the vorticity on the wake blows up near the first released vortex element. Therefore, one should be very careful on the numerical analysis of this first wake point. In fact, the strength of Professor Wu's method resides exactly in this combination of analytical and numerical methods used to catch the behavior of the wake near the trailing edge. In contrast, Krasny's method considers this very first released element as an extension of the body, computing its circulation purely numerically by inverting a linear system.

This can be seen better when comparing the results given by the two methods with the analytical result. For a wing advancing with a speed $U_0 = 10$, at an angle of 18 degrees, and the wake circulation computed after the wing traveled a distance of 0.005, the analytical wake circulation from equation (3.24) is $\Gamma_w = -0.61804$, the same circulation computed with Wu's method is $\Gamma_w = -0.6510$ and the one computed using Krasny's method is $\Gamma_w = -0.7131$. Such a discrepancy will be propagated in the wake later, and this is why we are seeing much better results for Wu's method.

3.4.6 Convergence Analysis

A very conclusive test to demonstrate the accuracy of Wu's method is the convergence analysis of the outer wake both with respect to time and blob. The outer wake represents a cut of the whole wake as it is depicted in figure 3.15 (a).

For a blob size of 0.2 we vary the time step, choosing dt=0.0005, 0.00025, 0.000125, and 0.0000625. We stop our computation after 1000, 2000, 4000 and respectively 8000 steps. This means the wing travels the same distance but we have more points in the wake, or a finer mesh in other words. We compute the distance between the resulting outer wakes by computing the distance between corresponding points on these wakes. In figure 3.15 (b) we can see a plot of these distances. The green plot represents the point distances between the outer wakes with dt=0.0005 and dt=0.00025, the red one the point distances between the outer wakes with dt=0.00025 and dt=0.000125, while the blue one corresponds to the point distances between the outer wakes with dt=0.000125 and dt=0.0000625. It is obvious

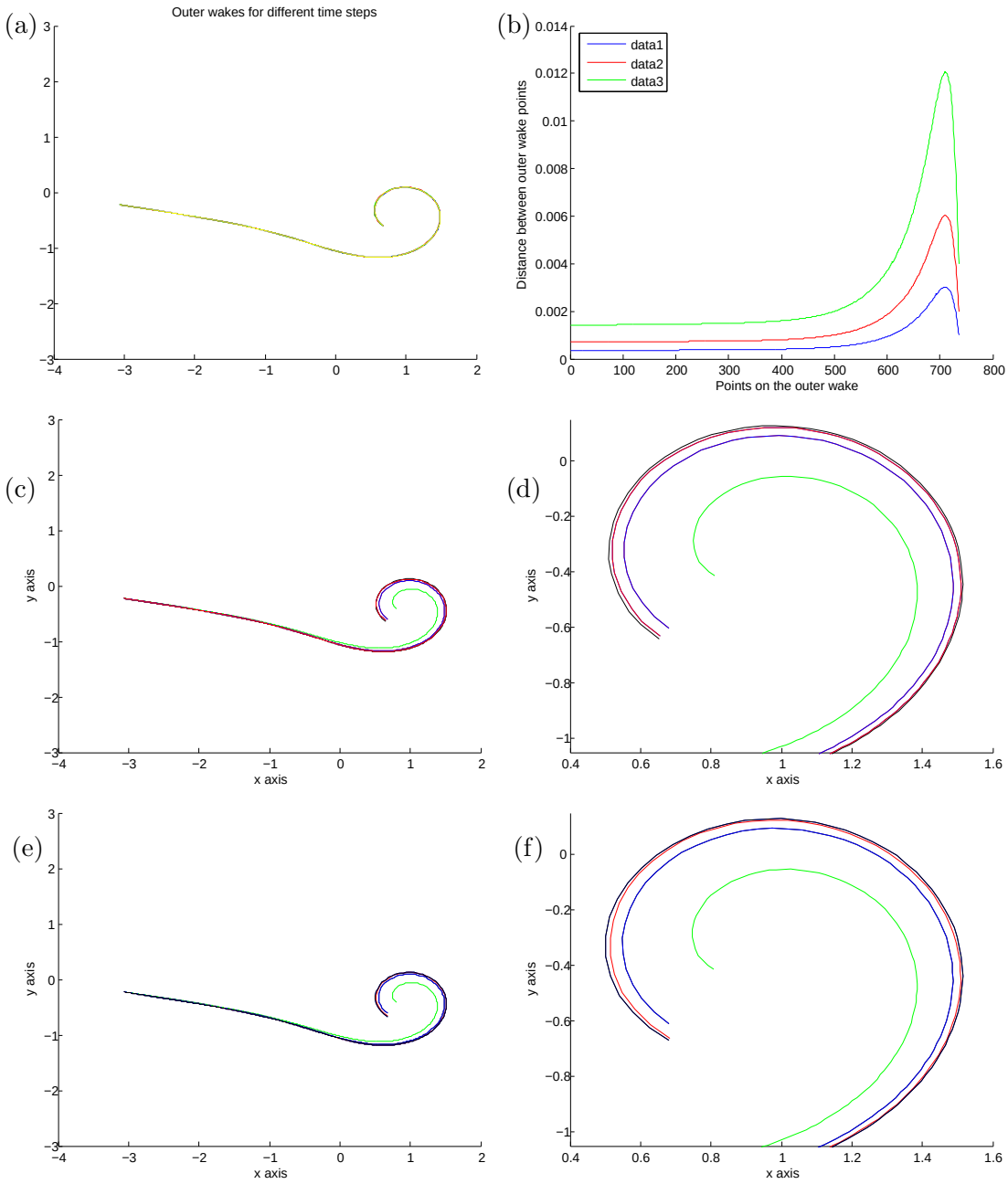

Figure 3.15: (a)The outer wake; b) distances between points on the wakes for a constant blob but variable time step; (c)&(d) Outer wake and a zoom for a constant time step dt=0.000125 but variable blob; (e)&(f) Outer wake and a zoom for a constant time step dt=0.0005 but variable blob. For plots (c), (d), (e) and (f) the green wake has δ=0.4, the blue one 0.2, the red one 0.1 and the black one 0.05.

how these distances decrease as time step decreases. More than that, the average distance between the outer wakes are 0.0028, 0.0014 and 0.0007 going from the coarsest mesh to the finest. This shows how the outer wake converges with respect to time step.

We perform a similar convergence study by varying the blob size. For a time step of 0.000125 and 4000 time steps we choose the blob size to be 0.4, 0.2, 0.1 and 0.05. Again we compute the distance between the points on the outer wake and it turns out that the average distance between these points goes from 0.0250 to 0.0057 and to 0.0015. Hence, the method is convergent with respect to the blob size. A representation of these outer wakes can be seen in figure 3.15 (c) with a zoom of the outer part of the vortex in figure 3.15 (d). Here the green plot corresponds to $\delta = 0.4$, the blue one to $\delta = 0.2$, the red one to $\delta = 0.1$ and the black one to $\delta = 0.05$.

We go even further and do the same computations for a different time step, dt=0.0005 and 1000 points in the wake. This case is similar to the above one in terms of the distance traveled by the wing. The blobs are again the same. The results show that the distance between the outer wakes are this time 0.0253, 0.0062 and 0.0027 respectively. Again, a representation of these outer wakes can be seen in figure 3.15 (e) with a zoom of the outer part of the vortex in figure 3.15 (f). Here the green plot corresponds to $\delta = 0.4$, the blue one to $\delta = 0.2$, the red one to $\delta = 0.1$ and the black one to $\delta = 0.05$.

It can be seen that in this case, for a bigger time step, the convergence is slower in delta. In other words, if we choose our blob size carefully, by decreasing the time step we will get a faster convergence of the outer wake. This shows that our method is more dependent on the time step than on the blob itself.

Some other experiments that are not included here show the dependence of the methods to the incidence angle. These experiments demonstrate that for a given time, for both methods the wake flattens more and more as we decrease the angle, approaching the horizontal. Of course, this is an expected result since for a plate advancing at a zero angle of attack we expect to get a linear wake.

Another experiment tries to feed the first n vortex elements (where n is 30, 50, 100) from Wu's method into Krasny's method hoping that these points, having less error near

the trailing edge, will correct Krasny's method and will produce an outer wake closer to the one given by Wu's. The experiment is not very conclusive because of the effect the core of the vortex has on the outer wake. Unfortunately, by feeding all these points from one method to the other, the accuracy is lost in the center of the vortex and this chaotic behavior affects the whole wake.

To show how the methods converge to a common result for the outer wake after we minimize the the impact of the error introduced in the first released vortex element, we also try to make the initial jump of the plate from the horizontal to angle α smoother. This experiment again does not prove to be very successful since, after all, we end up adding the contribution of all the smaller steps and the total error introduced in the wake is almost the same as in the non-smooth case.

3.4.7 Verifying Wagner's Result

A validation of professor Wu's method and of the numerical method may be given by Wagner's (1925) classical problem for a flat plate airfoil making a time-step increase in incidence angle so that $\Gamma_0(t) = H(t)$, the unit Heaviside step function. With the nonlinear terms dismissed, equation (2.86) reduces in the linear limit to

$$\int_1^{1+Ut} \gamma_w(\xi,t)\sqrt{\frac{\xi+1}{\xi-1}}d\xi = -1 \quad (t>0), \tag{3.26}$$

with γ_w properly scaled to have the unit change of the integral as a standard. Using the results of Karaman and Sears (1938), we change the variable $s = 1 + Ut - \xi$, so that $\gamma_w(\xi,t) = \gamma(1+Ut-s,t) = \hat{\gamma}(s,t)$, s being the distance measured along $S_w(t)$ from the tip of the starting vortex (at $\xi = \xi_m$) backward toward the trailing edge, by which (3.26) becomes

$$\int_0^{Ut} \hat{\gamma}(s,t)\sqrt{\frac{2+Ut-s}{Ut-s}}ds = -1 \quad (t>0). \tag{3.27}$$

We are interested in the beginning of the motion and therefore $0 \leq Ut - s \ll 1$, so the

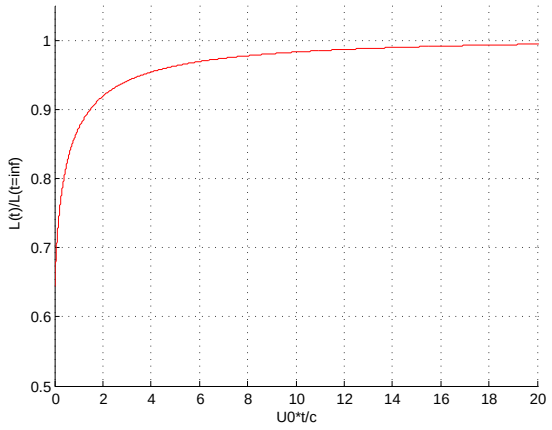

Figure 3.16: Variation of lift after the initiation of a sudden forward motion of a two-dimensional flat plate.

leading order of the small-time asymptotic representation of (3.27) is

$$\int_0^{Ut} \hat{\gamma}(s,t)\sqrt{\frac{2}{Ut-s}}ds = -1 \quad (0 < Ut \ll 1). \tag{3.28}$$

But now this is Abel's integral equation and it has the solution

$$\hat{\gamma}(s,t) = -(\pi\sqrt{2s}) \quad (Ut \ll 1). \tag{3.29}$$

Again following Karaman and Sears (1938), Wagner's lift-deficiency function $\Phi(Ut)$ is found to be

$$\Phi(Ut) = -\int_1^{1+Ut} \frac{\gamma(\xi)}{\sqrt{\xi^2-1}}d\xi = -\int_0^{Ut} \frac{\hat{\gamma}(s)}{\sqrt{2(Ut-s)}}ds = \frac{1}{2} \quad (as\ t \to 0), \tag{3.30}$$

which is Wagner's result, stating that an impulsively started flat-plate airfoil generates instantly half the final lift, which it eventually achieves, $1-\Phi(Ut) \to 1$ as $t \to \infty$, i.e., after a time delay, which is known as Wagner effect.

The designed numerical method is used to compute the initial lift and the lift at every later time step. After a sufficiently long time the lift is considered to be $L(t=\infty)$ or the final lift. The plot is presented in Figure (3.16). The result is obtained with blob 0.2, speed 10, time step 0.001 angle of attack $\alpha = \pi/20$ and the final lift considered after the wing has

traveled 8k time steps or approximately 40 chord lengths.

We compute the lift using the theory in (Sears [1938]). Sears shows how the total momentum of continuously distributed vortices (consisting of the airfoil and its wake) is

$$I = \rho \int_{-1}^{1} \gamma(x) x dx + \rho \int_{1}^{\xi_m} \gamma(\xi) \xi d\xi. \tag{3.31}$$

Using the fact that the lift is given by $L = -dI/dt$, the decomposition of vorticity $\gamma(x) = \gamma_0(x) + \gamma_1(x)$ and Kelvin's theorem of conservation of circulation, we get

$$L = -\rho \frac{d}{dt} \int_{-1}^{1} \gamma_0(x) dx + \rho U \Gamma_0 + \rho U \int_{1}^{\xi_m} \frac{\gamma(\xi) d\xi}{\sqrt{\xi^2 - 1}}, \tag{3.32}$$

where the first term represents the contribution of the apparent mass, the second one the quasi-steady lift, and the last one the lift given by the wake. The apparent mass behaves like a delta function centered at zero (γ_0 is constant after $t = 0^+$) and we will explain in more detail how we compute the main contribution of this term. We will compute

$$\frac{L(t)}{L_\infty} = \frac{-\frac{1}{U}\frac{d}{dt}\int_{-1}^{1}\gamma_0(x)dx + \Gamma_0 + \int_{1}^{\xi_m}\frac{\gamma(\xi)d\xi}{\sqrt{\xi^2-1}}}{-\frac{1}{U}\frac{d}{dt}\int_{-1}^{1}\gamma_0(x)dx + \Gamma_0 + \int_{1}^{\infty}\frac{\gamma(\xi)d\xi}{\sqrt{\xi^2-1}}}. \tag{3.33}$$

This is how we compute the contribution of the apparent mass: since this contribution comes only from a very small time interval around t=0, we consider the first time step a bit bigger, dt1=0.05. In this time interval we compute the apparent mass analytically by linearly varying the angle of attack from 0 to $\alpha = \pi/20$. As a consequence, we get

$$-\frac{1}{U}\frac{d}{dt}\int_{-1}^{1}\gamma_0(x)dx = -\frac{1}{U}\frac{d}{dt}\int_{-1}^{1} -2U_n\sqrt{\frac{1-x}{1+x}}dx =$$
$$2\frac{d}{dt}\sin(\alpha(t))\int_{-1}^{1}\sqrt{\frac{1-x}{1+x}}dx = 2\cos(\alpha(t))\alpha'(t)\int_{-1}^{1}\sqrt{\frac{1-x}{1+x}}dx,$$

where $\alpha'(t)$ will be the slope of the linear function going from 0 to $\pi/20$ in the interval dt1.

This is indeed a very nice way of verifying Wagner's result and it can be seen that the theoretical result (initial lift is half the final lift) and the numerical one (about 0.64)

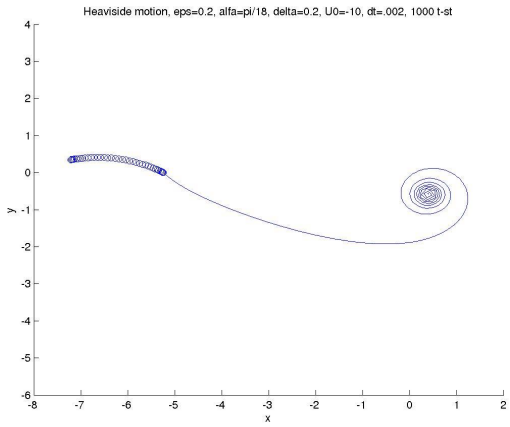

Figure 3.17: Heaviside Motion

are very close and that our numerical result is significantly better than some other ones. For instance Joseph Katz and Allen Plotkin (2001) get a result of about 0.85. Again, this demonstrates the robustness of Wu's method.

3.4.8 Analyzing the Lift for an Abrupt Heaviside Flexible Motion and an Abrupt Fourier Flexible Motion

Our theory provides new theoretical results. Similar to the case studied for the Wagner effect, one can analyze what happens when an abrupt Heaviside flexible motion is sought. In other words, at time $t = 0^-$ our wing coincides with the segment $[-1, 1]$ on Ox and at time $t = 0^+$ the wing undergoes abruptly a transformation that will deform it into a parabolic wing by $x(\xi) = \xi,\ y(\xi) = \epsilon(1 - \xi^2)\ for\ \xi\ \in\ [-1, 1]$. Then the wing is rotated with angle α with respect to the trailing edge, so that it will make an α incident angle with the flow. The rotation will transform the coordinates as follows

$$x^1 = 1 + \epsilon(1 - \xi^2)\sin(\alpha) - (1 - \xi)\cos(\alpha)$$
$$y^1 = \epsilon(1 - \xi^2)\cos(\alpha) + (1 - \xi)\sin(\alpha).$$

Hence, the outer normal will be given by $N(2\epsilon\xi\cos(\alpha) + \sin(\alpha), -2\epsilon\xi\sin(\alpha) + \cos(\alpha))$. Furthermore, the normal component of the fluid velocity reduces to

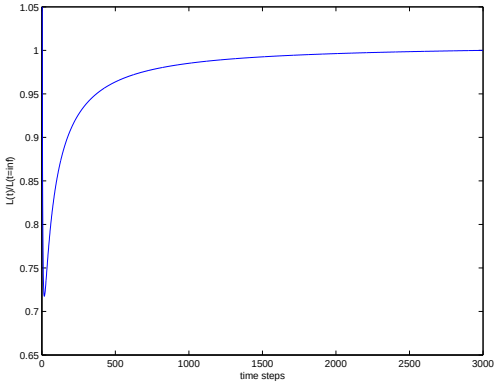

Figure 3.18: Behavior of Lift for a Heaviside Motion

$U_n = U_\infty \frac{2\epsilon\xi\cos(\alpha)+\sin(\alpha)}{\sqrt{1+4\epsilon^2\xi^2}}$.

Again, we get a very nice resolution of the vortex core (see Figure 3.17) while the behavior of the lift can be seen in Figure (3.18). The plots are obtained for deformation $\epsilon = 0.05$, angle of attack $\alpha = \pi/18$, blob $\delta = 0.2$, flow velocity $U_0 = -3.12$, time step $dt = 0.002$ and 10^3 time steps. This corresponds to the wing traveling 10 chord lengths to the left. The amplitude of deformation ($\epsilon = 0.05$) will give an effective angle of attack of approximately $\pi/18 + \pi/36 = \pi/12$ or 15 degrees.

The plot of the lift shows that in this case the initial lift would be about 0.72 of the final lift (see Figure 3.18) for this generalization of Wagner's result.

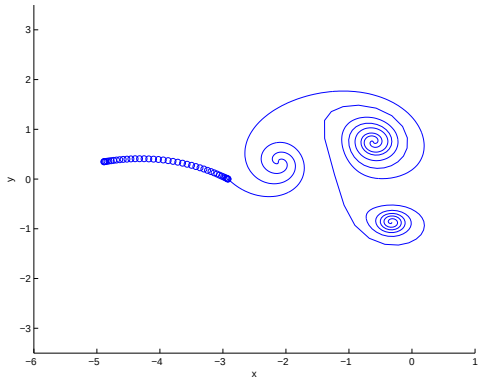

Figure 3.19: Fourier Motion

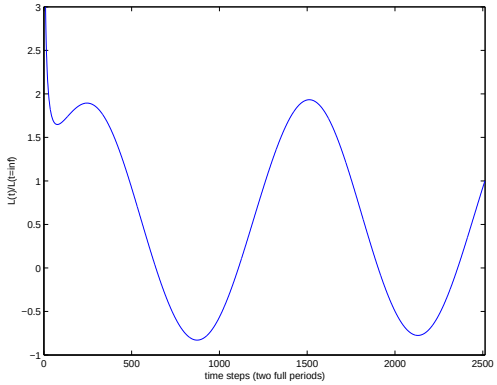

Figure 3.20: Behavior of Lift for a Fourier Motion

For the Fourier movement, the equation of the motion is similar to the one in the Heaviside case except that now, the amplitude of the deformation is variable, i.e. $\epsilon = \epsilon(t)$ where $\epsilon(t) = \epsilon_0 \cos(\omega t)$. The equations given above will remain the same up to this change. For the numerical simulations we chose $\epsilon_0 = 0.2$ and $\omega = 5$ so that after 1256 time steps (see Figure 3.19) the 2π period of the cosine has been covered. At a time step of $dt = 10^{-3}$ and a flow velocity of $U_0 = -3.12$ this corresponds to 2 chord lengths of flight.

Because of the periodic motion, the lift will also show periodicity. The effective angle of attack will be given by the chord angle (10 degrees) and the angle due to the wing curvature. For $\epsilon_0 = 0.05$ the angle due to curvature varies between ± 5 degrees which means that the effective angle of attack could be anywhere between around 15 degrees and 5 degrees. As a consequence, we expect to get lift during the motion. In Figure (3.20) it can be seen that the average lift is somewhere around 0.55 after two full periods.

Chapter 4

Three-Dimensional Model

This chapter will try to take the discussion even further and analyze the three dimensional model of a wing. We are not using a generalization of Wu's method, since this is still under research. Instead we use a panel-method combined with Krasny's vortex-blob method. The three-dimensional model we are using is a direct generalization of the two-dimensional vertically-moving flat plate studied in section (3.1.2). The modeling and simulations will use a square flat plate but we will justify our method by validating it in the next section against the two-dimensional model by using a rectangular very high-aspect ratio plate. We will assume again the presence of potential flow and the viscosity will be mimicked by the blob in the wake.

Now let's try to describe the method we are using. The main procedure is somehow similar to the two-dimensional case, however the equations are different. The idea is to form a linear system using the Biot-Savart law by imposing the normal flow conditions on the plate, and to determine the circulation of the plate filaments by solving this system. For that we will apply a rectangular mesh over the plate having more mesh points near the corners to give a better resolution. The mesh will form some panels on the wing and we will apply the no-through flow condition in the center of each one. After having computed the bound circulation for the panels, we will compute the circulation for each filament on the plate and then apply the two-dimensional method along all the longitudinal and transversal sections. The two-dimensional method will then compute the circulation of the currently shed vortex filament considering that a filament is shed at every time step along the mesh lines. The circulation of all the other free filaments will be preserved in time and therefore

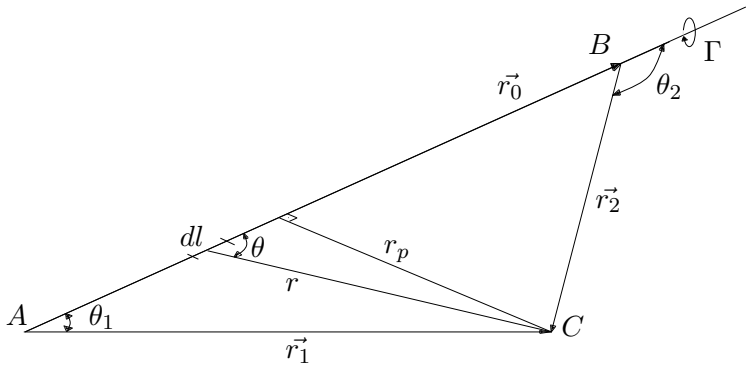

Figure 4.1: Velocity induced by vortex segment $\vec{AB}$ at location C.

having all the unknowns we could compute the velocities of all the free filaments. We then move these filaments to the updated locations and go to the next time step.

Bound Sheet It is known that the velocity induced by a vortex filament of strength Γ and a length of dl is given by the law of Biot and Savart

$$d\vec{V} = \frac{\Gamma(\vec{dl} \times \vec{r})}{4\pi r^3}. \tag{4.1}$$

From Figure (4.1) the magnitude of the induced velocity is

$$dV = \frac{\Gamma \sin\theta dl}{4\pi r^2}. \tag{4.2}$$

Since we are interested in the flow field induced by a straight segment, let us use the above equations to calculate this effect. Let AB be such a segment, with the vorticity vector directed from A to B. Let C be a point in space whose normal distance to line AB is r_p. Since

$$r = \frac{r_p}{\sin\theta} \qquad \text{and} \qquad dl = r_p(\csc^2\theta)d\theta, \tag{4.3}$$

we can integrate between A and B to find the magnitude of the induced velocity

$$V = \frac{\Gamma}{4\pi r_p}\int_{\theta_1}^{\theta_2} \sin\theta d\theta = \frac{\Gamma}{4\pi r_p}(\cos\theta_1 - \cos\theta_2). \tag{4.4}$$

Now let $\vec{r_0}, \vec{r_1}$ and $\vec{r_2}$ designate the vectors $\vec{AB}, \vec{AC}$ and $\vec{BC}$, respectively, as shown in Figure (4.1). Then

$$r_p = \frac{|\vec{r_1} \times \vec{r_2}|}{r_0}, \qquad \cos\theta_1 = \frac{\vec{r_0} \cdot \vec{r_1}}{r_0 r_1}, \qquad \cos\theta_2 = \frac{\vec{r_0} \cdot \vec{r_2}}{r_0 r_2},$$

where for a vector $\vec{r}$, we denote by r its magnitude. Substituting these expressions into equation (4.4) and noting that the direction of the induced velocity is given by the unit vector

$$\frac{\vec{r_1} \times \vec{r_2}}{|\vec{r_1} \times \vec{r_2}|},$$

we get

$$\vec{V} = \frac{\Gamma}{4\pi} \frac{\vec{r_1} \times \vec{r_2}}{|\vec{r_1} \times \vec{r_2}|^2} \left[\vec{r_0} \cdot \left(\frac{\vec{r_1}}{r_1} - \frac{\vec{r_2}}{r_2} \right) \right]. \tag{4.5}$$

Now in order to implement this, we write the components of the induced velocity $V = (u, v, w)$

$$\begin{cases} u = K \cdot (r_1 \times r_2)_x \\ v = K \cdot (r_1 \times r_2)_y \\ w = K \cdot (r_1 \times r_2)_z \end{cases}, \qquad K = \frac{\Gamma}{4\pi |r_1 \times r_2|^2} \left(\frac{r_0 \cdot r_1}{r_1} - \frac{r_0 \cdot r_2}{r_2} \right) \tag{4.6}$$

with

$$\begin{cases} r_0 \cdot r_1 = (x_2 - x_1)(x_p - x_1) + (y_2 - y_1)(y_p - y_1) + (z_2 - z_1)(z_p - z_1), \\ r_0 \cdot r_2 = (x_2 - x_1)(x_p - x_2) + (y_2 - y_1)(y_p - y_2) + (z_2 - z_1)(z_p - z_2) \end{cases} \tag{4.7}$$

and $|r_1 \times r_2|^2 = (r_1 \times r_2)_x^2 + (r_1 \times r_2)_y^2 + (r_1 \times r_2)_z^2$,

$$\begin{cases} r_1 = \sqrt{(x_p - x_1)^2 + (y_p - y_1)^2 + (z_p - z_1)^2}, \\ r_2 = \sqrt{(x_p - x_2)^2 + (y_p - y_2)^2 + (z_p - z_2)^2}, \end{cases} \tag{4.8}$$

and finally

$$\begin{cases} (r_1 \times r_2)_x = (y_p - y_1)(z_p - z_2) - (z_p - z_1)(y_p - y_2), \\ (r_1 \times r_2)_y = -(x_p - x_1)(z_p - z_2) + (z_p - z_1)(x_p - x_2), \\ (r_1 \times r_2)_z = (x_p - x_1)(y_p - y_2) - (y_p - y_1)(x_p - x_2). \end{cases} \tag{4.9}$$

We will consider a 2 by 2 square plate and a $N * N$ point-mesh on it, with N odd so

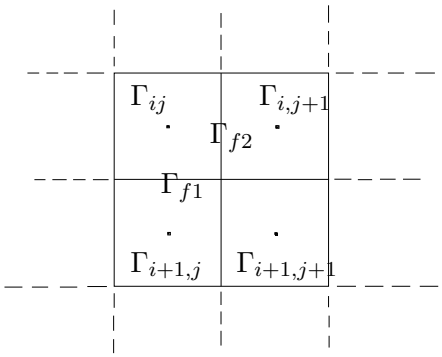

Figure 4.2: Computing the filament circulations from the panel circulations.

that a vortex point will be placed in the center of the plate. By imposing the no-through flow conditions in the center of the mesh panels we will get $(N-1)^2$ linear equations using formula (4.5). To each panel we assign a circulation Γ_{ij}. However, in order to be able to construct this linear system we should rearrange this circulation matrix into an array using a natural counting method from right to left and from up to down. At time $t = 0^+$, before anything is shed into the free sheet, the linear system will look like this

$$\begin{aligned}
&a_{11}\Gamma_1 + a_{12}\Gamma_2 + a_{13}\Gamma_3 + \ ... \ + a_{1,(N-1)^2}\Gamma_{(N-1)^2} = U_0 \\
&a_{21}\Gamma_1 + a_{22}\Gamma_2 + a_{23}\Gamma_3 + \ ... \ + a_{2,(N-1)^2}\Gamma_{(N-1)^2} = U_0 \\
&... \\
&a_{(N-1)^2,1}\Gamma_1 + a_{(N-1)^2,2}\Gamma_2 + a_{(N-1)^2,3}\Gamma_3 + \ ... \ + a_{(N-1)^2,(N-1)^2}\Gamma_{(N-1)^2} = U_0.
\end{aligned} \tag{4.10}$$

Whenever we compute the velocity induced by a panel on a certain point (centers of the panels), we will add the contribution from each segment filament bordering the considered panel so every segment will give two contributions. One segment filament will enter the calculations from both panels it belongs to, having the circulations assigned to those panels. Therefore, after inverting the matrix and solving the system, we have to recalculate the circulation of each bound filament. Thus, the circulation of a certain filament will be given by the difference of the circulations of the panels the filament borders. To do this, we will

have to reconstruct the circulation matrix from the circulation array obtained by solving the system. As in Figure (4.2) we will get

$$\Gamma_{f1} = \Gamma_{i,j+1} - \Gamma_{ij}, \quad \text{and} \quad \Gamma_{f2} = \Gamma_{i+1,j} - \Gamma_{ij}. \tag{4.11}$$

We are doing this because the velocity induced by a filament is taken into consideration two times, one time for every panel it belongs to. When we are at the edge, the circulation for the corresponding missing panel will be considered zero.

Free Sheet We found a very simple and elegant way to solve for the free sheet. At this point we know how to solve for all the quantities on the bound sheet. We do know the circulation along all the chord-wise and span-wise sections. From now on, we will switch to the two-dimensional method and apply it for all these sections with the given steady-state bound circulation, imported from the three-dimensional model. As in Section (3.1.2), we will compute for every such two-dimensional slice the sheet strength value at the edge γ_e, which will give us the slip velocities at both edges $\overline{U}$. Furthermore, we will compute the slip velocities above and below the edge and impose the non-attached slip flow condition. With the updated slip velocities we will recompute $\overline{U}$, which is now the velocity of the currently released vortex filament, and also the circulation of this free vortex from (2.22).

Having all the information about the first free vortex element we can now move it according to $\overline{U}$. Going to the next time steps, we will solve the corresponding section's two-dimensional linear system. However, from now on the contributions from the previously released free vortices will enter the system. Their circulation will be known since it is preserved in time, and therefore we can write the system as

$$A\tilde{\Gamma} = \tilde{b}, \tag{4.12}$$

where A is the matrix of coefficients from the two-dimensional model, $\tilde{\Gamma}$ is the new bound circulation to be computed, and $\tilde{b}$ is the known vector, including the circulation induced by the free vortex elements. We can look at this system as a perturbed system from its original state. Consider $\tilde{b} = b + \delta b$, where b is the vector from time step one consisting only

of the imposed normal velocities, to which we add some perturbation δb which is in fact the velocity induced by the free vortices. Then, we can also write $\tilde{\Gamma} = \Gamma + \delta\Gamma$, where Γ is the wake-less bound circulation imported from the three-dimensional model. Hence we get

$$A(\Gamma + \delta\Gamma) = b + \delta b. \tag{4.13}$$

But A, Γ and b solve the initial linear system at time $t = 0$ so $A\Gamma = b$ and therefore (4.13) becomes

$$A \cdot \delta\Gamma = \delta b. \tag{4.14}$$

Solving this system we get $\delta\Gamma$ and hence the new bound circulation $\Gamma + \delta\Gamma$. All the other quantities: the edge strength, the slip velocities and the velocities of the free vortices, are computed at every time step from the two-dimensional model, using the known bound circulation.

4.1 Validation of the Three-Dimensional Model Using the Two-Dimensional Results

To verify the accuracy of our three-dimensional model, we try to compare our results with the ones obtained in the two-dimensional formulation. One way to do that would be to take a very high aspect-ratio wing and check what happens in the middle section. Since the wing is very long, the fact that it is finite should have very little influence in the center and we expect the center section to behave very similar to the two-dimensional plate we studied in Section (3.1.2). We analyze a three-dimensional plate of length 62 and width 2. The mesh consists of 31x31 points and they are placed according to some cosine distribution so that we have more points in the corners and therefore better accuracy. We will compare the steady-state circulation (no wake influence) of the center section of this plate with the two-dimensional model which has a length of 2 and a mesh of 31 points as well. The wings will advance upwards with a speed $U = 1$.

Figure (4.3) (a) shows the wing and the section we are considering and part (b) shows

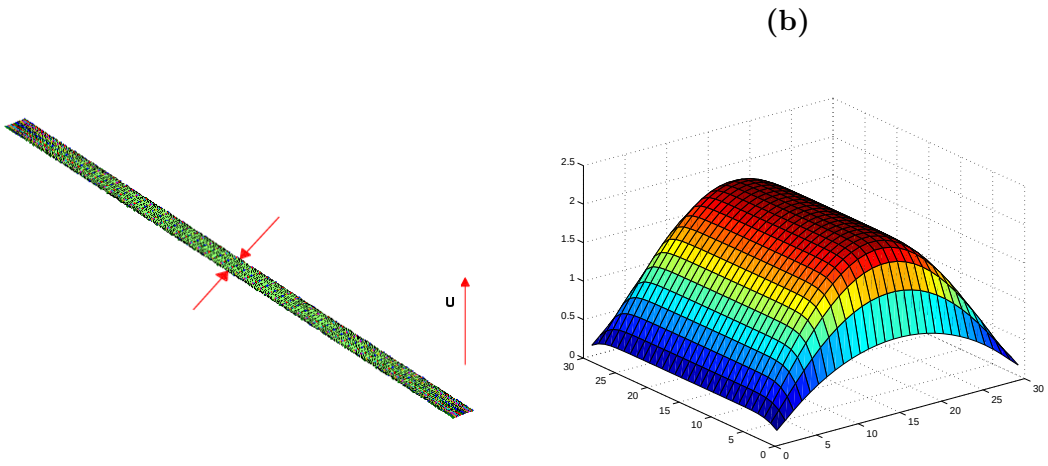

Figure 4.3: (a) three-dimensional high aspect ratio wing and section considered; (b) Plot of steady-state circulation as given by Equation (4.5).

what the steady-state circulation looks like on the wing. This is to be understood in the sense of Equation (4.5). To get similar results to the two-dimensional case we have to use Equation (4.11) and compute the circulation of the filaments on the section considered. Plotting this on top of the two-dimensional circulation (see Figure (4.4) plot (a)) we get results so close they cannot be differentiated just by the plots. The norm of their difference is very small, $2.4842 \cdot 10^{-4}$ however it is bigger than computer precision which shows the presence of the three-dimensional effect.

Plot (b) in Figure (4.4) shows the circulation in the section which is closest to the edge of the wing in a chord-wise section. We can notice that even though the shape looks similar, the absolute value of the circulation of the filaments is lower than in the center section, being about half the later. Plot (c) shows the circulation along the center section in a span-wise plane, and this is quite different than the other two. The circulation being very small for the main part of this section shows that the edge effects become very small as we go further from the plate's edges. In fact it says that only about 22% of the plate near every edge will feel the finite-wing effect. The last plot, (d), gives the circulation on the plate for a section near the edge in a span-wise plane. Note that this is significantly smaller than the circulation for the corresponding center section, being about 6 times smaller. In conclusion, our model proves to be very accurate when compared with the two-dimensional one and

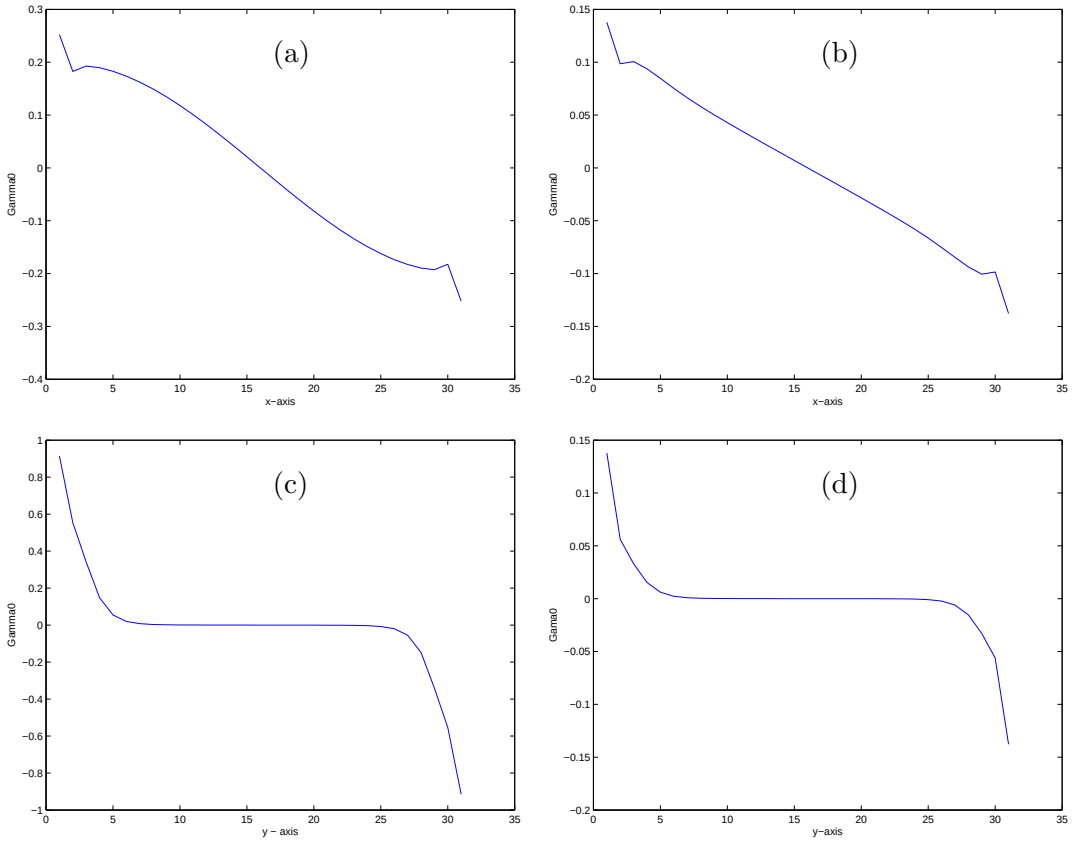

Figure 4.4: (a)&(b) chord-wise sections; (c)&(d) span-wise sections; (a) Superposition of circulation obtained in the two-dimensional case and the one obtained in the three-dimensional center chord-wise section; (b) Circulation obtained in the three-dimensional case, on an edge chord-wise section; (c) Circulation for the three-dimensional case on the central span-wise section; (d) Circulation for the three-dimensional case on an edge span-wise section.

plots (b), (c) and (d) show how important the three-dimensional effect is in the motion of the plate, especially at the edges. They also show that the finite-plate effect tends to reduce the vorticity in the near-edge cross sections compared to the center ones.

4.2 Numerical Results vs. Experiment for a Rectangular Wing

In this section we will try again to refer to more concrete examples taken from nature. To do that we will try to consider some wings with aspect ratios (AR) found in various birds and insects. Aspect ratio here will be defined as b^2/S, where b is the span of a single wing,

instead of the conventional definition, which is the distance between both wing tips; S is the single-wing plan-form (top-view) area.

Flying insects have AR's between about 2.75 and almost 6 (Ellington [1984] & Dickinson [1999]) while hummingbirds have AR's of around 4 (Dhawan [1991]); a soaring bird, such as albatross, has an AR of about 9 (Dhawan [1991]). A finite aspect-ratio wing, compared to one of infinite span, experiences aerodynamic effects due to the tip, which increase relatively as the aspect ratio decreases. Therefore for low aspect ratio wings the influence of the tip is very significant.

In this chapter we will refer extensively to the experiments done by Ringuette (see Ringuette [2004]) in the GALCIT towing tank at California Institute of Technology. Given the aspect ratios found in insects and hummingbirds mentioned above, he made some experiments with flat plates of rectangular planforms, having $AR = 2$ and $AR = 6$. Next, we will compare these experiments with the result obtained with our numerical method.

One thing the reader should be aware of is the presence of vortex separation in Ringuette's work. He argues that the circulation of the vortex ring does not grow indefinitely. Therefore, the experiments will show separation which happens at a time called "formation number". Formation number is the non-dimensional time at which a vortex achieves its maximum circulation before pinch-off. Pinch-off occurs when a vortex is no longer being fed by the shear-layer that generated it and the two become distinct entities in terms of vorticity. This separation was found in the experiment, however the numerical method is unable to observe it. Of course, if we wanted to mimic the experiment even better we could artificially detach the leading edge vortex (LEV) in our numerical method and let another one begin forming.

Aspect Ratio 2 For a wing of aspect ratio 2, the effects due to the tip are more prevalent then in the $AR = 6$ case. It can be seen from Figure (4.5) that the vortices near both chord-wise and span-wise center sections have more roll-ups than the ones near the corresponding edges. This is in perfect agreement with what we found in a previous section, where we showed (see Figure (4.4)) that there is more circulation near the bound center sections than near the edges. This will imply that less circulation is shed in the free sheet near the edges, making the vortices weaker. Also from the same plots (see Figure (4.4)) we expect

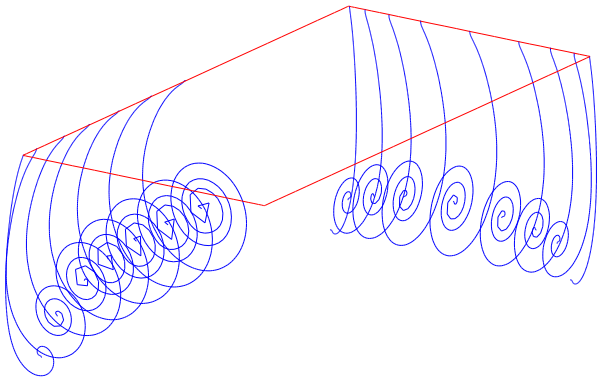

Figure 4.5: Wake shape for $AR = 2$.

the vortices to be stronger along the chord wise sections compared to those released along span-wise sections since the corresponding total circulation is bigger.

In both numerical and experimental setup a plate with chord $c = 5$ and aspect ratio $AR = 2$ is used (for the experiment the measuring unit was centimeter). The plate velocity is $U_0 = 6$ and for the numerical method we choose a time step of $dt = 0.003$ and a blob $\delta = 0.2$. Our numerical bound sheet is represented by a 31x31 point mesh.

In Figure (4.6) we make a comparison between the experiment (plot (a)) and our numerical method (plot (b)). We plot here the total circulation of a chord-wise section in the wake versus the formation time. The formation time is a non-dimensional time defined as $t_{form} = U_0 \cdot t/c$ where c is the chord. The plots are for three different chord-wise sections: triangles denote the circulation at 50% of span, circles at 75% of span and diamonds at 90% of span. It can be seen that the plots look very similar until the pinch-off occurs. After that, the circulation from the experiment would not grow as fast anymore and trail after the numerical results. This can be seen even better in Figure (4.7).

Plots (a) and (b) show the total circulation at 50% span from experiment and numerical method, respectively. We can see that the plots are identical until about formation time

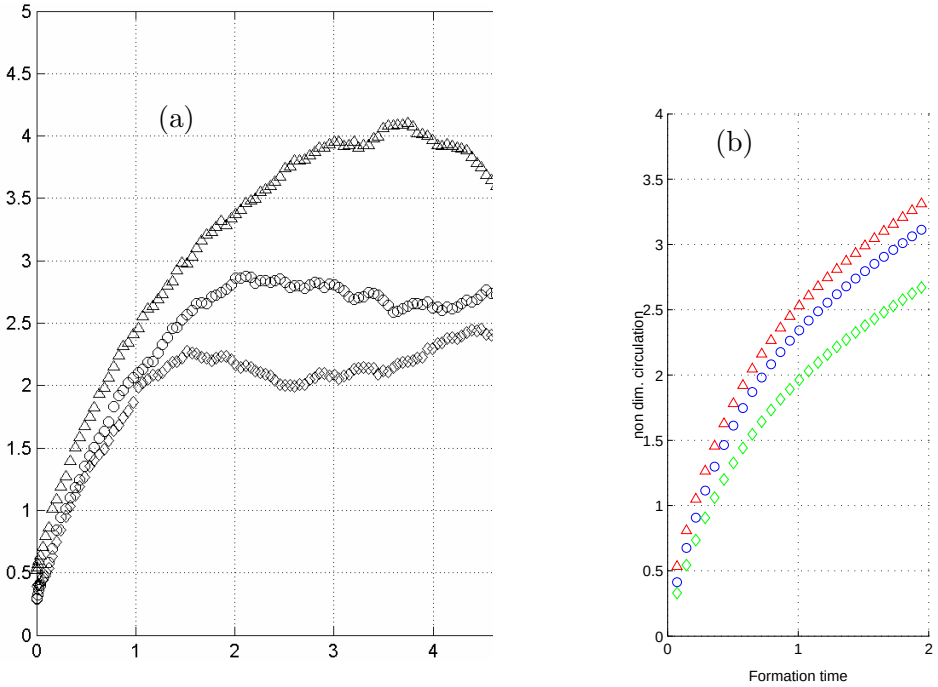

Figure 4.6: Circulation vs. formation time from (a) Ringuette's experiment and (b) numerical method, for $AR = 2$, triangles - 50% span, circles - 75% span, diamonds - 90% span.

$t_{form} = 3$, i.e., until the plate has traveled three chord lengths. Accordingly, plots (c) and (d) show the circulation at 75% span while (e) and (f) show the circulation at 90% span. On the right is always the experimental result. We can see that for the 75% case the similarity goes up to $t_{form} = 2$ while in the 90% case up to $t_{form} = 1.5$. On the left, we also have the shapes of the corresponding sections taken from the experiment at given formation times.

Aspect Ratio 6 For a wing of aspect ratio 6, the effects due to the tip are less significant than in the $AR = 2$ case. It can be seen from Figure (4.8) that the vortices near both chord-wise and span-wise center sections have more roll-ups than the ones near the corresponding edges. This is, again, in perfect agreement with what we found in a previous section, where it was showed (see Figure (4.4)) that there is more circulation near the bound center sections than near the edges. This implies that less circulation is shed in the free sheet near the edges, making the vortices weaker. However, in this case this can be seen better along span-wise sections due to the higher aspect ratio plate. Also, from the same plots (see Figure (4.4)) we expect the vortices to be stronger along the chord wise sections compared to those

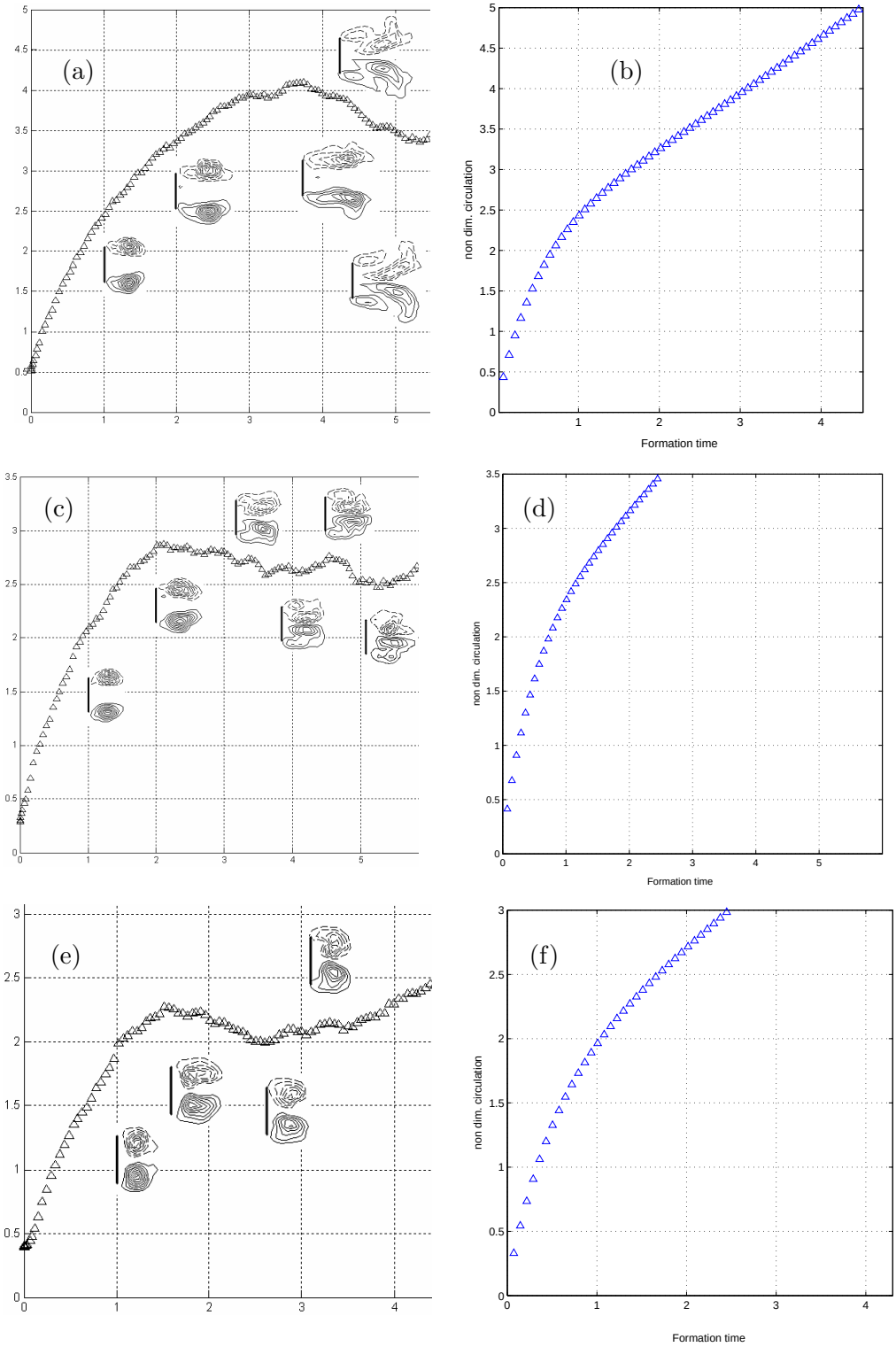

Figure 4.7: Total circulation versus formation time for $AR = 2$. Left column - Ringuette's experiment results, right column - our numerical results. (a)&(b) 50% span, (c)&(d) 75% span, (e)&(f) 90% span.

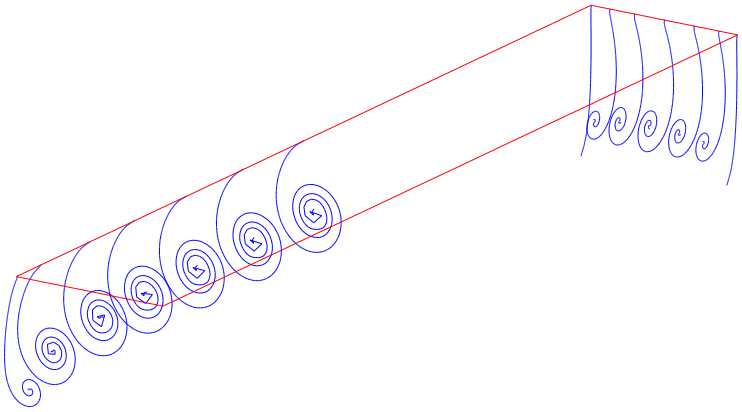

Figure 4.8: Wake shape for $AR = 6$.

released along span-wise sections since the corresponding total circulation is bigger. This is obviously more pronounced here than in the $AR = 2$ case.

In both numerical and experimental setup, a plate with chord $c = 5$ and aspect ratio $AR = 6$ is used (for the experiment the measuring unit was centimeter). The plate velocity is $U_0 = 6$, and, for the numerical method, we choose a time step of $dt = 0.003$ and a blob $\delta = 0.2$. Our numerical bound sheet is represented by a 31x31 point mesh.

In Figure (4.9) we make a comparison between the experiment (plot (a)) and our numerical method (plot (b)). We plot here again the total circulation of a chord-wise section in the wake versus the formation time. The plots are for three different chord-wise sections: triangles denote the circulation at 50% of span, circles at 75% of span and diamonds at 90% of span. It can be seen that the plots look very similar until the pinch-off occurs. After that, the circulation from the experiment would not grow as fast anymore and trail after the numerical results. This can be seen even better in Figure (4.10).

Plots (a) and (b) show the total circulation at 50% span from experiment and numerical method, respectively. We can see that the plots are identical all the way up to formation time $t_{form} = 4.5$, i.e., until the plate has traveled four and a half chord lengths. Accordingly,

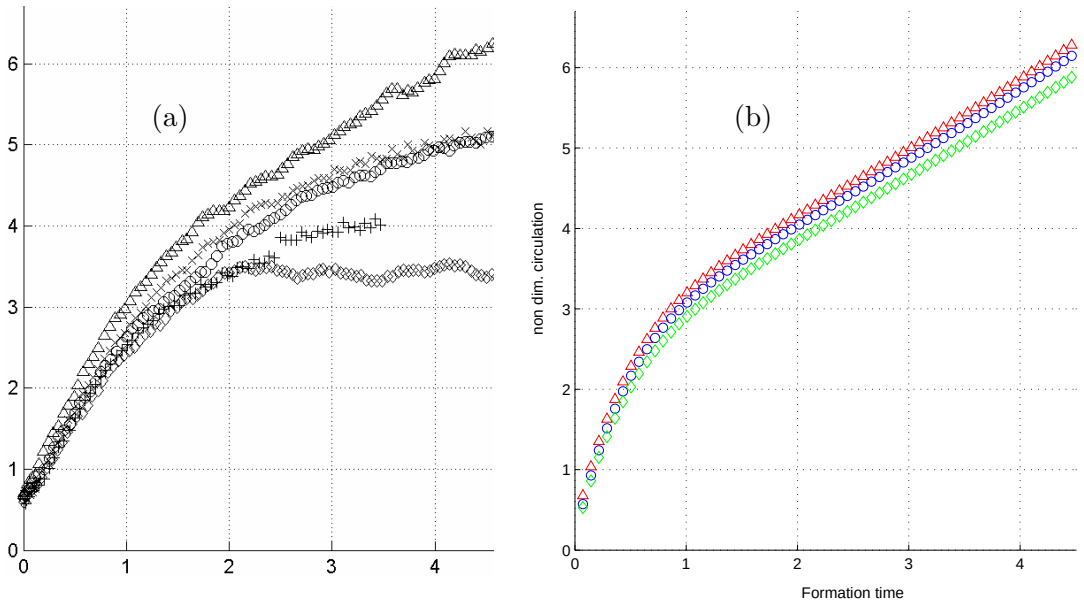

Figure 4.9: Circulation vs. formation time from (a) Ringuette's experiment and (b) numerical method, for $AR = 6$, triangles - 50% span, circles - 75% span, diamonds - 90% span.

plots (c) and (d) show the circulation at 75% span, while (e) and (f) show the circulation at 90% span. On the right is always the experimental result. We can see that for the 75% case the similarity goes up to $t_{form} = 3$ while in the 90% case up to $t_{form} = 2$. On the left, we also have the shapes of the corresponding sections taken from the experiment at given formation times. The plot of the circulation of the leading edge vortex is also included in some of these plots (x's and/or crosses). One can see that after a while the circulation of this LEV will trail the total circulation, implying separation.

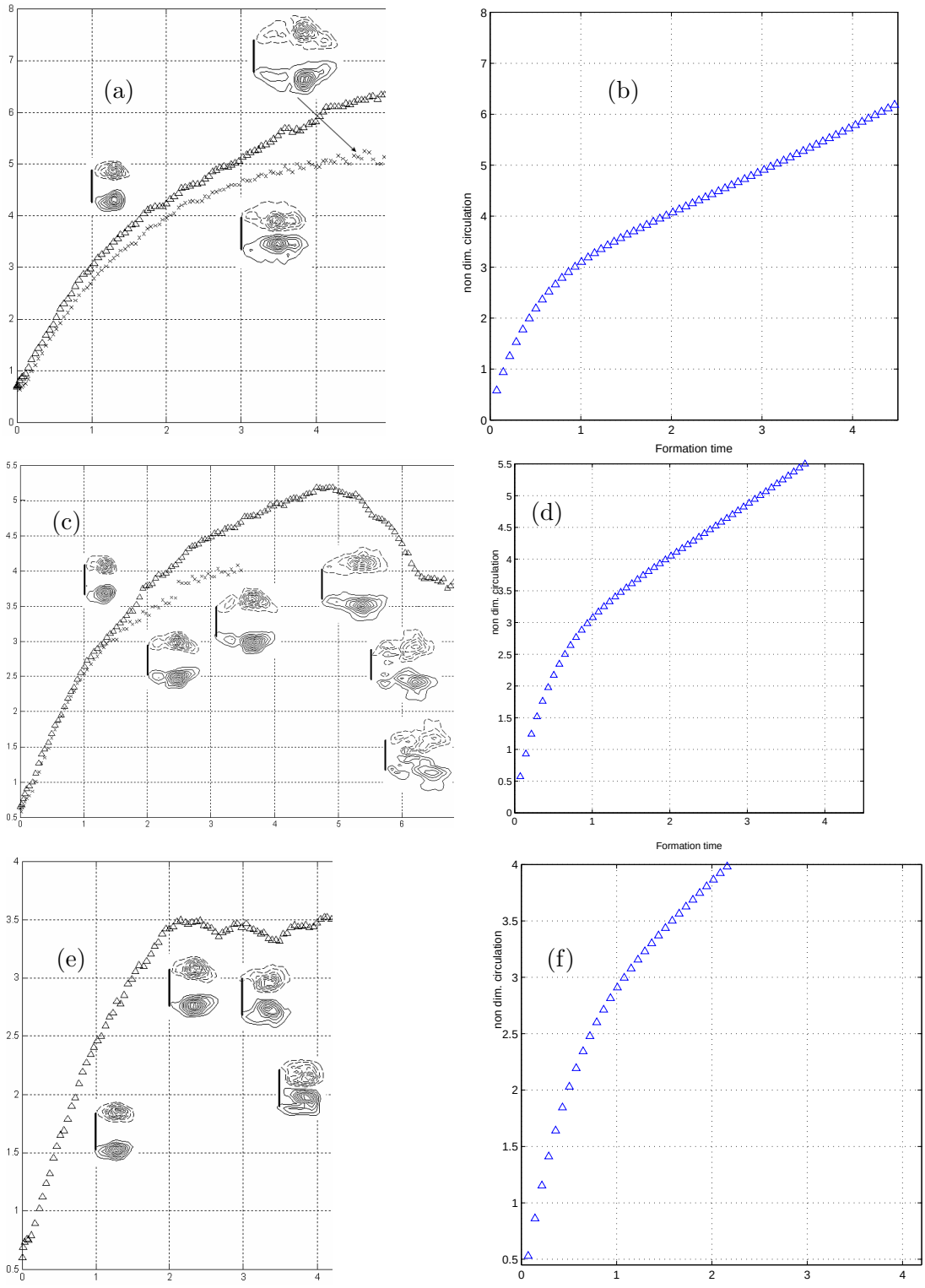

Figure 4.10: Total circulation versus formation time for $AR = 6$. Left column - Ringuette's experiment results, right column - our numerical results. (a)&(b) 50% span, (c)&(d) 75% span, (e)&(f) 90% span.

4.3 Numerical Results for a Three-Dimensional Square Wing

We thought it would be interesting to post here the numerical results for a square plate when $AR = 1$. Of course, in this case the finite-wing effects are the strongest. Unfortunately we couldn't find an experiment to match the square plate model but based on the previous comparisons for $AR > 1$ we are very confident our results are correct.

For the numerical simulations, we choose a square plate of length 2 represented by a 31x31 point mesh. The plate is moving upwards with a velocity $U_0 = 1$ and data is collected every $dt = 0.01$ time step. The blob again is chosen to be $\delta = 0.2$, and the code is stopped after 400 time steps. This is equivalent to a formation time of 4.

In Figure (4.11) (a)&(b), we plot a quarter of the wake. Of course, the wake will be symmetrical. From this plots we can see very well how the increased circulation shed in the wake near the center sections makes the vortices stronger, with more roll-ups, while the vortices near the edges are weaker with fewer roll-ups. Due to the lack of circulation, the edge vortices are more elongated because the normal velocity is dominant. Plots (a) and (b) are similar, with the only difference that in plot (b) we have half as many vortices as in (a) for a better visualization.

Figure (4.12) contains a plot similar to the ones we have already seen in $AR = 2$ and $AR = 6$ cases: total circulation versus formation time. This time though, due to the more powerful finite-wing effects, the separation between the three curves ($\triangle$'s - 50% span, $\circ$'s - 75% span and $\diamond$'s - 90% span) is even more accentuated.

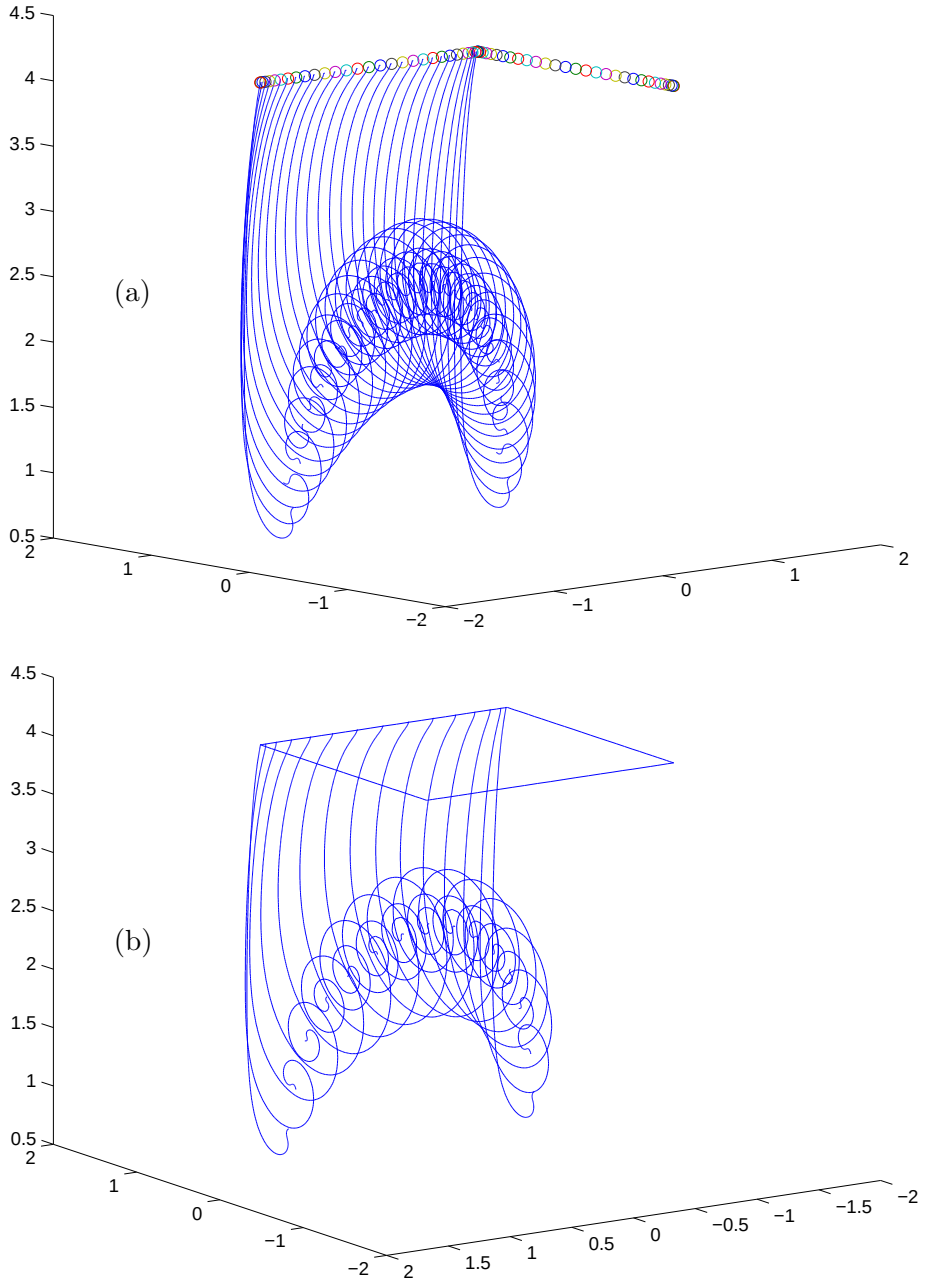

Figure 4.11: Wake shape in the case of a square plate. (a) has twice as many vortices as (b).

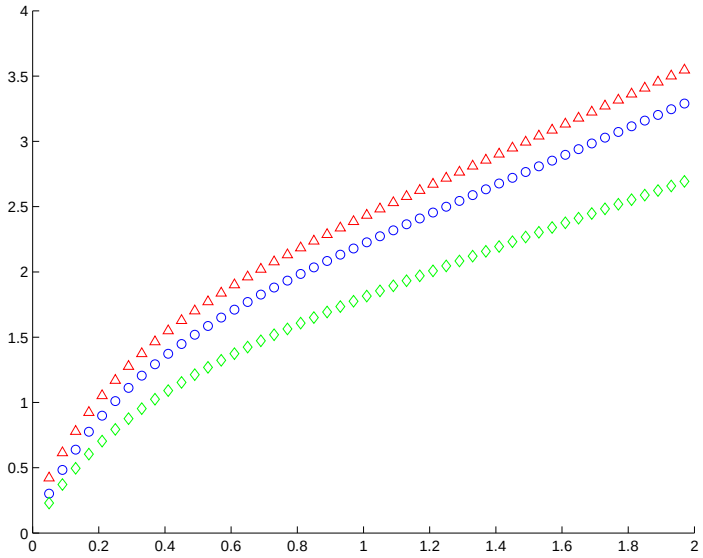

Figure 4.12: Circulation vs. formation time - numerical results, for $AR = 1$, triangles - 50% span, circles - 75% span, diamonds - 90% span.

Chapter 5

Concluding Remarks and Future Directions

Concluding Remarks The main goal of this thesis was to get more insight into fish and bird locomotion. Even though the topic is incredibly vast, we tried to explain some features found in nature, such as the effect of the trailing wake on the thrust and lift. This was done using the new and efficient method of Professor Wu which we demonstrated to be more reliable than the previous ones.

The new method can better capture the leading singular effect near the trailing edge, which improves the accuracy when dealing with some high nonlinear movements. The vorticity blows up near the the first released vortex element, and the analytical analysis provided by our method succeeds in better resolving this issue. We showed that the current method is better than the other methods when verifying Wagner's result. We also discussed the convergence of the outer wake and were able to demonstrate that using a blob in Wu's method did not affect its accuracy, since the method is more dependent on the time step than on the blob size. All the results compared very well with the experiments, and the method showed a great deal of robustness and accuracy on all the models and simulations we tried it on. When compared to Davenport's experiment, Wu's method gives a much better position and size of the outer wake than Krasny's method.

The three-dimensional model presented here is just a start for what could be an analysis of the same depth as the two-dimensional one. We consider it just a teaser for the reader and a good start for a better understanding of the natural three-dimensional movement. The current method shows some very nice behavior compared with the experiment and

demonstrates how efficient a direct generalization of the two-dimensional theory could be when some three-dimensional considerations are also taken into account.

Future Directions There are several directions to follow in the future to continue what we have started here.

We began working on this project fascinated by Gray's paradox. He proved in 1936 that given the muscle power and the frictional drag experienced during the motion, a fish could not swim as fast as some of the species do. One explanation for this might be the effect of the vortices released by the lateral fins on the tail fin. The tail fin could just take advantage of this vorticity present in the fluid and generate a greater thrust for the fish. Another unexplained fish behavior would be the extremely rapid U-turn a trout, for example, could make when approaching a wall at very high speed. All these examples involve extremely nonlinear motions and require some very fine mathematical analysis. We are confident that the new method presented in this thesis could help in solving some of these mysteries. The two-dimensional, semi-analytical approach of Professor Wu could capture these sensible details when dealing with highly-curved movements and wake-crossing maneuvers by S_b.

From a technical point of view, it would be a big step forward to better understand the necessity of the numerical blob, and to try to develop a numerical method that avoids using it, therefore becoming even more precise.

In three dimensions, our method already captures a lot of the experimental details, and therefore it could be a very good start for developing a more sensitive mathematical model. Just like in two dimensions, where we started with Krasny's method just to help in developing Wu's approach, this three-dimensional model could provide the basis for a further investigation of a possible generalization of Wu's method in three dimensions. This may be a very difficult theoretical task, but it could lead to some very nice results. However, even the further development of the present method could bring some valuable information about the three-dimensional flight. The idea of a three dimensional wing advancing at a given angle of attack with the finite-wing effects taken into consideration is extremely tempting especially for the visualization and effects of the trailing wake. A more immediate task would be to model and understand the helical pattern observed by Ringuette in 2004

in the corner regions of a three-dimensional plate advancing perpendicular to the flow.

Appendix A

Cauchy Integral Equation of the First Kind

Lemma. *The solution of the Cauchy integral equation of the first kind,*

$$\frac{1}{\pi\imath}\fint_{-1}^{1}\frac{\phi(y)}{y-x}dy = 1 \quad is \quad \phi(y) = \imath\sqrt{\frac{1+y}{1-y}}, \quad for\ any\ y \in (-1,1).$$

Proof. Let's define

$$\Phi(z) = \frac{1}{2\pi\imath}\fint_{-1}^{1}\frac{\phi(y)}{y-z}dy,$$

and assume that the solution is Hölder continuous, so that the Plemelj formulas (see Muskhelishvili [1946], §17, eq. (17.2)) apply

$$\Phi_{\pm}(x) = \pm\frac{\phi(x)}{2} + \frac{1}{2\pi\imath}\fint_{-1}^{1}\frac{\phi(y)}{y-x}dy.$$

Since

$$\Phi_{+}(x) + \Phi_{-}(x) = \frac{1}{\pi\imath}\fint_{-1}^{1}\frac{\phi(y)}{y-x}dy = 1 \tag{A.1}$$

$$and \quad \Phi_{+}(x) - \Phi_{-}(x) = \phi(x), \tag{A.2}$$

the task of solving the integral equation becomes that of solving (A.1), which is an inhomogeneous multiplicative Riemann-Hilbert problem.

To find an analytic function satisfying (A.1), we first try to find a function that satisfies

the homogeneous version of this problem. Let $\Phi(z) = H(z)\Psi(z)$, where

$$H_+(x) + H_-(x) = 0$$

across the interval [-1,1]. We rearrange this equation and apply a logarithm to turn it into an additive Riemann-Hilbert problem

$$\log H_+(z) - \log H_-(x) = \imath\pi.$$

The solution to this additive problem is

$$\begin{aligned} \log H(z) &= \frac{1}{2\pi\imath}\int_{-1}^{1}\frac{\imath\pi}{\xi - z}d\xi + k(z) \\ &= \frac{1}{2}\log(\xi - z)\Big|_{\xi=-1}^{\xi=1} + k(z) \\ &= \frac{1}{2}\log\left(\frac{z-1}{z+1}\right) + k(z), \end{aligned}$$

where $k(z)$ is any entire function. We will not have any need for $k(z)$ in this problem so we set $k(z) = 0$, but it is sometimes helpful to choose an appropriate $k(z)$ to make later calculations more convenient. We have now determined that

$$H(z) = \sqrt{\frac{z-1}{z+1}}.$$

Since we want $H(z)$ to have a branch cut along the interval [-1,1], let's restrict $\arg(z-1)$ and $\arg(z+1)$ to $[0, 2\pi)$. This choice of angle restriction produces

$$H_\pm(x) = \lim_{y\to 0^\pm} H(x + \imath y) = \pm\imath\sqrt{\frac{1-x}{1+x}}.$$

(Of course, $H(z)$ satisfies $H_+(x) + H_-(x) = 0$.)

Knowing $h(z)$ allows us to turn the original inhomogeneous multiplicative Riemann-Hilbert problem into an additive one. Substituting $\Phi_\pm(x) = H_\pm(x)\Psi_\pm(x)$ into (A.1) and

rearranging, we obtain

$$\Psi_+(x) - \Psi_-(x) = \frac{1}{H_+(x)} = -\imath\sqrt{\frac{x+1}{1-x}}.$$

We use the Discontinuity Theorem to find $\Psi(z)$.

$$\begin{aligned}
\Psi(z) &= \frac{-\imath}{2\pi\imath}\int_{-1}^{1}\sqrt{\frac{\xi+1}{1-\xi}}\frac{d\xi}{\xi - z} \\
\boxed{\text{Let } t = \sqrt{(\xi+1)(1-\xi)}.} &= \frac{2}{\pi(z-1)}\int_0^\infty \frac{t^2 dt}{(t^2+1)(t^2+\frac{z+1}{z-1})} \\
\boxed{\text{Decompose fractions}} &= \frac{1}{\pi(z-1)}\int_0^\infty \left[\frac{z+1}{t^2+\frac{z+1}{z-1}} - \frac{z-1}{t^2+1}\right] dt \\
\boxed{\text{Use } \textstyle\int_0^\infty dx/(x^2+a^2) = \pi/(2a).} &= \frac{1}{2(z-1)}\left[(z+1)\sqrt{\frac{z-1}{z+1}} - (z-1)\right] \\
&= \frac{1}{2}\left[\sqrt{\frac{z+1}{z-1}} - 1\right].
\end{aligned}$$

Using the same angle restrictions as before, we find that

$$\Psi_\pm(x) = \frac{1}{2}\left[\mp\imath\sqrt{\frac{x+1}{1-x}} - 1\right].$$

Now all that remains is to recall that $\Phi_\pm(x) = H_\pm(x)\Psi_\pm(x)$ and work through some algebra to obtain the solution to the integral equation,

$$\phi(x) = \Phi_+(x) - \Phi_-(x) = -\imath\sqrt{\frac{1-x}{x+1}}.$$

■

Bibliography

Abbott, I. H. and Doenhoff, A. E. von [1958], Theory of wing sections, *Dover Publications, Inc. New York*.

Anderson, J. D. Jr. [2001], Fundamentals of aerodynamics, *McGraw-Hill Higher Education*, 3^{rd} edition.

Baker, R. G., D. I. Meiron, S. A. Orszag [1982], *Journal of Fluid Mechanics* **123**, 477–501

Baker, R. G., J. T. Beale [2004], Vortex blob methods applied to interfacial motion, *J. Comput. Phys.*, **196**, 233–258

Batchelor, G. K. [1990], An introduction to fluid dynamics, *Cambridge University Press*.

Beale, J. T. [2004], A grid-based boundary integral method for elliptic problems in three dimensions, *SIAM J. Numer. Anal.* textbf42, 599–620

Bertin, J. J., M. L. Smith [1979], Aerodynamics for engineers, *Prentice-Hall, Inc., Englewood Cliffs, New Jersey*.

Brady, M., A. Leonard, D. I. Pullin [1998], Regularized vortex sheet evolution in three dimensions, *Journal of Computational Physics* **146**, 520–545

Bratt, J. B. [1953], Flow patterns in the wake of an oscillating airfoil, *Aeronautical Research Council, R&M* **1773**

Breguet, L. [1925], Le vol a voile dynamique des oiseaux; analyse des effets des pulsations du vent sur la resultante aerodynamique moyenne d'un planeur, *Paris, Gauthier-Villars*.

Bulirsch, R. [1965], Numerical calculation of elliptic integrals and elliptic functions, *Numerische Mathematik* **7**, 78–90

Chamara, P. A., B. D. Coller [2001], Double flutter in an aeroelastic system, *AIAA Journal* **39**

Chorin, A. J. and Bernard, P. S. [1973], Discretization of a vortex sheet, with an example of roll-up, *J. Comput. Phys.* **13**, 423

Davenport, W. J., M. C. Rife, S. I. Liapis, G. J. Follin [1995], The structure and development of a wing-tip vortex, *Journal of Fluid Mechanics* **312**, 67–106.

Dhawan, S. [1991], Bird flight, *Bangalore: Indian Academy of Sciences.*

Dickinson, M. H., F. O. Lehmann, S. P. Sane [1999], Wing rotation and the aerodynamic basis of insect flight, *Science* **284**, 1954–1960.

Didden, N. [1979], On the formation of vortex rings: rolling up and production of circulation, *Z. Angew. Math. Phys.* **30**,101

Durand, W. F. [1943], Aerodynamic theory, *Pasadena, Calif. : California Institute of Technology, 1943.*

Earls, K. D. [2000], Kinematics and mechanics of ground take-off in the starling Sturnis Vulgaris and the quail Coturnix Coturnix, *The Journal of Experimental Biology* **203**, 725–739

Ellington, C. P. [1984], The aerodynamics of hovering insect flight, *Phil. Trans. R. Soc. Lond.* B **305** 1–181

Glauert, H. [1926], The elements of aerofoil and airscrew theory, *Cambridge - The University Press*

Hou, T. Y. [1995], Numerical solutions to free boundary problems, *Acta Numerica* **(1995)**, 335–415

Hou, T. Y., J. Lowengrub, R. Krasny [1991], Convergence of a point vortex method for vortex sheets, *SIAM J. Numer. Anal.* **28**, 308–320

Jones, K. D., C. M. Dohring, M. F. Platzer [1998], Experimental and computational investigation of the Knoller-Betz effect, *AIAA Journal* **36**, 1240–1246

Jones, R. T. [1990], Wing theory, *Princeton University Press*.

Karamcheti, K. [1966], Principles of ideal-fluid aerodynamics, *John Wiley and Sons, Inc.*

Karman, von Th. and Sears, W. R. [1938], Airfoil Theory for Non-Uniform Motion, *Journal of the Aeronautical Sciences* **5**, 6–17.

Katz, J., D. Weihs [1978], Behavior of vortex wakes from oscillating airfoils, *J. Aircraft* **15**, 861–863.

Katz, J. & Plotkin, A. [2001], Low-speed aerodynamics, *Cambridge University Press* **2nd edition**.

Koochesfahani, M. M. [1989], Vortical patterns in the wake of an oscillating airfoil, *AIAA Journal* **27**, 1200-1205.

Krasny, R. [1991], Vortex Sheet Computations: Roll-Up, Wakes, Separation, *Lectures in Applied Mathematics* **28**, 385–402, American Mathematical Society.

Kuethe, A. M., J. D. Schetzer [1950], Foundation of Aerodynamics, *New York, John Willey & Sons, Inc.*

Lai, J. C. S., J. Yue, M. F. Platzer [2002], Control of backward-facing step flow using a flapping foil, *Experiments in Fluids* **32**, 44–54

Lamb, H. [1938], Hydrodynamics, *Cambridge - The University Press*, 6^{th} edition

Lindsay, K. and Krasny, R. [2001], A particle method and adaptive treecode for vortex sheet motion in three-dimensional flow, *Journal of Computational Physics* **172**, 879–907

Massey, B. S. [1983], Mechanics of fluids, *Van Nostrand Reinhold (UK) Co. Ltd.* **5th edition**.

McCormick, B. W. [1979], Aerodynamics, aeronautics, and flight mechanics, *John Wiley and Sons, Inc.*

McCune, J. E., C. M. G. Lam, M. T. Scott [1990], Nonlinear aerodynamics of two-dimensional airfoils in severe maneuver, *AIAA Journal* **28**, 385–393

Moore, D. W. [1976], The stability of an evolving two-dimensional vortex sheet, *Mathematika* **23**, 35–44.

Moran, J. [1984], An introduction to theoretical and computational aerodynamics, *John Wiley & Sons, Inc.*

Murdock, J. W. [1976], Fluid mechanics and its applications, *Houghton Mifflin Company*

Muskhelishvili, N. I. [1946], Singular integral equations; Boundary problems of function theory and their application to mathematical physics, *Groningen, P. Noordhoff [c1953]*, **17, 23**.

Nitsche, M. and Krasny, R. [1994], Numerical study of vortex ring formation at the edge of a circular tube, *Journal of Fluid Mechanics* **276**, 139–161.

Peerless, S. J. [1967], Basic Fluid Mechanics, *Pergamon Press.*

Pennycuick, C. J., M. Klaassen, A. Kvist, A. Lindstrom [1996], Wingbeat frequency and the body drag anomaly: wind-tunnel observations on a Thrush Nightingale (*Luscinia Luscinia*) and a Teal (*Anas Crecca*), *The Journal of Experimental Biology* **199**, 2757–2765.

Plapp, J. E. [1968], Engineering fluid mechanics, *Prentice-Hall, Inc., Englewood Cliffs, New Jersey.*

Poore, S. O., A. Sanchez-Haiman, G. E. Goslow Jr. [1997], Wing upstroke and the evolution of flapping flight, *Nature* **387**, 799–802.

Pullin, D. I. [1978], The large-scale structure of of unsteady self-similar rolled-up vortex sheets, *J. Fluid Mech.* **88**, 401–430

Reid, E. G. [1932], Applied wing theory, *McGraw-Hill Book Company.*

Ringuette, M. J. [2004], Vortex formation and drag on low aspect ratio, normal flat plates, *Ph.D. Thesis, California Institute of Technology.*

Rott, N. [1956], Diffraction of a weak shock with vortex generation, *J. Fluid. Mech.* **28**, 111–128.

Russel, D. and Wang, Z. J. [2003], A cartesian grid method for modeling multiple moving objects in 2D incompressible viscous flow, *Journal of Computational Physics* **191**, 177–205

Sabresky, R. H., A. J. Acosta [1964], Fluid flow, a first course in fluid mechanics, *The Macmillan Company, New York.*

Saffman, P. G. [1992], Vortex Dynamics, *Cambridge University Press.*

Streeter, V. L. [1966], Fluid mechanics, *McGraw-Hill, Inc.* **4th edition**.

Srikwerda, J. C. [1989], Finite Difference Schemes and Partial Differential Equations, *Chapman & Hall, New York, NY.*

Theodorsen, T. [1935], General theory of aerodynamic instability and the mechanism of flutter, *National Advisory Committee for Aeronautics*, Report No. **496**.

Wang, Z. J., J. M. Birch, M. H. Dickinson [2004], Unsteady forces and flows in low Reynolds number hovering flight: two-dimensional computations *vs* robotic wing experiments, *The Journal of Experimental Biology* **207**, 449–460

Wang, Z. J. [2000], Vortex shedding and frequency selection in flapping flight, *J. Fluid Mech.* **410**, 323–341.

Wang, Z. J. [2000], Two dimensional mechanism for insect hovering, *Physical Review Letters* **85**, 2216–2219.

Weissinger, J. [1947], The lift distribution of swept-back wings, *NACA Technical Memorandum* **1120**.

White, F. M. [1986], Fluid mechanics, *McGraw-Hill, Inc.*

Wu, T. Y. [1961], Swimming of a waving plate, *J. Fluid Mech* **10**, 321–344.

Wu, T. Y. [1971], Hydromechanics of swimming propulsion, I. Swimming of a two-dimensional flexible plate at variable forward speeds in an inviscid fluid, *J. Fluid Mech* **46**, 337–355.

Wu, T. Y. [1971], Hydromechanics of swimming propulsion, II. Some optimum shape problems, *J. Fluid Mech* **46**, 521–544.

Wu, T. Y. [1971], Hydromechanics of swimming propulsion, III. Swimming and optimum movements of slender fish with side fins, *J. Fluid Mech* **46**, 545–568.

Wu, T. Y. [1971], Hydrodynamics of swimming fishes and cetaceans, *Advances in Applied Mechanics*, Vol.II, 1–63, Academic Press, London, New York.

Wu, T. Y., C. J. Brokaw, C. Brennen [1975], Swimming and flying in nature, *Plenum Press, New York*.

Wu, T. Y. [1977], Introduction to the scaling of aquatic animal locomotion, In *Scale Effects in Animal Locomotion*, 203–232, Academic Press, London, New York.

Wu, T. Y. [2001], On Theoretical Modeling of Aquatic and Aerial Animal Locomotion, *Advances in Applied Mechanics* **38**, 291–352.